

The Texas Medical Center Library

DigitalCommons@TMC

The University of Texas MD Anderson Cancer
Center UTHealth Graduate School of
Biomedical Sciences Dissertations and Theses
(Open Access)

The University of Texas MD Anderson Cancer
Center UTHealth Graduate School of
Biomedical Sciences

5-2021

The impact of synchrony on neuronal coding and behavior

Natasha Kharas

Follow this and additional works at: https://digitalcommons.library.tmc.edu/utgsbs_dissertations



Part of the [Neurosciences Commons](#), and the [Neurosurgery Commons](#)

Recommended Citation

Kharas, Natasha, "The impact of synchrony on neuronal coding and behavior" (2021). *The University of Texas MD Anderson Cancer Center UTHealth Graduate School of Biomedical Sciences Dissertations and Theses (Open Access)*. 1088.

https://digitalcommons.library.tmc.edu/utgsbs_dissertations/1088

This Dissertation (PhD) is brought to you for free and open access by the The University of Texas MD Anderson Cancer Center UTHealth Graduate School of Biomedical Sciences at DigitalCommons@TMC. It has been accepted for inclusion in The University of Texas MD Anderson Cancer Center UTHealth Graduate School of Biomedical Sciences Dissertations and Theses (Open Access) by an authorized administrator of DigitalCommons@TMC. For more information, please contact digitalcommons@library.tmc.edu.



**THE IMPACT OF SYNCHRONY ON NEURONAL CODING AND
BEHAVIOR**

by

Natasha Kharas, B.S.

APPROVED:

Valentin Dragoi, Ph.D.
Advisory Professor

Ruth Heidelberg, M.D. Ph.D.

Xaq Pitkow, Ph.D.

Matthew McGinley, Ph.D.

Fabricio H. Do Monte, D.V.M., Ph.D.

Louise D. McCullough, M.D., Ph.D.

APPROVED:

Dean, The University of Texas
MD Anderson Cancer Center UTHealth Graduate School of Biomedical Sciences

THE IMPACT OF SYNCHRONY ON NEURONAL CODING AND BEHAVIOR

A
DISSERTATION

Presented to the Faculty of
The University of Texas
Health Science Center at Houston
McGovern Medical School
MD Anderson Cancer Center
UTHealth Graduate School of Biomedical Sciences

in Partial Fulfillment
of the Requirements
for the Degree of

DOCTOR OF PHILOSOPHY

by
Natasha Kharas, B.S.

Houston, Texas

May 2021

DEDICATION

~ ~ ~

This work is dedicated to my parents. In particular, to my mother, who instilled in me the love of mathematics at a young age.

~ ~ ~

Acknowledgements

Thank you to all my friends and family for their love and support over the years. In particular, thank you to my parents who provided me with every opportunity imaginable. Also, thank you to my fiancée, Victoria, and her family their support during my PhD. My lifelong friends, Grace, Janine, and Amber have always provided me their undying support. My close medical school friends, Peter, Sarah, Kanwal, Rachel, Helena, Ryan, Deb, and Meaghan made the MD/PhD journey lots of fun. My clinical mentors, Drs. David Sandberg and Casey Halpern, always appropriately guided me and are my role model neurosurgeon-scientists.

Thank you to all the faculty and staff in the Neurobiology and Anatomy Department, Neuroscience Program, and Graduate School of Biomedical Science for your support throughout the years.

I am grateful to be part of a cohesive lab group, where I can call each member of the lab a good friend. Sam and Ariana were instrumental in the experiments described in Chapter 3. Sam was my first collaborator in the lab and has become like a sister to me. We always have fun whether it is coordinating t-shirts to wear to lab meeting or coordinating experiments for our projects. Ariana taught me not only how to perform electrophysiological recordings in nonhuman primates but also how to do optogenetics in nonhuman primates, and she was an excellent teacher. Mircea and Arun have been key collaborators in the experiments described in Chapter 4. Arun helped set up the electrical stimulation experiments. Mircea has been working on an integrate-and-fire network model to explain our experimental findings. Mircea and I have had interesting conversations on a range of topics over the years. Although I did not overlap with Sarah in the lab, she set-up polysomnography in the lab and it has been great collaborating with her. Thank you to Neda, who took me under her wing and taught me how to code. Thank you to Adam as well for

teaching me several coding tricks that I continue to use today. Russell and I wrote our first NIH grants together, have been roommates at several neuroscience conferences and have had the many interesting scientific debates over beers. Sunny embodies why it is important to pick a lab with good post-docs, he has mentored me effortlessly, providing me with guidance in several scientific domains. Sorin and Melissa have been fantastic to work with on projects that probe how animals process subconscious stimuli. Melissa also helped me with the videography analysis in the Chapter 4 project and is equally enthusiastic about implementing new technology as she is about her dance moves.

I am indebted to our animals, without whom this work would not be possible. Thank you for helping us understand the inner workings of the brain. I appreciate all the staff at CLAMC that take great care of our animals.

Thank you to my advisory committee members, Xaq, Fabricio, Drs. Heidelberger, McCullough, and McGinley for their time over the years providing me with crucial feedback about my research, appropriately questioning my logic, and constructively criticizing my work to help me become a better scientist.

Lastly, I would like to thank my PhD advisor, Valentin Dragoi, who has been an excellent mentor to me. He strikes a perfect balance between challenging my work and being a cheerleader. He has taught me reanalyze questions until we reach a meaningful and impactful conclusion that advances the way we think about the brain.

Thank you to all my funding sources for recognizing my research as worthy including but not limited to the NIH/NEI NRSA F31 grant, Kopchick Fellowship, Hawkins Scholarship, Osborne Endowment, and Terry Crow Scholarship.

The impact of synchrony on neuronal coding and behavior

Natasha Kharas, B.S.

Advisory Professor: Valentin Dragoi, Ph.D.

Abstract

Cortical columns represent the elementary functional and computational module of the neocortex. Although much is known about its laminar structure and synaptic connectivity, how patterns of spiking activity propagate within columnar circuits when the state of the brain changes remains poorly understood. We used multi-electrode laminar arrays to reveal that brain state modulates the propagation of neural activity across the layers of early and mid-level visual cortex (areas V1 and V4). We found a high prevalence of neuronal synchrony (vigorous (On) and weak (Off) spiking) in rest but low prevalence of synchrony during wakefulness. We next tested whether propagation of synchrony across cortical circuits is state dependent. By optogenetically inducing On and Off state transitions within a single cortical layer during wakefulness, we found that synchronized neural activity propagates to other layers only weakly, and the extent of spread is inversely related to arousal level. In contrast, during rest, optogenetically-induced population activity vigorously propagates throughout the entire cortical column even when neurons are in a desynchronized wake-like state prior to optogenetic stimulation. The influence of the global brain state on the propagation of spiking activity across laminar circuits was explained by changes in the coupling between neurons, where neurons were weakly coupled during wakefulness but strongly coupled during rest. The state-dependent propagation of synchronous activity revealed here could constitute a general principle of signal transmission within the sensory cortex.

In addition to understanding how neuronal coupling modulates synchrony propagation in wakefulness and rest, we probed the functional significance of synchrony by studying the influence of NREM sleep (where high levels of synchrony are observed) on coding and cognitive performance. We used non-human primates to record the changes in activity of single neurons, neuronal populations, and local field potentials in V4 that occur before, during, and after NREM sleep. To test the cognitive effects of naps, monkeys performed a visual discrimination task before and after taking a nap. We found that high levels of synchrony during NREM sleep drive the brain to be further asynchronous after sleep compared to before sleep. Thus, synchrony in NREM sleep improves behavior by modulating population level dynamics., which we mechanistically tested by performing local microstimulation to induce synchrony in V4 of awake animals. Local microstimulation in V4 replicated the changes in neuronal coding and behavioral performance observed after sleep. We uncovered how synchrony in sleep influences neuronal coding changes in single neurons and in neural ensembles that lead to sleep dependent improvement in cognitive performance. Overall, these findings expand our understanding of the functional significance of synchrony, the neurobiology of sleep, and the neuronal coding that drives perception.

Table of Contents

Approval Page.....	i
Title Page	ii
Dedication	iii
Acknowledgements	iv
Abstract.....	vii
Table of Contents	viii
Chapter 1: Introduction.....	1
1.1 Canonical visual circuits.....	1
1.2 Coding in single neurons and neuronal populations.....	3
1.3 Synchrony in cortical circuits	5
1.4 Behavioral states and brain activity	6
1.5 Hypothesis and research aims.....	7
Chapter 2: Materials and Methods.....	8
2.1 Surgical procedures.....	8
2.2 Electrophysiological recordings	9
2.3 Behavioral tasks	11
2.4 Optogenetics	19
2.5 Microstimulation.....	21
2.6 Data analysis	23
Chapter 3: Brain state modulates synchrony propagation in visual cortical circuits.....	28
3.0 Abstract.....	28
3.1 Introduction.....	29
3.2 Results.....	31
3.3 Discussion.....	57
Chapter 4: Synchrony in NREM sleep desynchronizes cortical circuits and improves behavior	61
4.0 Abstract.....	61
4.1 Introduction.....	62
4.2 Results.....	64
4.3 Discussion.....	81
Chapter 5: Conclusions and future directions.....	83
Bibliography	87
Vita	109

Chapter 1: Introduction

1.1 Canonical visual circuits

Seeing and identifying objects in our environment is essential for survival. Visual information from our surroundings enters the eye in the form of light. This information is processed and transmitted by the retina to the lateral geniculate nucleus (LGN) in the thalamus and subsequently to the primary visual cortex (V1)^{1,2}. This relay from the eye (retina) to a subcortical structure (thalamus) and then to the cortex (V1) occurs rapidly, over the course of hundreds of milliseconds^{1,3}.

Once the visual information is in the cortex (V1), it travels dorsally to the parietal cortex and ventrally to the temporal cortex^{2,3}. Brain areas in the dorsal stream, including the middle temporal and lateral intraparietal area, respond to motion of objects and the relationships between them^{2,4}. In contrast, brain areas in the ventral stream, including primary visual area (V1), the mid-level visual cortex (V4), and the inferior temporal cortex, are essential for object recognition². In this dissertation, I will focus on the brain areas in the ventral stream involved in object recognition, specifically areas V1 and V4.

Information flow is bidirectional in the ventral visual pathway. There is feedforward input from LGN to V1 to V2¹, but there is also feedback from V2 to V1⁵. In fact, top-down feedback (modulatory) connections can influence neuronal encoding more than bottom-up feedforward (driving) connections^{4,6}. For example, V2 sends 10-times more feedback connections to V1 compared to the LGN feedforward connections to V1 and thus, compared to LGN, V2 has a stronger influence on neuronal responses in V1⁷. The connections in the ventral visual pathway are very diverse. Anatomical tracer studies show that V1 indirectly

projects to V4 through V2, but V4 sends sparse yet direct feedback to V1^{5,8}. Further, V4 shares bidirectional connections with TEO (temporal occipital lobe involved in color⁹, priming¹⁰, and attention¹¹) as well as indirect projects to TEO through LOC (lateral occipital complex involved in 3D shape perception)^{5,8}. In this manner, recurrent feedforward and feedback connections between areas in the ventral visual pathway drive perception, as studies have shown both bottom-up and top-down connections modulate encoding of visual information¹²⁻¹⁴.

Visual information encoded becomes more complex along the feedforward pathway^{3,15}. Neurons in V1 respond to lines, edges, and luminosity^{3,16}, whereas neurons in V4 respond to color^{9,17,18}, shape^{19,20}, and depth^{21,22}. Thus, to elicit robust neuronal responses, when recording from V1, we used sinusoidal orientation gratings (chapter 3 experiments). While recording from V4 we used natural images (chapter 3 and 4 experiments)^{1,23,24}. These visual feature information are topographically organized in V1 and V4. Visual cortices are horizontally organized such that neurons that respond to adjacent locations (i.e. x and y coordinates) in the visual space are anatomically adjacent in the cortex²⁵⁻²⁷. The coordinates in visual space to which a neuron responds is dubbed its receptive field and is measured in degrees²⁸. Receptive fields of neurons in V1 and V4 range from 0.5-1 and 2-4 degrees in diameter, respectively²⁹.

Vertically (perpendicular to the cortical surface) arranged neurons across the depth of the cortex share receptive fields²⁶. A group of neurons across cortical layers I-VI that share receptive field properties and stimulus preference is termed a ‘cortical column’^{26,28}. A rudimentary example is a V1 or V4 cortical column that prefers the 90-degree orientation or the color red presented at 30 degree of eccentricity in visual space. Visual cortices show remarkable regularity, where neighboring cortical columns that span feature preference (ex. 0

to 272 degree orientations) are uniformly repeated every 2-3 millimeters, eventually covering the entire visual space³⁰. Cortical columns are believed to be the fundamental units of computation in the visual cortex and across the neocortex³¹. Thus, a key goal in visual neuroscience is to understand how information is encoded across cortical columns to drive perception and behavior.

1.2 Coding in single neurons and neuronal populations

Spikes are the currency of visual information coding in the brain. In electrophysiological recordings, several measures derived from the spiking activity of a single neuron or neuronal populations are used to understand how visual cortices encode information^{3,32}. A preferred visual stimulus in the receptive field of a neuron elicits an increase in firing rate of that neuron²⁶. Interestingly, there is variability in how a neuron responds to repeated presentations of the same visual stimulus³³. This variability in the responses provides a measure of the reliability of a neuron, and comparing the responses to different visual stimuli provides a measure of the discriminability of a neuron³⁴. Single neuron measures of reliability and discriminability increase with object familiarity, task learning, and task engagement indicating that they are important measures of stimulus encoding in the cortex^{35,36}. However, to understand how information coding in the brain influences perceptual decision-making and drives behavior, it is essential to move beyond single neurons and examine large neuronal populations^{33,37}.

In the past two decades, the availability of commercial multi-electrode arrays (MEAs) hardware to record data³⁸ and affordable computing power to store the data have made it possible for neuroscientists to record simultaneously from large neuronal populations and examine dynamics at the larger network scale³⁷. The importance of studying spiking across

neuronal populations is evident from studies that show that these populations outperform single neurons in encoding visual-/task-related information and more accurately predict behavioral performance^{3,37,39}. A popular measure to quantify neuronal dynamics is by correlating the variability in the spiking activity of pairs of neurons, an analysis termed ‘noise correlation’^{40–42}. Redundancy (high correlations) in spiking activity is information limiting, and thus, lower noise correlations have been shown to be beneficial for information coding in visual cortical areas and perceptual accuracy^{43,44}. A recent study showed that the timing of higher order (3 or more neurons) interactions in response to visual stimuli predicts behavior even better than pairwise interactions (2 neurons)⁴⁵. Although neuronal responses and coding measures have been classically studied in response to visual stimuli^{25,46}, spontaneous activity in the brain is far from “silent” in the absence of external stimuli^{47,48}. It has been shown that baseline activity just prior to the presentation of a visual stimuli can predict behavioral accuracy^{36,49}. After all, it makes sense that the “readiness” of the network read out by baseline firing would contribute to the efficacy of information coding. A measure of fluctuations in baseline spiking activity irrespective of neural identity is the coefficient of variation of the average population firing (termed PSI: population synchrony index)^{50,51}. Variations in PSI measured at the millisecond timescale have been shown to predict perceptual performance on a second-by-second basis⁵¹.

In addition to the coding measures summarized in this section, there are several ways to quantify network activity such as cross-correlograms, population vectors, synergistic/redundant interactions, linear generative models, and non-linear models including deep neural networks^{41,52–56}. Computational methods are rapidly expanding and appropriately scaling with the advancements in technology that now allow us to record hundreds of neurons simultaneously (as of three years ago⁵⁷) and image spiking activity of thousands of neurons (as

of a month ago⁵⁸), all aiming at better understanding how the cortex encodes information and drives perception and behavior.

In this dissertation, I use firing rates and population coupling in chapter 3 and discriminability, noise correlations, and PSI in chapter 4 to elucidate how brain state (wakefulness vs. rest) modulates signal propagation and influences information encoding, respectively. Spike rates, spike timing, correlated variability, and baseline synchrony all play a crucial role in encoding visual information and driving perceptual behavior^{43–45,51}.

1.3 Synchrony in visual cortical circuits

Synchrony is defined as co-fluctuations of the neuronal population firing where most neurons fire together or are silent⁵⁹. Synchrony can be measured in short- and long-time scales. Spike timing synchrony at shorter timescales (less than <10 ms) can be beneficial for information coding, whereas synchrony at longer time scales (tens to hundreds of ms) is detrimental to information coding^{42,45,51}. Synchrony in visual circuits is observed transiently in response to a preferred visual stimulus during wakefulness or ubiquitously when the animal is resting or sleeping⁶⁰. Specifically, in studies using imaging, extracellular and intracellular recordings show that spontaneous activity is dominated by synchrony during sleep and anesthesia but desynchronized during wakefulness^{59,61–65}. Indeed, desynchronized activity is the hallmark of wakefulness while synchronized activity is the hallmark of rest and sleep^{59,66}. This accepted dogma raises the following questions: (1) can synchrony be observed in wakefulness? and (2) why is synchrony transient in wakefulness, i.e., is it a limitation of previous recording techniques or it suggests that the cortex lacks the anatomical architecture/synaptic connectivity required to spread synchrony during wakefulness? To answer these questions, we (1) systemically quantified synchrony in thousands of neurons in

cortical columns of V1 and V4 during wakefulness and rest (chapter 3), (2) mechanistically examined the extent to which synchrony can spread in cortical circuits using optogenetics (chapter 3), and (3) measured the underlying synaptic connectivity in V1 cortical columns during wakefulness and rest (chapter 3).

1.4 Behavioral states and brain activity

Neuronal activity varies along a continuum from highly synchronized to desynchronized^{61,67}. During sleep, synchrony in neuronal network varies depending on the stage of sleep. For example, the duration and sequence of the synchronous ON (high firing rate) and OFF (low firing rate) states are non-uniform and drastically change during the various stages of sleep^{68,69}. During early sleep stages (i.e., non-rapid eye movement - NREM), sleep is characterized by synchronous firing whereas during later sleep stages (i.e., rapid eye movement - REM), relatively desynchronized firing is observed^{59,70,71}. Even during wakefulness, neuronal synchrony exists on a spectrum where quiet wakefulness has relatively increased levels of synchrony compared to active wakefulness^{50,72–74}. These baseline synchronous oscillations in firing rate during wakefulness are driven by factors such as arousal and attention. Several studies in anesthetized animals and a few studies in awake animals have shown that baseline synchrony influences neuronal coding^{54,72,75}. Indeed, neuronal coding measures described in section 1.2, for example reliability and noise correlations, are modulated with changes in brain state such as attention and arousal^{35,47,76,77}. Although ongoing oscillations in neural activity and fluctuations in brain state have been shown to influence neuronal coding in real-time, how they influence neuronal coding at subsequent time points remain poorly understood.

Specifically, how do prolonged epochs of synchronous oscillations influence sustained changes in neuronal coding, i.e., what is the functional significance of synchrony? To answer

this question, we studied NREM sleep (occurring during a short nap), as it is the behavioral condition where neuronal synchrony is robust and reliably observed (see also background information on sleep provided in section 4.1). Specifically, we tested how prolonged neuronal synchrony in short naps (20-min of sleep) influences changes in neuronal coding in V4 and behavioral performance in a visual discrimination task. We took advantage of the well-understood organization (section 1.1) and well-studied measures of coding (section 1.2) in the visual cortices. We tested changes in neuronal coding in single neurons and neuronal populations before and after sleep (Chapter 4). We also mechanistically tested the function of synchrony by using electrical microstimulation to induce synchrony and measuring the underlying changes in neuronal coding and behavioral performance (Chapter 4).

1.5 Research Aims

In this dissertation, I examine the prevalence of synchrony in cortical columns (Aim 1), the propagation of synchrony across laminar circuits (Aim 2), and the impact of synchronous activity during sleep on neuronal coding and behavioral performance (Aim 3).

Aim 1 (Chapter 3): Examine the presence of synchrony in cortical columns in V1 and V4 during behavioral states of wakefulness and rest.

Aim 2 (Chapter 3): Use optogenetics to mechanistically test whether the spread of synchrony across cortical columns in V1 is dependent on behavioral states of wakefulness and rest.

Aim 3a (Chapter 4): Examine whether synchrony in NREM sleep influences behavior and coding in single neurons and neuronal populations in V4.

Aim 3b (Chapter 4): Use electrical microelectrical stimulation to test the functional significance of synchrony on coding in single neurons and neuronal populations in V4.

Chapter 2: Materials and Methods

The data presented in this dissertation was recorded from 4343 units across 176 recording sessions in brain areas V1 and V4 in five nonhuman primates (Wh, Ch, Mo, To, and Ty). All experiments were performed in accordance with protocols approved by the US National Institutes of Health Guidelines for the Care and Use of Animals for Experimental Procedures and were approved by the Institutional Animal Care and Use Committee at the University of Texas Health Science Center at Houston.

2.1 Surgical procedures

A titanium head post used for head fixed experiments was implanted in the medial frontal region of the skull. After 3 weeks of recovery, we trained the animals on visual fixation, contrast detection, and image discrimination tasks. We considered the task to be successfully learned once the animal performed above chance level consistently for 2 weeks.

Upon successfully learning the task, a recording chamber (inner diameter of 17 mm) for single-unit multiple electrode recording were cemented over areas V1 and V4 (according to magnetic resonance imaging map and anatomical landmarks). The recording chamber was stabilized with two to five stainless steel screws inserted into the skull around the recording chambers. The recording chamber was further reinforced with cement. The animals recovered post-surgery for 4 weeks prior to using the recording chamber. The chamber was routinely examined for dura, and any additional dura was removed prior to insertion of recording electrodes. This set up was used to perform acute laminar recordings.

Chronic surface recordings were performed using 96 channel Utah arrays (Blackrock Microsystems) implanted in V4. The surgery was planned based on MRI and brain atlases.

Visual verification of the lunate sulcus and superior temporal sulcus to identify V4 was made in the operating prior to array implantation. In a subset of animals, we also used an neuronavigation software (Brainsight) to verify the anatomical location of V4 in the operating room. In addition to the array, a pedestal for chronic recordings was implanted on the caudal location on the skull off the midline. Animals had a 2-week recovery period before recordings.

2.2 Electrophysiological recordings

Electrophysiology recordings across the depth of the cortex (2.2.1) with identification of layers (2.2.2) or across the superficial layer (2.2.3) is described as follows.

2.2.1 Laminar recordings across the depth of the cortex

Laminar recording electrodes were used to record single unit and multi-unit activity. Unit was recorded using a laminar probe with 16–24 equally spaced contacts at 100 μm (U-Probe, Plexon). The electrode was advanced across the depth of the cortex using the NAN drive system (Plexon) attached to the recording chamber. Local field potential (LFP) was recorded in all channels, multi-unit activity was recorded in most channels, and single-unit activity was recorded on average in 50% of channels. Real-time spiking activity and LFP signals were recorded at 40 kHz, filtered by a preamplifier box and processed using a Multichannel Acquisition Processor System (MAP, Plexon Inc) and filtered by a preamplifier⁴³. In addition, spiking activity of isolated single units was heard through a speaker. Unit activity was sorted into single units using an offline spike-sorting program (Plexon Inc). High- and low-amplitude noise was manually removed using an offline sorter. Units were manually sorted in principal component analysis spaces chosen based on the spike waveform shape and low signal-to-noise ratio.

2.2.2 Current Source Density (CSD) analysis to identify cortical layers

In order to identify the relative position of cortical layers in areas V1 and V4, current source density analysis (CSD) was performed⁷⁸. Evoked response potentials to a high contrast stimulus were recorded from equally spaced laminar contacts (100 μm intercontact spacing). The second spatial derivative of the evoked response potentials was computed using the iCSD toolbox for Matlab. The granular layer was identified by finding the maximum sink, measured by nA/mm^3 . Channels located in the primary sink were assigned to the granular layer, while channels above the sink were assigned to the supragranular layer and channels below the sink were assigned to the infragranular layer. Several controls were performed to ensure that the above protocol for laminar characterization is reliable: (i) small movements of the entire laminar probe shift the CSD plot towards the performed direction of movement. (ii) shuffling contact position on the laminar probe destroys the deliverable CSD plot. (iii) total laminar length was verified with anatomical measurements.

2.2.3 Surface recording using Utah arrays

We recorded single-unit, multi-units, and local field potentials from all 96-channels (400 μm apart) of chronically implanted Utah arrays (Blackrock Microsystems). Data was sampled at 30 kHz using a Cerebus Neural Signal Processor¹⁷. Spike wave forms with signal to noise ratio of 4 standard deviations were saved and processed through the spike sorting Plexon software as described in section 2.2.2.

2.2.4 LFP analysis

LFP was recorded at 1 KHz. We corrected the filter-induced timing delays of LFP data by using the FPAlign utility from Plexon Inc⁵². We then filtered the LFP channels with a band

pass filter (0.5-80 Hz) and we applied an 8th order Butterworth notch filter at 60 Hz. The LFP power was then computed for each recording channel independently using the MATLAB R2015b function `bandpower`, which calculates the average power via a rectangle approximation of the integral of the power spectral density estimate. The power was then z-scored across trials.

To define rest in chapter 3, the LFP power ratio (PR) was computed by dividing the LFP power in the lower-frequency bands (0.5-10 Hz) by the LFP power in the higher-frequency bands (30-80 Hz). LFP PR was used as a measure of brain state, as changes in these specific lower- and higher-frequency bands have been known to be associated with wakefulness compared to rest^{50,51}. Rest sessions where the LFP PR was significantly different from task sessions using a Wilcoxon rank sum test were considered valid.

To characterize sleep in chapter 4, band power in all frequency bands was computed in sleep and no sleep conditions. Power in delta (0.5 - 4 Hz) was calculated for sleep and no sleep sessions. The relative increase in delta was calculated by dividing the peak in delta band power from the baseline delta activity. Relative increases in delta were compared between sleep and no sleep sessions using Chi-squared test (Figure 4.6A).

2.3 Behavioral tasks and conditions

Behavioral tasks (fixation, detection, and discrimination) and behavioral conditions (rest and sleep) are summarized as follows in sections 2.3.1 to 2.3.7.

2.3.1 Visual stimuli

Natural images (ex. penguin, dog, tree landscape) were using in discrimination task. The natural images were gray-scale such that the images had identical luminosity and contrast.

Orientation gratings were used for detection task. Gratings were generated via MATLAB Psychophysics Toolbox. Stimuli ranged in size from 1–5°, and were presented at 2–6° of eccentricity. In each recording session, stimuli were displayed within the receptive fields of neurons recorded. All visual stimuli (natural images and gratings) were presented on a 19” CRT color video monitor (Dell, 60 Hz refresh rate). The precise timing of visual stimuli presentation was recorded using a photodiode placed on the monitor screen. Photodiode timing combined with strobed markers in the task allowed us to align neuronal data with visual stimulus presentation recording with millisecond precision (ECM device, FHC Inc)⁴³.

2.3.2 Fixation task

Animals were trained to fixate on a central point (0.1 deg in size) presented on a 19” CRT video monitor (Dell, 60 Hz refresh rate) on a dark background in a dark room. Fixation was maintained within a 1-deg window for 1000 ms in the absence of sensory stimulation. Successful fixation was rewarded with 5 drops of juice. If fixation was broken, trials were aborted. Each session consisted of 120-480 trials. We recorded 3,840 trials across 32 sessions (608 units).

2.3.3 Detection task

Animals were trained to detect visual stimuli presented binocularly on a 19” CRT video monitor (Dell, 60 Hz refresh rate). Monkeys were required to signal the presence of the stimulus by releasing the lever or maintaining contact if no stimulus was displayed. Correct behavioral responses were rewarded with 5 drops of juice. Visual stimuli consisted of gray-scale sinusoidal gratings created in Psychophysics Toolbox in MATLAB and were presented on a dark background in a dark room. Each trial started with a 0.1 deg fixation point presented

on the screen. Once the animal established stable fixation (within a 1-deg window) for 450 ms, a sinusoidal grating with a diameter of 2-3 deg were displayed at 2-4 deg eccentricity was transiently presented for 300 ms. and was followed by a delay period of 1.1s (blank screen). Peak luminance values (0.107, 0.120, 0.133, 0.280 cd/m²) for visual stimuli were calculated and measured for consistency (Tektronix, J17)⁴³. 50% of trials contained a stimulus. Each session consisted of 360-720 total trials. A total of 11,520 trials across 32 sessions were recorded.

2.3.4 Discrimination task

During each recording session, monkeys performed a delayed-match-to-sample task in which they had to indicate whether two successively presented natural images had the same or different orientation. Monkeys sat in conventional primate chairs, head-restrained, in front of a computer monitor 90 cm away⁵¹. Eye position was continuously monitored as described in “Eye movement control” section below. Receptive field selectivity was examined as described in detection task. The units recorded had largely overlapping receptive fields (Figure 3.1B), thus, ensuring that we were recording from a cortical column. The 2 to 5 deg natural image stimuli was presented in the receptive field of cells being recorded. For every trial, once the animal established stable fixation (within a 1-deg window) for 400 ms, a target stimulus was flashed for 367 ms, and after a delay period of 1250 ms, a test stimulus flashed for 367 ms. In approximately half of the trials, the test stimulus had the same orientation as that of the target (‘match’ condition). In the other half of the trials, the test orientation was rotated from the target by 3°, 5°, 10° or 20° (‘non-match’ condition)⁵¹. Animals were trained to release a bar on match trials and hold the bar on non-match trials in order to receive a juice reward. Match and non-match trials were randomly interleaved (we collected at least 500 trials in each

session). The inter-trial interval was 10 s. Each session consisted of 500 total trials. In data analysis for chapter 3, 3507 trials with stimulus and 493 trials without stimulus were recorded across 8 sessions with 91. In data analysis for chapter 4, 47 sessions were recorded with 2080 units.

2.3.5 Eye movement control

Eye position was calibrated at the beginning of each session using a five-point calibration procedure. On each trial, monkeys were trained to fixate on a dot (0.2 deg in size) at the center of the screen within a small rectangular 1-2 deg window⁵². To ensure fixation, eye position was constantly monitored by using an eye tracker operating at 1 KHz (EyeLink II; SR Research). The eye-tracker gains were adjusted so that they were linear for horizontal and vertical eye deflections. Microsaccades were analyzed every 10 ms by using a vector velocity threshold of 10 deg/s (this corresponds to a 0.1 deg eye movement between consecutive 10-ms intervals)⁵². If a detected microsaccade exceeded 0.25 deg (fixation instability), the trial was automatically aborted. Thus, if at any point during the trial, eye position exceeded 0.25 deg outside the boundaries of the rectangular box, the trials described in the fixation and detection tasks below were automatically aborted. For analysis in rest, eye closure was calculated based on eye X and Y traces using custom MATLAB scripts. Only sessions in which eye closure exceeded 85% of the total session time were considered valid rest sessions. Pupil size was continuously measured monocularly at 1 kHz sampling frequency (EyeLink II; SR Research). We included in the analysis only the time periods in which luminance was constant and the fixation point was the only stimulus displayed on the screen (during the delay period, see Figures 3.3A and 3.3B). For the pupil analysis (see Figures 3.9 and 3.25B), pupil size was downsampled at 100 Hz and the median value was

taken over the entire delay period in each trial. The pupil size trace was z-scored to compare across sessions. The average pupil size was calculated per trial and correlated with state transitions/s using the Pearson correlation coefficient R . P values < 0.05 were considered significant.

2.3.6 Rest (Chapter 3)

In the rest condition, either performed before or after the passive fixation or contrast detection tasks, monkeys remained in the same experimental set-up in a dark room and stimulus screen with a dark background for 20–45 minutes. Monkeys began to rest at approximately 2 p.m., which is around the time monkeys naturally take daytime naps⁷⁹. A total of 31 rest sessions with 523 units were recorded across three monkeys, W, T and C (see ‘Quantification of rest sessions’ below).

In chapter 3, in conditions where we performed laser stimulation (passive fixation/wakefulness and rest), experimental conditions were well controlled. That is, animals were in the same experimental setup in a dark room, and in both conditions, the monitor had a dark background and there was no visual stimulus in either condition. Furthermore, neurons’ firing rates were not significantly different between passive fixation and task conditions ($P > 0.05$, Chi-squared test). Thus, experimental conditions during wakefulness and rest were identical: dark room, dark monitor, and no visual stimulation. These identical experimental conditions allowed us to evaluate the effect of laser stimulation during wakefulness (passive fixation) and rest.

2.3.6a Quantification of rest period

To ensure that animals were resting during the designated rest sessions, we coordinated the start of the rest condition to occur at the time of day when monkeys naturally take daytime

nap⁷⁹, with sessions starting at approximately 2 pm each day. A rest session was considered valid if (i) the monkey's eyes were closed for > 85% of total session duration and (ii) PR was significantly higher (Wilcoxon rank sum test, $P < 0.05$) in rest compared to wakefulness (fixation and task). Eye position was monitored using a camera-based system sampling at 1 KHz (EyeLink II, SR Research). Eye closure was derived from eye position using custom MATLAB scripts. A total of 31 rest sessions across three monkeys, W, T and C met our criteria, in which we recorded 523 units.

2.3.7 Sleep (Chapter 4)

2.3.7a Videography Analysis

We used deep neural network-based software (DeepLabCut) to extract features from videos of the monkeys' face during experimental recordings⁸⁰. We used DeepLabCut to recognize and label time-points when the monkey's eyes were closed and the jaw was slacked. To do so, we followed the detailed steps under the function Details.md in the DeepLabCut repository on github⁸⁰. In brief, we created a training data set by manually labeling 200 video frames of the monkeys' face with the following labeled markers: (1) right pupil, (2) left pupil, and (3) jaw (lower lip area) (Figure 4.5A). We trained the default resnet50 network on the training dataset (all default settings were utilized). We next manually evaluated the trained network to check for appropriate labeling of left pupil, right pupil, and lower lip. Upon verification of appropriate labeling, the model was trained on the video dataset of the monkeys in the 'sleep' and 'no sleep' conditions. If the left and right pupils were extracted with greater than 90% probability, we considered that the monkey's eyes were open. If the probability of left and right pupil in the frame was less than 1% (i.e. pupils were undetectable as eyelids

covered them), we considered that the monkey's eyes were closed (Figure 4.5B). In addition, if the position of the lower lip moved in the frame along the y-axis with greater than 90% probability, we considered that the monkey's jaw was slacked (Figure 4.5C). Only sessions where the monkeys' eyes were closed and the jaw was slacked for greater than 20 minutes were considered as valid sleep sessions. Importantly, in both sleep and no sleep conditions, the lighting was identical to avoid any confounds in video training or feature extraction.

2.3.7b Polysomnography (PSG) recording setup

We created a polysomnography cap for nonhuman primates according to the strict guidelines of the AASM Manual for scoring human sleep⁸¹. We placed 3 electrodes on the frontal, 3 electrodes on the central, and 1 electrode on the occipital regions of the brain based on the international standard of 10-20 system of EEG sites used in polysomnography⁸¹. Electrodes were standard 6 mm cast silver, gold-plated, cup electrodes (Grass technologies) that were sewn to straps together forming the custom-made electroencephalogram (EEG) cap. The cap was secured to the primate's head using elastic straps and electrodes were applied on the scalp using Ten20 conductive paste. Electrooculography (EOG) was collected by positioning electrodes that were placed above the right eye and below the left eye to detect eye movements. Electromyography (EMG) was measured by an electrode placed on the mentalis muscle was used to detect muscle tone. All electrodes were referenced to a clip electrode placed on the right ear and grounded to a clip electrode placed on the left ear⁸¹. Data was sampled at 500 Hz. EEGs and EOGs were low-pass filtered online at 150 Hz and EMGs were bandpass filtered between 10 Hz and 250 Hz. Offline EEGs and EOGs were bandpass filtered between 0.3 and 35 Hz. In this manner, EEG, EOG and EMG were combined to measure PSG in nonhuman primates.

2.3.7c PSG analysis

We employed an automated sleep software (NeuroScore, DSI) that characterized epochs of time during the ‘sleep’ and ‘no sleep’ sessions into the following sleep stages: REM, non-REM (N1, N2, N3), Wake and Active Wake. In addition, we had two expert neurologist technicians (technicians from Dr. Jeremy Slater and Dr. Samden Lhatoo clinical group) manually verify the automated classifications. We did so by designing a custom-made matlab graphical user interface (GUI) that displayed the EEG, EMG, EOG and pupil traces all together. The interface allowed the data to be viewed in scalable time windows and the GUI had buttons to assign data into awake, NREM (stage 1, 2, 3), and REM sleep. We had two technicians independently evaluate the sessions and found high degree of consistency between the scoring performed by the technicians and the automated sleep software. ‘Sleep’ sessions were considered valid only if animals had experienced 20 min of NREM sleep.

2.3.7d Sleep and no sleep controls

We controlled the lights in the room, the monitor darkness, and personnel such that the experimental set-up was identical in the sleep, control (no sleep), and task conditions. The personnel inside the room paired with each monkey was the same in sleep and no sleep sessions. In the ‘no sleep’ condition, the personnel used a verbal cue to signal to the monkey to stay awake; in the absence of the verbal cue the monkey would sleep. The verbal cue was only provided at the end of ‘task pre’ so the animal did not have a priori indication of whether a session was going to be sleep or no sleep. Macaques are natural daytime nappers and thus, we did not have trouble training them to take a nap. Sleep or no sleep sessions were randomly interweaved. The sleep and no sleep conditions were verified by PSG and videography analyses as described in detail.

2.4 Optogenetics (Chapter 3)

2.4.1 Viral vector injections

Channelrhodopsin-2 (ChR2), a light-gated cation channel⁸², was transfected into excitatory neurons of primary visual cortex (V1). This was done by injecting high titers (> 10⁹ IU/ml) of purified lentivirus with a calcium/calmodulin-dependent protein kinase type II subunit alpha (α -CAMKII) promoter that specifically targets excitatory neurons (North Carolina Gene Therapy Vector Core). The virus was injected using a 29-gauge needle connected to a Hamilton syringe. The syringe and needle were mounted to a micro-manipulator (NAN instruments) which allowed for precise computerized control of the injections. The needle was lowered to the edge of the infragranular layer (lowest depth at which stable neurons were recorded). 1 μ l of virus suspension was slowly injected over 10 minutes. The needle was then retracted slowly upwards (0.1 mm/min) in 200-300 μ m steps and additional viral injections were made at 5 additional depths until the top edge of the supragranular layer was reached (highest depth at which stable neurons were recorded). This ensured that ChR-2 was injected across the entire depth of the cortex covering supragranular, granular and infragranular layers.

2.4.2 Optogenetic stimulation and electrophysiology.

A 100 mW DPSS blue (473 nm) laser (RGBLase) was coupled to a 200 μ m optical fiber and inserted into a 356 μ m stainless steel cannula for stability⁴³. The cannula encased fiber optic was mounted onto a computer-controlled NAN Microdrive allowing for precisely lowering the fiber optic to desired depths in the cortex. Light intensity was kept below 50 mW/mm² to avoid tissue heating⁴³. Importantly, light intensity was kept the same throughout

an experimental session. Laminar recording electrodes (U-probe, Plexon Inc) were advanced through the dura mater to adjacent sites on the recording grid at 0.6 mm (center-to-center) distance from the fiber. The optical fiber and electrodes were mounted separately and could be manipulated independently. The optical fiber and electrodes were positioned to minimize the distance between the optical fiber tip and the probe, with the devices often touching at the target depth. After advancing the optical fiber and recording electrode into the cortex and reaching the injection depth, optical stimulation of the neurons was achieved by delivering 10 ms light pulses at 20 Hz (15 cycles; 2 sessions) or 35 Hz (10 cycles; 4 sessions). The laser output was regulated via TTL pulses driven by a waveform generator (Model 3220A, Agilent Technologies), controlled by the experiment control module (FHC Inc).

2.4.3 Optogenetic stimulation in wakefulness and rest

To examine signal propagation in different brain states, a total of 18 sessions (200-720 total trials) were performed with 342 V1 units recorded in monkeys W and C. An experimental day consisted of wakefulness and rest sessions either arranged in rest-awake-rest or awake-rest-awake blocks on a given recording day. The reason for repeating the 1st block (either rest or awake) was to ensure that the effects observed are stable and robust. On average, the ‘awake’ lasted 45 min while a ‘rest’ session lasted 20 min (there was a 15-min inter-block interval). We optogenetically stimulated a subset of units (described in detail in ‘Layer-specific optogenetic stimulation’ section) in the laminar column and simultaneously recorded from the entire depth of cortex using laminar U-probes. Optogenetic stimulation was triggered on trials during passive fixation while no visual stimulus was presented on the screen. On each stimulation trial, laser was triggered 300 ms after the monkey acquired fixation (the average ITI was 14 s). Optogenetic stimulation and control (no laser) trials were matched in number

and they were randomly and evenly distributed across all trials. During rest, the optogenetic stimulation protocol performed in wakefulness was repeated while lights were turned off (stimulation and no-stimulation trials were randomly interleaved). The duration and number of light stimulation and control trials were identical for the wakefulness and rest conditions. As a control, we varied the frequency of optogenetic stimulation while making sure that the total duration of laser stimulation (100 ms) was held constant throughout a recording session: 35 Hz, 10 cycles, 10 ms width; 20 Hz, 10 cycles, 10 ms width; 1 Hz, 1 cycle, 100 ms width. The frequency of stimulation was held constant across brain state conditions.

In conditions where we performed laser stimulation (passive fixation/wakefulness and rest), experimental conditions were well controlled. That is, animals were in the same experimental setup in a dark room, and in both conditions, the monitor had a dark background and there was no visual stimulus in either condition. Furthermore, neurons' firing rates were not significantly different between passive fixation and task conditions ($P > 0.05$, Chi-squared test). Thus, experimental conditions during wakefulness and rest were identical: dark room, dark monitor, and no visual stimulation. These identical experimental conditions allowed us to evaluate the effect of laser stimulation during wakefulness (passive fixation) and rest.

2.5 Microstimulation (Chapter 4)

We used Synapse software suite along with RZ5 digital signal processing unit and IZ2-32 stimulator (Tucker-Davis Technologies, Alachua, Florida, USA) to generate waveforms to electrically stimulate neuronal populations through a maximum of 8 channels on a 96-channel Utah array (surface array) implanted in V4 ($n = 2$ animals). The current from IZ2-32 stimulator was injected into the electrodes on the Utah array via the 'Stim Switch Controller' and 'Stim

Switch Headstage' (Blackrock Microsystems). Stim Switch Headstage is a capacitively coupled electrode-switching control interface for neural stimulation that allows switching between recording and stimulating modes.

The stimulation current waveform was designed such that the net cumulative charge delivered to the brain through all the electrodes did not exceed 20nC, which is well below 30nC charge safely delivered per-phase in other studies. Stimulating the brain with low frequency sinusoid current waveforms would lead to a large amount of net cumulative charge buildup per-phase (above the 30nC safety limit) even with low amplitudes. This is not desirable as it has potential to damage both brain tissue and the electrodes. Therefore, we achieved 4Hz stimulation by superimposing two high frequency sinusoid current waveforms at 150Hz and 154Hz that resulted in an electric field envelope modulated at 4Hz (Figure 4.15B). The intrinsic low-pass filtering of electrical signals by the neural membrane [1] causes the neurons to follow the low frequency (4Hz) modulation of the envelope of the resulting interference field pattern [2]. Charge injected in one phase is immediately drawn out in the subsequent opposite phase and we carefully set the amplitude of the constituent sinusoids (150Hz and 154Hz sinusoids) to small equal values so that the net charge delivered never exceeded 20nC per phase. To control for the sensation of microstimulation, we stimulated at higher envelope frequencies: 40 Hz (150Hz and 110 Hz), 30 Hz (150 Hz and 120 Hz), 25 Hz (150 Hz and 125 Hz), 20 Hz (150 Hz and 130 Hz), and 15 Hz (150 Hz and 135 Hz).

We verified the current waveforms from the stimulator had the correct amplitude and temporal dynamics by driving the current through 50KOhm and 100KOhm resistors (approximating a typical range of input impedance values of Utah array electrodes) and measuring the induced voltage across them with both an oscilloscope and the ADC monitors

in the IZ2-32 stimulator. The electrodes on the Utah array were coated with Sputtered Iridium Oxide Film (SIROF) and thus, ideal for electrical microstimulation. To confirm preservation of the array, we also tested the impedance on all of the channels (stimulated and non-stimulated) and the impedance measurements were unaltered by the electrical microstimulation.

The experimental room conditions including light, monitor brightness, and personnel were strictly controlled as described in detail in section 2.3.7d ‘Sleep and no sleep controls.’ These controls were in place in the microstimulation, sleep, and no sleep sessions. We also used videography analysis (DeepLabCut, see section 2.3.7a) to confirm that the animals were awake in the microstimulation and no sleep sessions.

2.6 Data analysis

2.6.1 Hidden Markov Model Analysis

We fit a hidden Markov model (HMM) to our spiking data as described previously (Engel et al., 2016). Briefly, the spiking data were binned every 10 ms, and the HMM model was fitted to population spiking data to identify two states (on state and off state) and the transition probabilities between these states on the dataset using the `hmmtrain` function in MATLAB R 2017b. The output was analyzed using the `hmmviterbi` function, which utilizes the Viterbi algorithm to classify the spiking data into the two states for all time points. The model was trained on 50% of the data set and tested on 50% of the data set. Two states were selected by analyzing the average cross-validation error for n states (where $n = 1$ to 5). The addition of states greater than two did not significantly reduce the cross-validation error indicating that two states was the most parsimonious model for the dataset (combined rest, task

and fixation data). Because the HMM is an unsupervised learning model, only the number of states and the convergence threshold were set. The higher firing rate state was designated the on state, and the lower firing rate state was designated the off state. The output was analyzed to determine the average firing rates in the on and off states and the durations of the on and off states. As a control, the HMM model was also trained on shuffled data (temporal structure was shuffled). The final output was calculated as the output of the model trained on the original data subtracted from the output of the model trained on shuffled data. The final output was analyzed to determine the average firing rates in the on and off states and the durations of the on and off states. Minimal overlap between firing rates of on and off states indicated appropriate clustering by the model. Lastly, for the time period of a second, the switch between on and off states was calculated and labeled as transition/s. Transitions measured during laser duration of 300 ms were labeled as ‘transitions’. This transition rate measure was used in further analysis, as it is a derivative of not only the presence of on/off states but also the fluctuation between them. The fluctuation between states was examined during passive fixation, during the task, and during rest. All transition rate differences between behavioral states (fixation, task and rest) were significant within each monkey ($P < 0.05$, Wilcoxon rank sum). Furthermore, there were no statistically significant differences between monkeys ($P > 0.05$, Chi-squared test).

2.6.2 Population coupling

Population coupling is computed by calculating the cross-correlation between the smoothed firing rate of a neuron and the spike-triggered average of the population (stPR)⁸³. Population rate used for stPR computation for an individual unit excluded the spikes of that unit. Population rate was computed by accumulating spiking activity of all (multi and single)

units with 1 ms resolution and smoothing the resulting vector with a Gaussian of half-width 12 ms⁸³. The baseline level of each stPR was subtracted. For individual units, the firing rate of a unit was computed with 1 ms resolution while smoothing the resulting vector with a Gaussian of half width of $12/\sqrt{2}$ ms. The population coupling of unit i is calculated as (where f represents the smoothed firing rate of a single unit, μ represents the firing rate of a single unit and $\|f_i\|$ represents its norm):

$$c_i = \frac{1}{\|f_i\|} \int f_i(t) \sum_{j \neq i} (f_j(t) - \mu_j) dt$$

stPRs were normalized by the median size of the stPR of the shuffled data in each recording such that stPRs could be compared across recordings. Spikes were shuffled according to the raster marginals model. This shuffling procedure produces a uniform sample that preserves the mean firing rate and population rate distribution to that of the original data⁸³. In brief, the data was divided into non-overlapping 1 ms bins, and a binary matrix was constructed with one column for each time bin and one row for each recorded unit. To shuffle data, we randomly chose and shuffled 2-by-2 submatrices and switched the position of 0s and 1s. Whereas 1 indicated that a unit spiked at the corresponding time bin, 0 indicated no spikes. Swapping 0s and 1s preserved the firing rate while destroying the spike timing structure of the data successfully shuffling the data.

2.6.3 Putative excitatory/inhibitory (E/I) ratio

Spike waveforms of well-isolated single units were spline interpolated to a 2.5 μ s resolution. We then computed the time from the trough to the peak of the average waveform and set a threshold of 200 μ s to classify the single units as broad-spiking (putative excitatory) and narrow-spiking (putative inhibitory) based on previous studies^{84,85}. We used the peak-to-

trough time to classify units as this measure provides the most reliable separation of excitatory and inhibitory neurons⁸⁶. The mean waveform width of the putative inhibitory neurons was $183.4 \pm 7.9 \mu\text{s}$ and putative excitatory was $400.6 \pm 9.6 \mu\text{s}$ ⁸⁴⁻⁸⁶ (excitatory vs. inhibitory, Wilcoxon rank sum test, $P < 0.0001$). Of the 208 single units analyzed, 15% were inhibitory. The E/I ratio was calculated by dividing the mean firing rate of putative excitatory cells by the mean firing rate of putative inhibitory cells for each session.

2.6.4 Linear decoder

We decoded the neural activity by implementing a linear classifier, which fits a multivariate normal density with a pooled estimate of covariance using the MATLAB function, `classify`⁵¹. The classifier was trained on 50% of the data and tested on 50% of the data. The classification performance was calculated by averaging the output of 100 train-test cycle. Data was separately analyzed for sleep and no sleep sessions.

2.6.5 Population synchrony index (PSI)

The PSI was calculated in each trial by using the coefficient of variation of the population spike count across 100 windows of $T = 10 \text{ ms}$: $\text{PSI} = \text{Cv} = \sigma (\text{population spike counts}) / \mu (\text{population spike counts})$ ⁵¹. PSI was computed over the delay (black screen) period of a given trial. Recalculating PSI using 20 windows of 50 ms duration did not change the results.

2.6.6 Correlations (Rsc)

Correlated variability (Rsc) was computed for each pair of neurons using the Pearson correlation coefficient as previously described in detail^{43,44}. Only stable pairs of neurons were

included in the analysis. We computed Rsc for the 367 ms duration of the visual stimulus (test and target windows in Figure 4.1B).

2.6.7 Statistical analysis

We used non-parametric statistical tests throughout the analysis. For rest or sleep and wakefulness comparisons, Wilcoxon rank sum test was used. In other cases, we used Chi squared test and Pearson's correlation for significance analysis. The Holm-Bonferroni correction was applied wherever multiple comparisons were performed. All differences reported in spontaneous and optogenetically induced state transitions were significant in each individual monkey ($P < 0.05$, Wilcoxon rank sum). Furthermore, there were no significant differences between monkeys ($P > 0.05$, Chi-squared test).

Chapter 3: Brain state modulates synchrony propagation in visual cortical circuits

Note: This chapter is based upon: Kharas N, Andrei AR, Debes SR, and Dragoi V. Brain state limits propagation of neural signals in laminar cortical circuits. This manuscript is currently under review at PNAS.

3.0 Abstract

Cortical column represents the elementary functional and computational module of the neocortex. Although much is known about its laminar structure and synaptic connectivity, how patterns of spiking activity propagate within columnar circuits when the state of the brain changes remains mysterious. Here, we used multi-electrode laminar arrays to reveal that brain state modulates the propagation of neural activity across the layers of early and mid-level visual cortex (areas V1 and V4). During periods of rest, neurons exhibit frequent, spontaneous fluctuations between phases of vigorous (On) and weak (Off) spiking synchronously. In contrast, synchronized fluctuations in population activity are rare events during wakefulness. By optogenetically inducing On and Off state transitions within a single cortical layer during wakefulness, we found that synchronized neural activity propagates to other layers only weakly, and the extent of spread is inversely related to arousal level. Surprisingly, light-induced population activity vigorously propagates throughout the entire cortical column during rest even when neurons are desynchronized prior to light stimulation. The influence of global brain state on the propagation of spiking activity across laminar circuits can be explained by changes in the coupling between neurons. The state-dependent propagation of population activity revealed here could constitute a general principle of signal transmission within sensory cortex.

3.1 Introduction

For over a century, neuroscientists have observed remarkable regularity in cortical microarchitecture: clusters of cells are synaptically connected to form small columns orthogonal to cortical surface^{26,87}. These microcolumns constitute the elementary functional units of cortical circuitry⁸⁸, and consist of distinct layers that each contain a characteristic distribution of cell types and connections with other layers^{2,26,89,90}. Deciphering the functional principles of cortical column operation requires an understanding of how neural signals propagate across laminar circuits. Indeed, physical signals are transformed into neural impulses that travel along the cortical column and then are transmitted to different brain regions. It is generally accepted that the extent and accuracy with which neural signals propagate along cortical columns play a critical role in shaping behavior. However, despite significant progress in our understanding of sensory coding across laminar circuits^{51,91}, the dynamics of neuronal responses across the entire depth of cortex and the extent to which electrical signals propagate across the cortical column in different brain states^{59,73,75,92} remain unknown.

In principle, the strong intracortical connections within and between layers^{2,4,89,90} may suggest that signals emitted by individual neurons would vigorously propagate across all layers. Indeed, during wakefulness, the input, granular cortical layers relay stimulus information to output, supragranular layers, which send feedforward projections to downstream areas^{4,90}. Furthermore, neurons in the supragranular layers project back to infragranular layers, which in turn project to granular layers, and hence signals are circulated across the entire microcolumn^{89,90}. From a theoretical standpoint, this dynamic flow of signal propagation raises the possibility that neurons across cortical layers would simultaneously become active or inactive even in the absence of sensory stimulation. One possible

consequence of this spatiotemporal pattern of activity across the microcolumn is that correlations in neuronal firing would rise across layers. Nonetheless, this is inconsistent with overwhelming evidence that neurons across the cortical surface are desynchronized during wakefulness^{40,41,59,73,93,94}, and that spike count correlations in sensory cortex are relatively small (around 0.1) and layer-dependent^{91,95,96}. Importantly, the dynamics of populations of cortical neurons in alert animals vary widely across different behavioral states^{73,75,97}. Thus, even in the absence of external stimulation, the state of the brain can fluctuate between synchronized activity during rest and sleep and highly desynchronized activity during alertness^{72,92,98,99}. However, whether the dynamics and propagation of electrical signals across columnar circuits exhibit state dependency is unknown.

Previous studies were unable to address these issues mainly due to inherent restrictions of techniques such as *in-vitro* slice recordings¹⁰⁰ and *in-vivo* recordings during anesthesia^{72,77,96} that severely limit the behavioral repertoire, and hence the interpretation of cortical dynamics across laminar circuits. Furthermore, studies focused on *in-vivo* laminar recordings did not investigate the state-dependent signal propagation across cortical layers^{95,101,102}. Here, we examined the dynamics and propagation of neural signals across the cortical column in different brain states using multi-electrode laminar arrays. We discovered that global brain state strongly modulates the propagation of neural activity across the layers of early and mid-level visual cortex (areas V1 and V4). While neurons exhibit spontaneous fluctuations between phases of vigorous (On) and weak (Off) spiking during rest, synchronized fluctuations in population activity were infrequent during wakefulness. Further, we optogenetically activated specific cell populations during wakefulness to find that synchronized neural activity propagates to other layers only weakly, and that arousal controls the extent of spread. In

contrast, the light-induced activity of the same neural population propagated throughout the entire cortical column during rest even when neurons were desynchronized prior to light stimulation. We found that the differential propagation of electrical signals in different brain states relies on the degree of coupling of individual neurons to their neighbors. These findings provide mechanistic insight into the role of brain state dependent propagation of neural signals in sensory cortex.

3.2 Results

State-dependent dynamics of laminar population activity

We examined the spiking activity of 2,263 cells across the layers of visual cortical areas V1 and V4 of three behaving rhesus monkeys using 16 and 24-channel linear array microelectrodes^{91,103} (1,407 units in V1 and 856 in V4; $n = 129$ sessions). These arrays allowed us to record multiple neurons with largely overlapped receptive fields across the entire depth of cortex (Figures 3.1 and 3.2). Neuronal responses were recorded in different brain states while animals performed a fixation or a behavioral task (see Methods), and during 20 min of rest. To avoid stimulus-induced confounds we measured neurons' responses in the absence of external stimulation during visual fixation or before stimulus presentation during the task, and during periods of rest when monkeys had their eyes closed in a dark room (Figures 3.3A-C; 17,534 trials during wakefulness, and 9,110 pseudo-trials of identical length during rest). We controlled the lights in the room and the monitor brightness such that the experimental set-up was identical in all three conditions. As revealed by analyzing the local field potentials (LFPs), wakefulness was associated with increased high-frequency LFP power (30-80 Hz) and decreased low-frequency power (1-20 Hz), while high-frequency power was decreased and low-frequency power was increased during rest^{92,99} (Figures 3.3A-C). As animals rested,

prominent On-Off transitions occurred synchronously across cortical layers (Figure 3.3C). However, during wakefulness, in agreement with previous results in sensory cortex in which neuronal activity was measured at multiple sites along the cortical surface^{59,73,99,104}, the population of cells emitted action potentials in a desynchronized manner (Figures 3.3A and 3.3B).

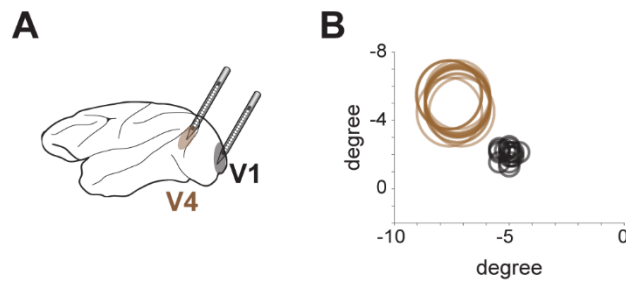


Figure 3.1. Overlapping receptive fields within V1 and V4. (A) Schematic of laminar recording using 16 channel U-Probe in macaque primary visual cortex (V1) and mid-level visual cortex (V4). (B) An example session is shown with overlapping V1 and overlapping V4 receptive fields. Circles represent receptive fields of individual neurons recorded along consecutive channels in V1 (black) and V4 (brown).

Trial

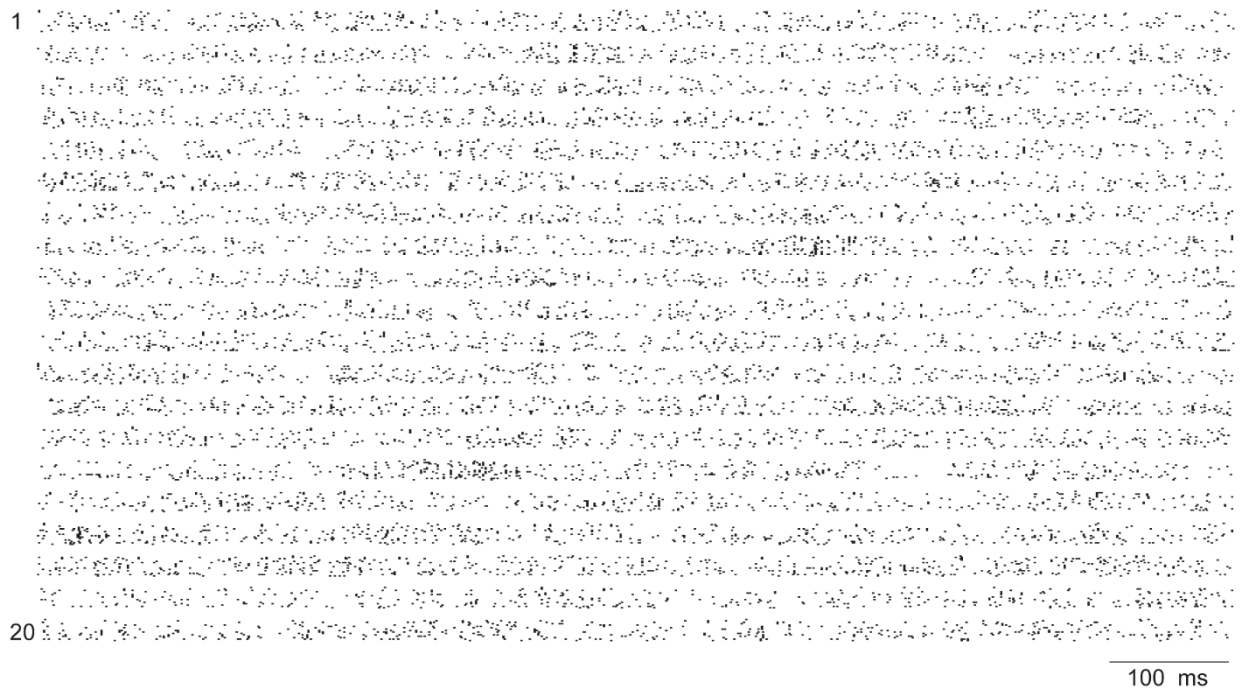


Figure 3.2. Desynchronized neural activity during wakefulness in V1. Population spike raster in a subset of fixation trials (n=20) in an example session in monkey W.

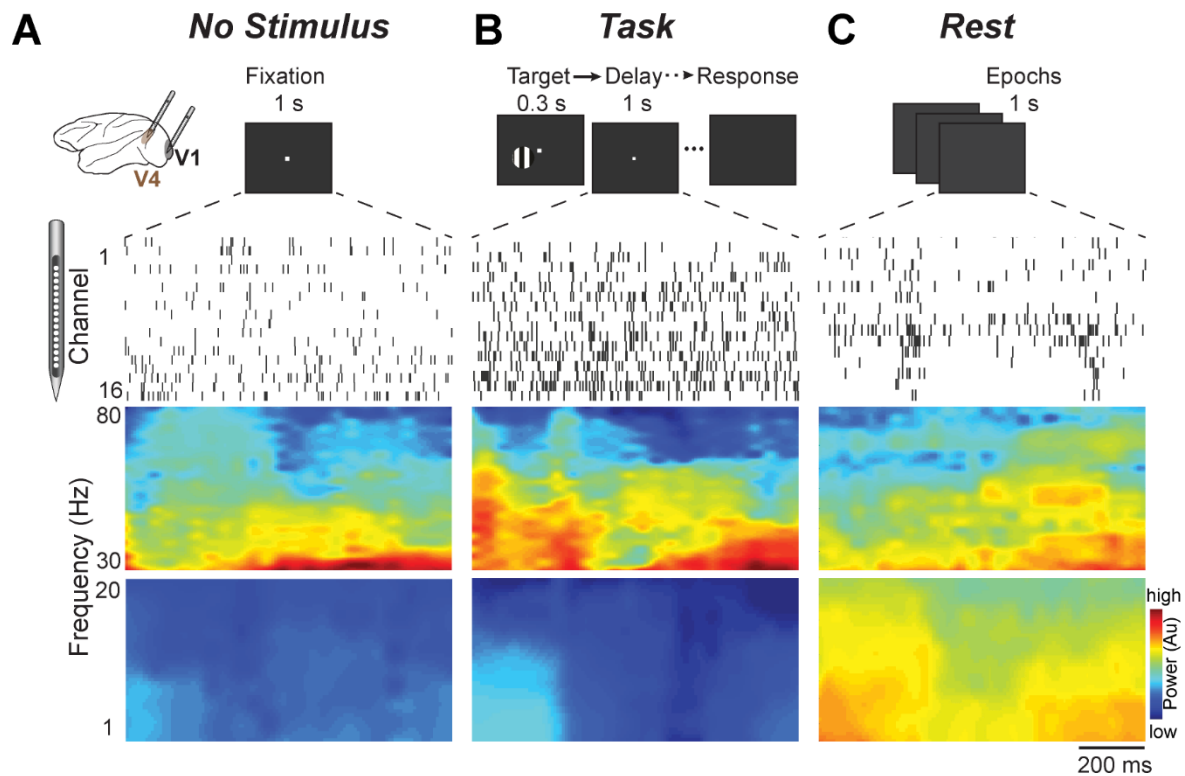


Figure 3.3. Dynamics of cortical population activity during wakefulness and rest across cortical layers. (A) Schematic representation of electrophysiological recordings using laminar probes in V1 and V4 (top). Diagram of ‘no stimulus’ condition: animals were trained to passively fixate in the center of a computer screen for 1-s. Raster plots represent single units recorded across 16 channels for example time epochs. The spectrograms on the bottom represent the corresponding low (1-20 Hz) and high frequency (30-80 Hz) LFP power. (B) Schematic representation of ‘task’ condition (top). Animals were trained to report whether a low-contrast visual stimulus was present on a computer screen. Example neuronal activity (middle) and LFP (bottom) for the 1-s interval (delay) following stimulus presentation. (C) Animals rested for 20-40 minutes (top). Example neuronal activity (middle) and LFP (bottom) during a 1s rest epoch.

To characterize the dynamics of neuronal responses across the population of cells ($n = 1,921$ units across 57 sessions in V1 and 54 sessions in V4) we counted spikes in 10-ms bins and used a two-state Hidden Markov Model^{105,106} (HMM, Figure 3.4A). We asked whether spontaneous transitions between episodes of robust (On) and weak (Off) spiking may occur synchronously during wakefulness. The HMM has a one-dimensional, latent variable representing an unobserved population state switching between the On and Off states¹⁰¹. We

fitted the HMM to our multiple single-unit spiking data across layers to transform the spike-count data into On and Off episodes under the assumption that spikes are generated via a Poisson process (Figure 3.4B). While On and Off episodes resembling the Up and Down states routinely found during anesthesia and slow-wave sleep^{59,76,99,107} were common during rest, they were scarce during wakefulness regardless of whether animals performed a behavioral task or simply fixated on a computer screen (Figures 3.3A-C).

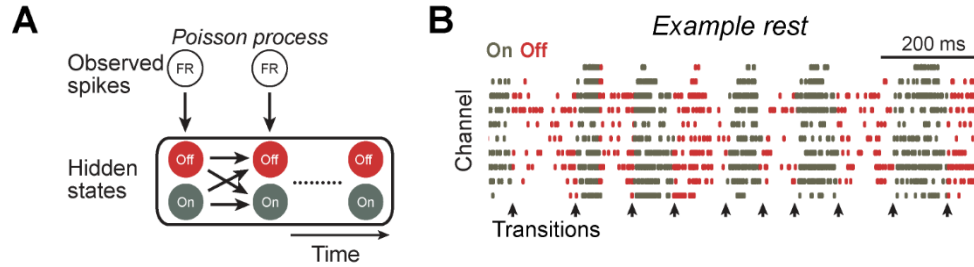


Figure 3.4. (A) Schematic of a two-state Hidden Markov Model to elucidate hidden states (On and Off) from population firing. (B) Example neuronal activity colored as On and Off states as predicted by the model; transitions between On and Off states are indicated by arrows.

We further used the HMM to infer the most likely sequence of On and Off episodes based on the observed spike trains on a trial-by-trial basis. Spike counts in On states were higher on average than those in Off states in both V1 and V4 areas (Figure 3.5). On a trial basis, we estimated the probability of staying in the On state (P_{on}), transitioning from On to Off state ($P_{on \rightarrow off}$), staying in Off state (P_{off}), and transitioning from Off to On state ($P_{off \rightarrow on}$, Figure 3.6). The probability of transitioning between On and Off states during wakefulness was almost zero, i.e., $P_{on \rightarrow off}$ ranged between 1-2% and $P_{off \rightarrow on}$ ranged between 1-3% in both V1 and V4 (Figure 3.6). In contrast, the probability to transition between

On-Off states was significantly higher during rest compared to wakefulness: $P_{on \rightarrow off}$ ranged between 18-20%, and $P_{off \rightarrow on}$ ranged between 6-11% (Figure 3.6, Wilcoxon rank sum test, $P < 0.01$). To examine the prevalence of synchronized fluctuations in population activity in different brain states, we measured the number of On-Off state transitions in 1 second (the corrected rate of transitions was computed by subtracting the rates from shuffled data, see Methods). Across sessions, columnar synchrony was significantly greater in rest compared to wakefulness in both V1 and V4 (Figures 3.4B, 3.7A, and 3.7B, Chi-squared test, $P < 0.0001$). The zero median transition rate during fixation and task indicates that synchrony in laminar circuits is largely absent during wakefulness (only 7% of trials had a transition rate > 0 , Figure 3.7A). During these epochs, the duration of On and Off states was significantly longer than that during rest (Figure 3.8).

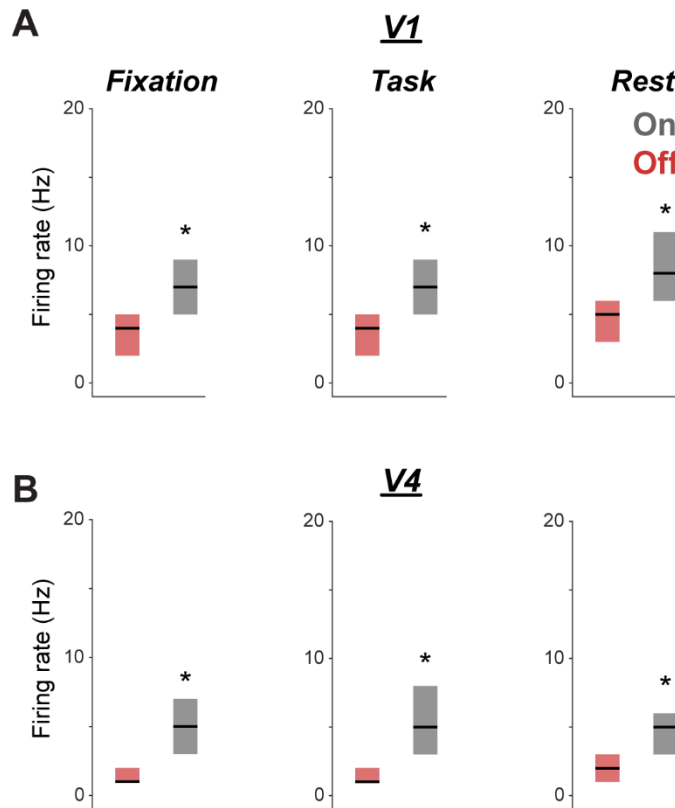


Figure 3.5. Firing rates in On and Off states in V1 and V4. Box plots show firing rates in states classified as On (grey) or Off (red) by the Hidden Markov Model (HMM) in fixation, task and rest in V1 (A) and V4 (B). Horizontal black bars indicate median and box edges

represents first quartile (bottom) and third quartile (top). Firing rates in On states is significantly different from Off states in all conditions of fixation, task and rest in V1 (A) and V4 (B) (On vs. Off durations in V1, $*P < 0.05$, Wilcoxon rank sum test, $n=27$ sessions; On vs. Off durations in V4, $*P < 0.05$, Wilcoxon rank sum test, $n=26$ sessions).

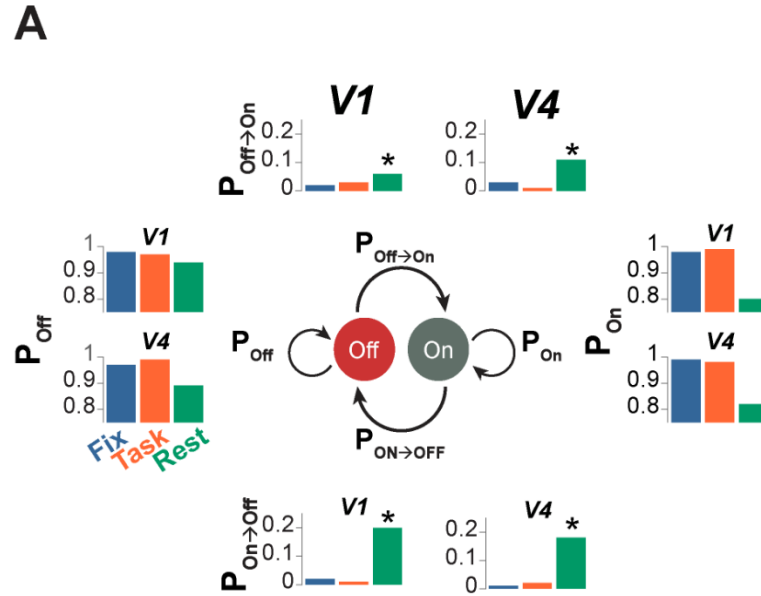


Figure 3.6. (A) Schematic showing the probability of staying in the same state and the probability of transitioning between states (center). Probability of staying in On and Off states during fixation, task, and rest (left and right) represented as bars. Probability of transitioning between On and Off states during fixation, task, and rest in both V1 and V4, as predicted by HMM ($P_{\text{Off} \rightarrow \text{on}}$ (top) and $P_{\text{On} \rightarrow \text{off}}$ (bottom) in rest vs. fixation and task in V1, $*P < 0.01$, Wilcoxon rank sum test, $n=27$ sessions; $P_{\text{Off} \rightarrow \text{on}}$ (top) and $P_{\text{On} \rightarrow \text{off}}$ (bottom) in rest vs. fixation and task in V4, $*P < 0.01$, Wilcoxon rank sum test, $n=26$ sessions).

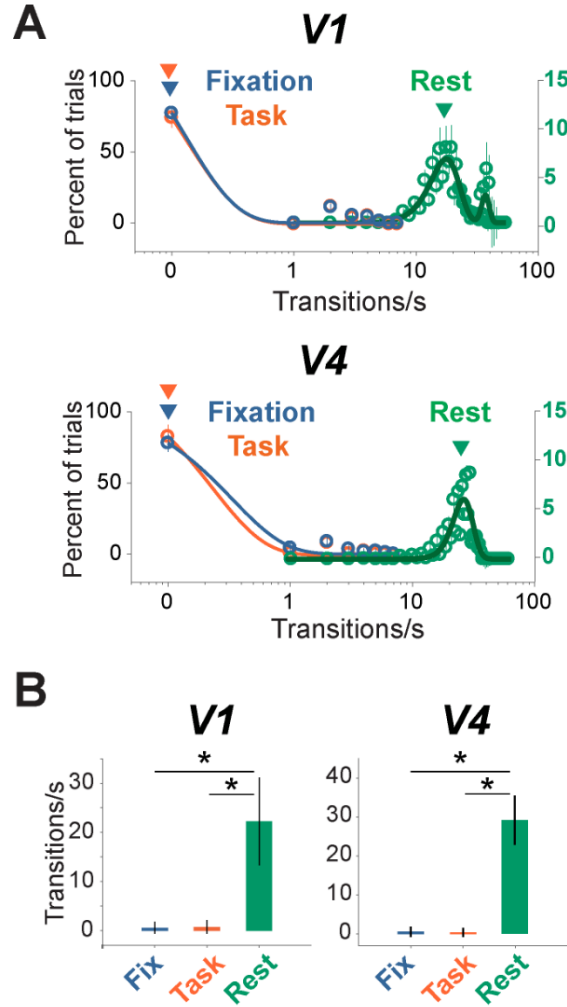


Figure 3.7. (A) Histograms of rate of transition between On and Off states during fixation, task, and rest in V1 (top) and V4 (bottom). Arrows indicate medians and error bars represent s.e.m. (B) Transitions/s plotted as mean and standard deviation during fixation, task, and rest in V1 and V4 (transition rate in rest vs. fixation and task in V1 (left), $*P < 0.0001$, Chi-squared test, $n=27$ sessions and V4 (right), $*P < 0.0001$, Chi-squared test, $n=26$ sessions).

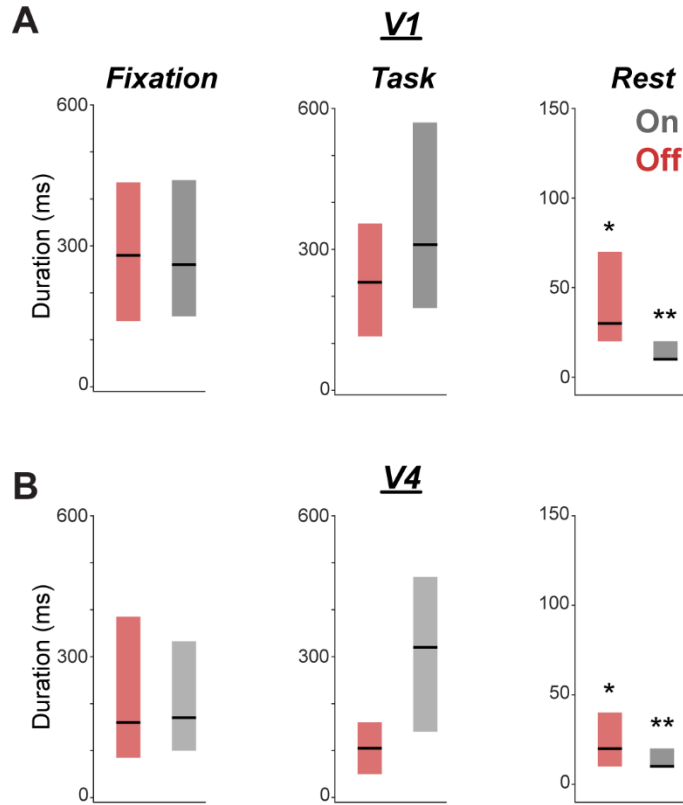


Figure 3.8. Duration of On and Off states in V1 and V4. Box plots show duration of states classified as On (grey) or Off (red) by the Hidden Markov Model (HMM). Horizontal black bars indicate median and box edges represents first quartile (bottom) and third quartile (top). In rest, the duration of On and Off states is significantly different from both awake conditions (fixation and task) in V1 (A) and V4 (B) On states, $**P < 0.05$, Chi-squared test, V1 (n=27 sessions) and V4 (n=26 sessions); Off states, $*P < 0.05$, Chi-squared test, V1 (n=27 sessions) and V4 (n=26 sessions).

In those rare wakefulness trials in which we observed On-Off transitions we examined whether the fluctuation in pupil size, a measure of global arousal, is related to the probability of occurrence of On and Off states. On a trial basis, there was a negative correlation between pupil size and rate of On-Off transitions in both V1 and V4 (Figure 3.9, Pearson's correlation coefficient, V1: $R = -0.10$, $P < 0.05$; V4: $R = -0.14$, $P < 0.05$). That is, high arousal (larger pupil) decreases the rate of On-Off synchrony during wakefulness, whereas low arousal (smaller pupil) increases it. In contrast, rest is accompanied by significantly higher On-Off

transition rates, 12-26 transitions/s, i.e., consistent with oscillations in the 6-13 Hz range reported during rest and early NREM sleep^{76,92,99} (see also Figures 3.3C and 3.7B). Our findings that columnar neurons are desynchronized during wakefulness are in contrast to a previous study in macaque V4 reporting striking On-Off state transitions during an attentional task¹⁰¹. However, brain state, such as reduced arousal or drowsiness, could contribute to increase the degree of population synchrony across laminar circuits. Additionally, contamination of waveform clusters identified as single units by spikes of other cells or noise¹⁰⁸, (Figure 3.10) could artificially give rise to spontaneous On-Off state transitions.

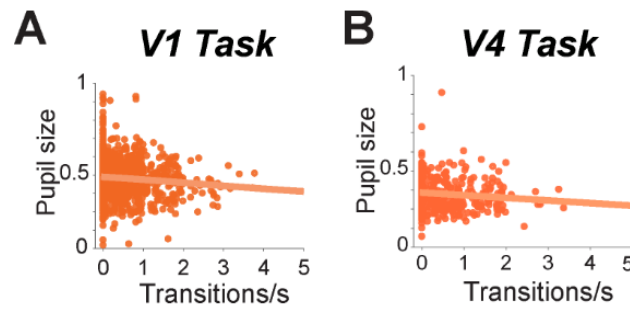


Figure 3.9. Scatter plot of mean pupil size and rate of transitions on a trial-by-trial basis. (A) V1, $R = -0.10$, $P < 0.05$, Pearson's correlation, $n=815$ trials. (B) V4, $R = -0.14$, $P < 0.05$, Pearson's correlation, $n=384$ trials.

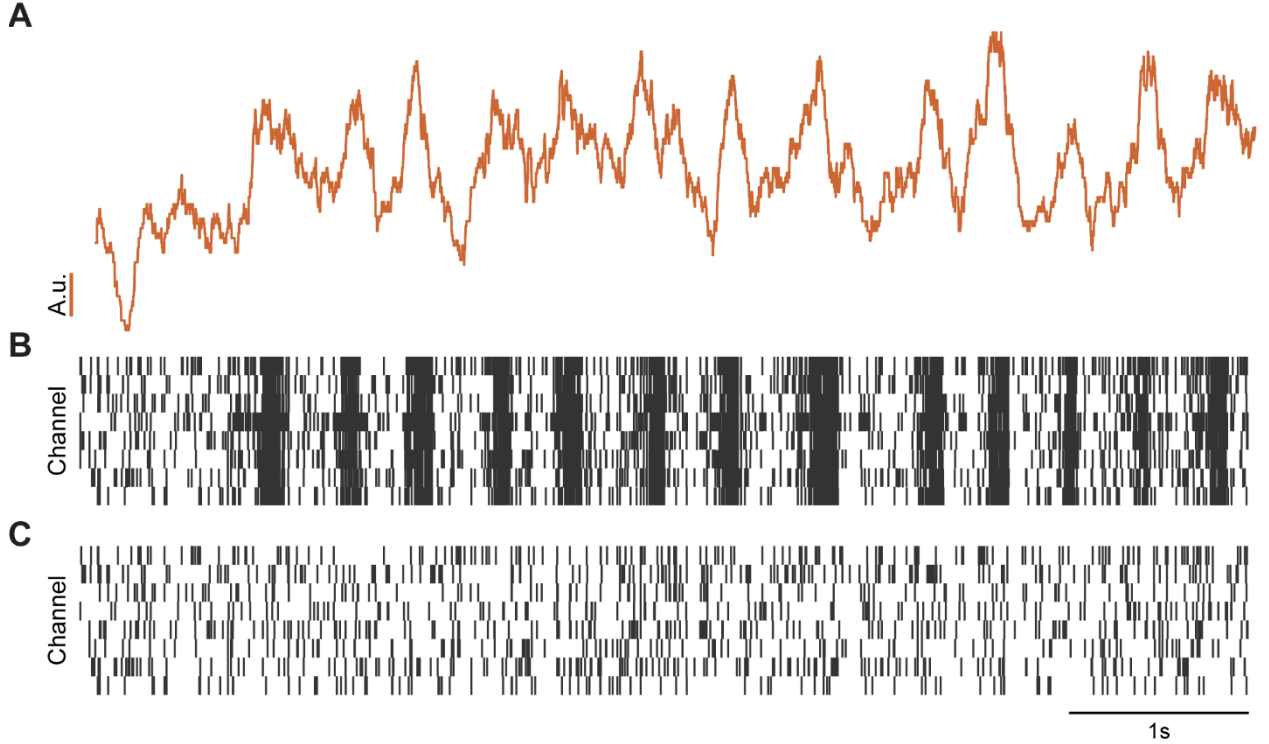


Figure 3.10. Muscle artifact in unsorted electrophysiological recordings. (A) Muscle movement, represented as the average distance between animal's lips, extracted from the video of monkey W chewing a cracker. To extract the movement of the lips we analyzed consecutive video frames every 100 ms. (B) Simultaneously recorded neural activity prior to noise removal, while monkey W was chewing. (C) Same as (B) but following noise removal and spike sorting.

On-Off state transitions in cortical layers

The HMM prediction that columnar populations are desynchronized during wakefulness does not rule out the possibility that individual cortical layers may exhibit synchronous On-Off transitions that are temporally offset among each other. One possible source of synchrony is the strong intra-layer recurrent connections within a cortical column^{2,28,60,88}. However, when we fitted the HMM to spiking activity in each layer (Figure 3.11A), the results mirrored those from the analysis of the entire column. That is, the median rate of On-Off transitions in the supragranular, granular, and infragranular layers in V1 and V4 was 0 (Figures 3.11B, 3.11C, 3.12A and 3.12C; Figures 3.13 and 3.14). This confirms that On-

Off state transitions are rare events during wakefulness, and they predominantly occur in isolation within a layer without spreading to adjacent layers (Figure 3.15). Thus, the lack of synchronous population fluctuations during wakefulness is a general property of cortical layers in early and mid-level visual cortex. In contrast, during rest we found significant rates of On-Off transitions in each layer without inter-laminar differences (Figures 3.11B, 3.11C, 3.12B and 3.12D, Chi-squared test, $P > 0.05$), which tend to spread to adjacent cortical layers (Figure 3.15).

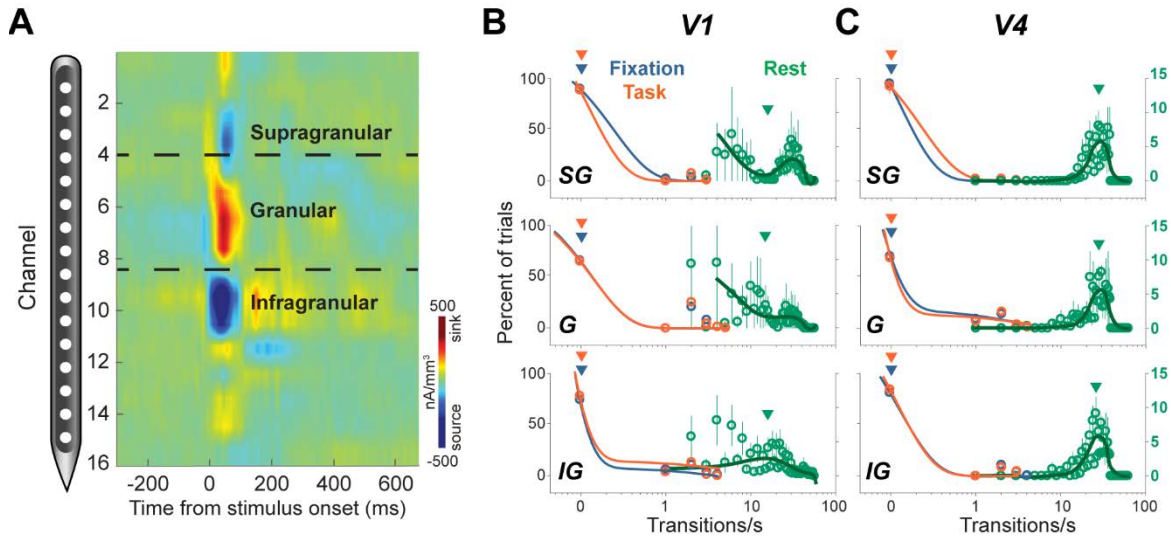


Figure 3.11. State-dependent fluctuations in population activity across cortical layers. (A) Current Source Density (CSD) analysis to identify layers by detecting the polarity inversion accompanied by the sink-source configuration at the base of the granular layer. Example current sink (shown as red) represents the granular layer and spans $\sim 400 \mu\text{m}$. (B and C) Histogram representation of transitions between On and Off states in supragranular (SG), granular (G), and infragranular (IG) layers in V1 (B) and V4 (C). Arrows indicate median and error bars represent s.e.m.

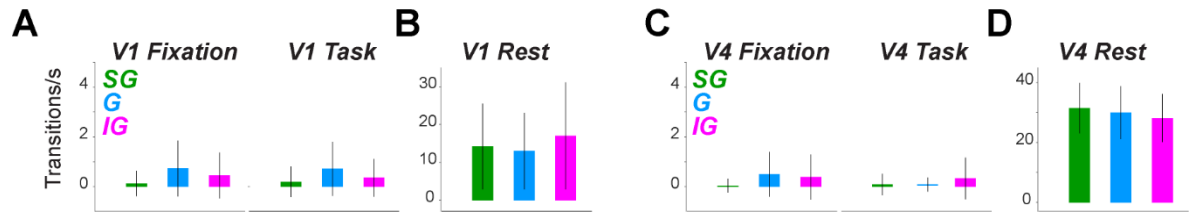


Figure 3.12. (A and C) Rate of transition between On and Off states in each cortical layer during fixation and task within V1 and V4 (During fixation, layer pairs of SG vs. IG, SG vs G, and G vs. IG in V1 (A, left) and V4 (C, left), $P > 0.05$, Chi-squared test, $n=13$ sessions; During task, layer pairs compared in V1 task (A, right) and V4 task (C, right), $P > 0.05$, Chi-square test, $n=13$ sessions). Bars represent mean and error bars represent standard deviation. (B and D) Rate of transition between On and Off states in each cortical layer during rest within V1 and V4 (Layer pairs of SG vs. IG, SG vs G, and G vs. IG in V1, $n=12$ sessions and V4, $n=9$ sessions, $P > 0.05$, Chi-squared test). Bars represent mean and error bars represent s.e.m.

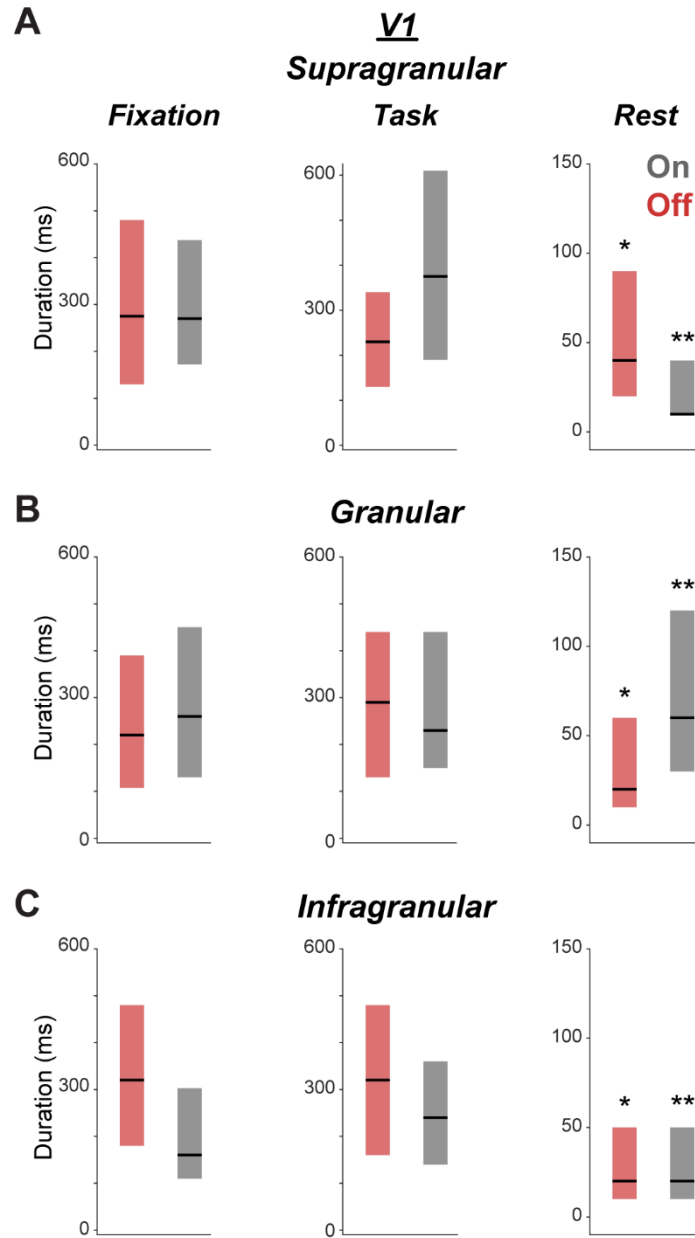


Figure 3.13. Durations of On and Off states in V1 cortical layers. Box plots show duration of states classified as On (grey) or Off (red) by the Hidden Markov Model (HMM). Horizontal black bars indicate median and box edges represents first quartile (bottom) and third quartile (top). In rest, the duration of On and Off states is significantly different from wakefulness (fixation and task) in supragranular (A), granular (B), and infragranular (C) layers. On states, $*P < 0.05$, Chi-squared test, V1 (n=22 sessions) and V4 (n=12 sessions); Off states, $*P < 0.05$, Chi-squared test, V1 (n=22 sessions) and V4 (n=12 sessions).

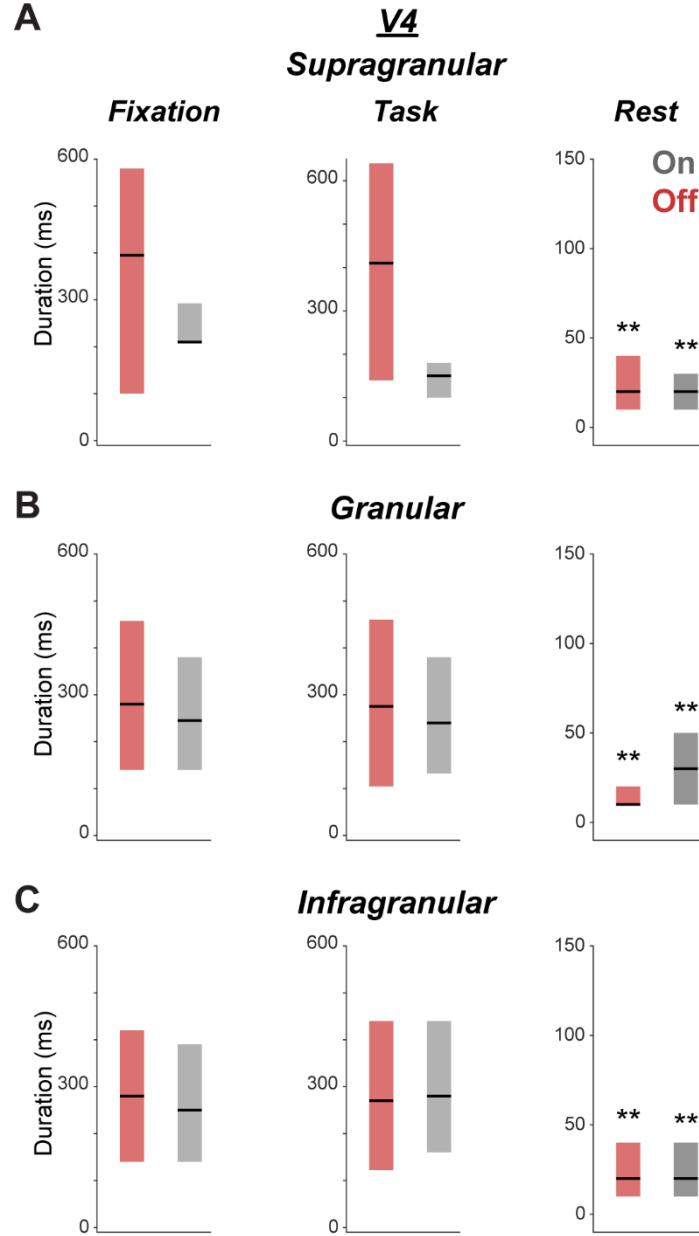


Figure 3.14. Durations of On and Off states in V4 cortical layers. Box plots show duration of states classified as On (grey) or Off (red) by the Hidden Markov Model (HMM). Horizontal black bars indicate median and box edges represents first quartile (bottom) and third quartile (top). In rest, the duration of On and Off states is significantly different from wakefulness (fixation and task) in supragranular (A), granular (B), and infragranular (C) layers. On states, $*P < 0.05$, Chi-squared test, V1 (n=22 sessions) and V4 (n=12 sessions); Off states, $*P < 0.05$, Chi-squared test, V1 (n=22 sessions) and V4 (n=12 sessions).

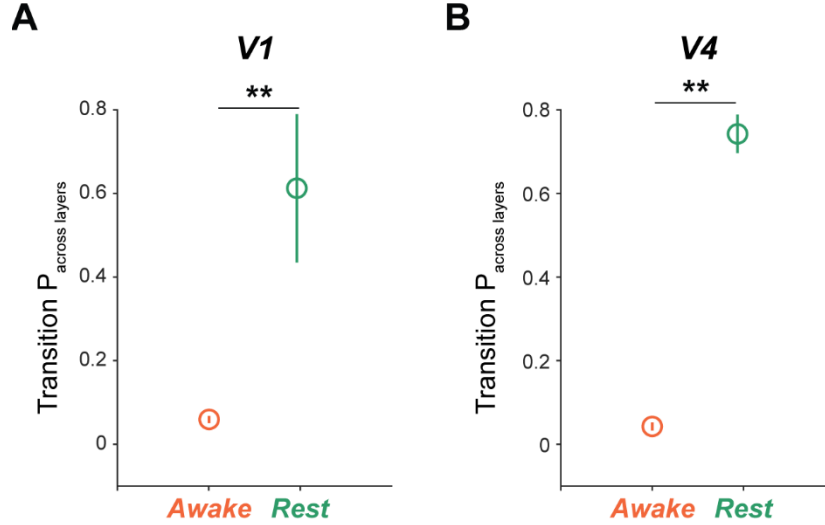


Figure 3.15. Probability of transitioning between On and Off states across layers. (A) Mean probability of a transition in a layer relative to a transition in adjacent layers in V1 during wakefulness and rest (40 ms window, $**P < 0.001$, Wilcoxon rank sum test, $n = 13$ sessions in awake and 12 sessions in rest) Bars represent s.e.m. (B) Same as A but in V4 (30 ms window, $**P < 0.001$, Wilcoxon rank sum test, $n = 13$ sessions in awake and 9 sessions in rest). Bars represent s.e.m.

Optogenetically induced state transitions remain local during wakefulness

These results further allowed us to examine, for the first time, the propagation of spiking patterns within columnar networks in different brain states. In principle, the strong intracortical connections within and between layers could underlie a vigorous transmission of cortical signals across layers. We directly examined the brain state dependency of signal propagation by optogenetically inducing synchronized On-Off transitions in a given layer while measuring the propagation of induced synchrony to adjacent layers during wakefulness ($n=18$ sessions in two fixating monkeys, Figure 3.16A). This was done by injecting lentivirus with an α -CAMKII promoter to express *ChR2* in V1 glutamatergic neurons¹⁰⁹, and then optically stimulating neurons while performing concurrent laminar recordings (stimulation and no stimulation trials were randomly interleaved). Using this procedure, neural populations in the granular layers were transiently activated using 10-ms light pulses presented at 20 or 35

Hz for 300 ms while electrical activity was recorded from all layers simultaneously (Figure 3.16A and 3.16B). We found both direct and indirect activation of neurons by light, indicating that optogenetic stimulation did spread across cells in the stimulated layer¹¹⁰ (Figure 3.19).

Given the strong recurrent connectivity between layers, we expected that the induced On-Off state transitions would propagate across the entire cortical column. Surprisingly, however, the light-induced population synchrony remained mostly local. Indeed, laser stimulation increased the firing rates of granular layer neurons significantly beyond control level to induce On-Off synchronized transitions (Figures 3.16B and 3.17, Wilcoxon rank sum test, $P < 0.0001$) reminiscent of the synchronized state during rest. In contrast, the neurons in adjacent layers had a significantly lower increase in firing rate (Figure 3.17, Wilcoxon rank sum test, SG: $P < 0.001$; G: $P < 0.0001$; IG: $P < 0.05$) while synchronous On-Off state transitions were absent (Figures 3.16C, 3.18A and 3.18B). These results were confirmed by the HMM predictions (Figures 3.16B and 3.16C, Chi-squared test, $P < 0.001$) that the synchronized state transitions induced in the granular layer spread only poorly to adjacent supragranular and infragranular layers (Figures 3.18A and 3.18B, Chi-squared test, $P < 0.001$). The weak spread of light-induced population spiking activity was observed regardless of which layer was optogenetically stimulated (Figure 3.20).

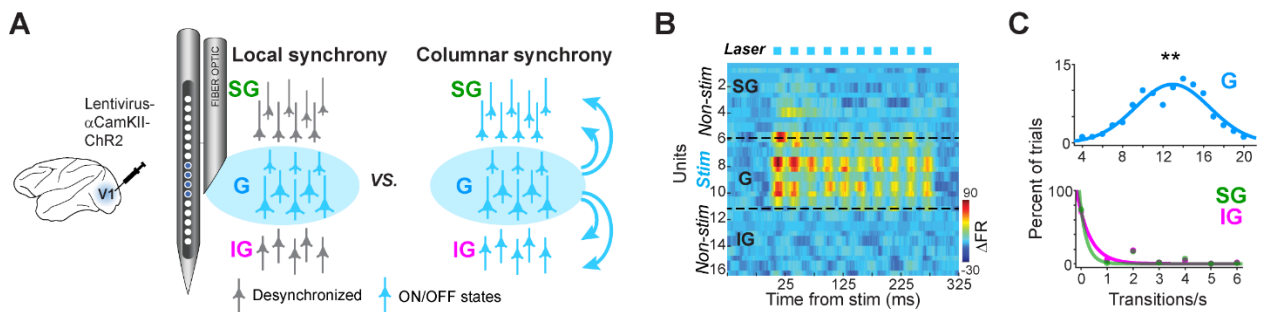


Figure 3.16. Optogenetically induced On-Off states remain local during wakefulness. (A) Schematic of two scenarios: (left) induced synchrony remains local at the light stimulation site,

and (right) induced synchrony spreads across the entire column. Area V1 was injected with Channelrhodopsin receptor 2 (ChR2) such as to optogenetically induce synchronous On-Off states. (B) Difference in firing rates (Δ FR) between ‘light stimulation’ and ‘control’ trials across all single units in an example session. Laser stimulation was performed at 35 Hz using 10-ms pulses for 300 ms (top). Optogenetically induced On (high FR) and Off (low FR) states in granular layer. (C) Histogram of transition rate between On and Off states for the example session in (B). Transition rate in the stimulated granular layer (blue) compared to non-stimulated supragranular (green) and infragranular (magenta) layers (G vs. SG, $**P < 0.001$; G vs. IG, $**P < 0.001$, Chi squared test, $n=1$ session).

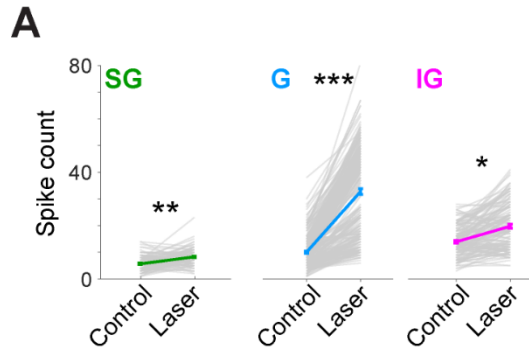


Figure 3.17. (A) Spike counts across sessions in laser trials compared to control trials for each layer, gray lines represent trials; solid bars represent mean spike counts. Error bars represent s.e.m. (G laser vs. G control, $***P < 0.0001$; SG laser vs. SG control, $**P < 0.001$; IG laser vs. IG control, $*P < 0.05$, Wilcoxon rank sum test, $n=5$ sessions).

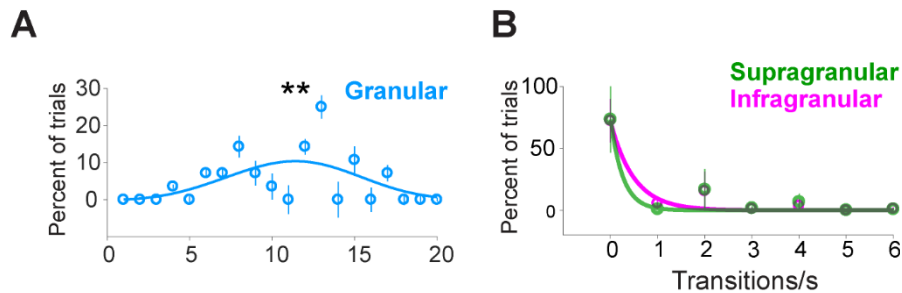


Figure 3.18 (A and B) Histogram of rate of transitions between On and Off states across all sessions. Transition rate in G (stimulated, blue) compared to SG (non-stimulated, green) and IG (non-stimulated, magenta) for all sessions (G vs. SG, $**P < 0.001$; G vs. IG, $**P < 0.001$, Chi squared test, $n=5$ sessions). Error bars represent s.e.m.

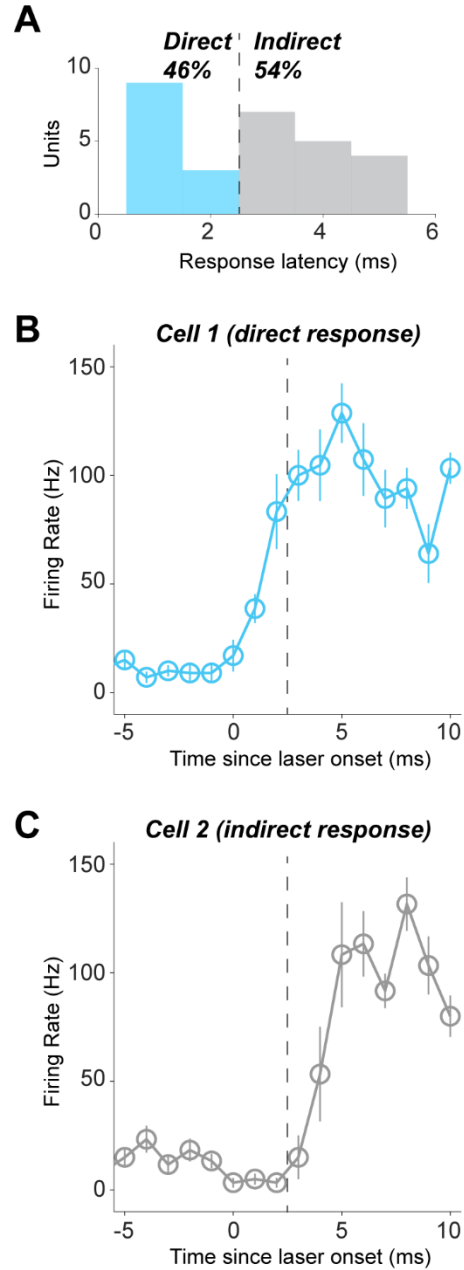


Figure 3.19. Optogenetic stimulation yields direct and indirect activation of neurons. (A) Example session – the histogram represents the number of neurons and their light-induced activation latency calculated as the time since laser onset when the firing rate in a given trial exceeded 50% of the peak response in that trial ($n=28$ units over 6 sessions). Direct responses typically occurred within 2 ms of laser onset (dashed line). Greater latencies were considered indirect¹¹⁰. Mean firing rates of two example neurons showing direct (B) and indirect (C)

responses to laser onset. Firing rates were calculated by averaging responses to laser onset across all trials. Error bars show s.e.m.

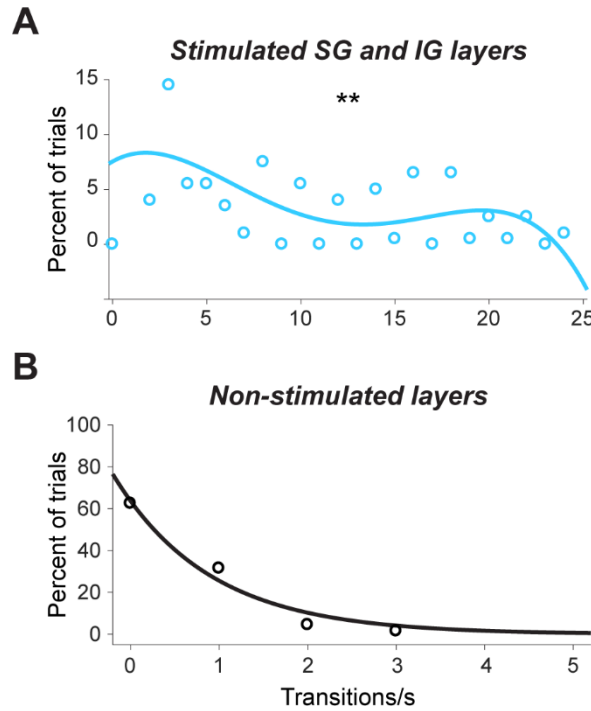


Figure 3.20. Optogenetically induced On and Off state transitions do not propagate across layers in V1. (A) Histograms representing the transition rates between the On and Off states in optogenetically stimulated supragranular (SG) and infragranular (IG) layers across trials. (B) Same as A, but in non-stimulated layers (transitions/s in stimulated layers vs. transitions/s in non-stimulated layers, $**P < 0.001$, Chi squared test, $n=2$ sessions).

Brain state modulates propagation of optogenetically induced neural signals

To further examine whether the propagation of cortical signals depends on global brain state, we optogenetically activated a subset of neurons in the 1-35 Hz frequency range while animals were resting or awake (Figure 3.21). The optogenetic stimulation duration, frequency, and number of stimulation trials were identical across behavioral state conditions of wakefulness and rest. Additionally, animals were in the same experimental setup in a dark room, and in both conditions, the monitor had a dark background and there was no visual stimulus in either condition. Furthermore, neurons' firing rates were not significantly different

between passive fixation and task conditions ($P > 0.05$, Chi-squared test). Thus, experimental conditions during wakefulness and rest were identical: dark room, dark monitor, and no visual stimulation. These identical experimental conditions enabled us to evaluate the effect of laser stimulation during wakefulness (passive fixation) and rest.

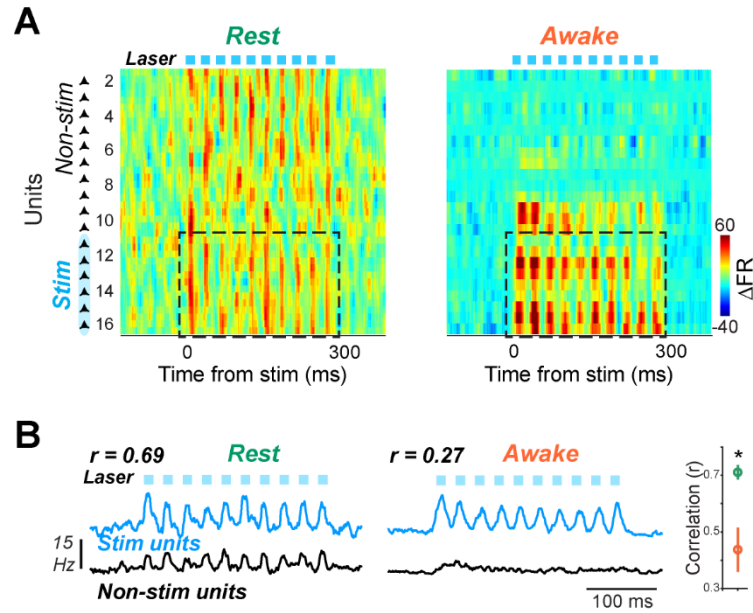


Figure 3.21. State-dependent propagation of cortical spiking activity. (A) Heat maps represent the difference in firing rates (ΔFR) between stimulated and control trials across all units in rest (20-min) and awake (40-min) recording sessions. Optogenetically induced On (high FR) and Off (low FR) states in units are indicated by dashed box. (B) Mean population firing rates represented for optogenetically stimulated and non-stimulated units in example sessions shown in (A). Pearson's correlation coefficient (r) computed between mean firing rates of stimulated and non-stimulated units (right, awake vs. rest, $P < 0.001$, Wilcoxon rank sum test, $n = 12$ sessions). Bars represent s.e.m.

As expected, at the site of optogenetic stimulation, the population of neurons increased their firing rates in both brain states to elicit On and Off transitions (Figure 3.22, left; firing rates of all units were statistically indistinguishable in non-laser (control) trials, data not shown, $P > 0.05$, Wilcoxon rank sum test). Remarkably, while synchronized spiking activity remained

relatively local during wakefulness, it spread vigorously during rest (Figures 3.21A and 3.21B). Indeed, while the increase in population responses significantly decayed as a function of the distance from the border of stimulated sites during wakefulness, elevated firing remained remarkably robust across layers during rest (Figure 3.22, right). This effect was observed irrespective of the frequency of optogenetic stimulation (Figure 3.23; stimulation frequency was held constant throughout a session). Furthermore, the correlation between the mean population response of optogenetically-stimulated and non-stimulated cells was significantly higher in rest compared to wakefulness (Figure 3.21B, inset, Wilcoxon rank sum test, $P < 0.001$). Accordingly, the On-Off transition rates were significantly increased for the optogenetically stimulated units compared to non-stimulated units in both wakefulness and rest (Figure 3.24A, left, $P < 0.001$, Chi-squared test). However, while the induced synchrony remained local to stimulated units during wakefulness, it spread to non-stimulated sites during rest (Figure 3.24A, left, $P < 0.001$, Chi-squared test; firing rates of simulated vs. non-stimulated units were statistically indistinguishable in awake and rest in non-laser (control) trials, data not shown, $P > 0.05$, Wilcoxon rank sum test). To ensure that the propagated optogenetically-induced synchrony is not due to naturally occurring synchronous activity during rest, we separately analyzed the trials in which the population of neurons was desynchronized for at least 1000 ms before light stimulation (i.e., zero On-Off transition rate pre-stimulation, Figure 3.24A, right). However, this did not alter the propagation of cortical signals – even in these conditions, the spread of light-induced population synchrony to non-stimulated units during rest was robust across the entire cortical column, whereas the extent of signal propagation was greatly reduced during wakefulness (Figure 3.24, Chi-squared test, $P < 0.001$).

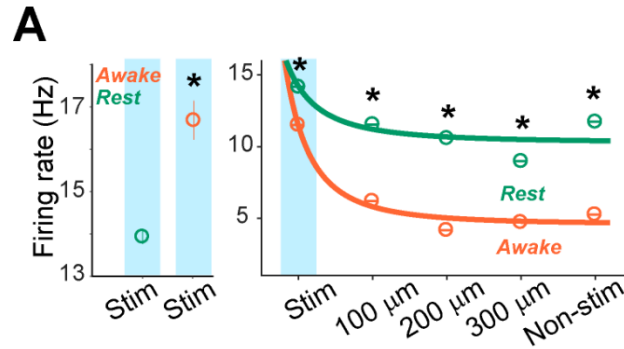


Figure 3.22. (A) Mean firing rates of stimulated units during wakefulness and rest in laser trials (left, awake vs. rest, $*P < 0.001$, Wilcoxon rank sum test, $n=12$ sessions). Bars represent s.e.m. (A, right) Mean firing rates of individual units, plotted as a function of distance from stimulated units, in rest compared to wakefulness (right, awake vs. rest, $*P < 0.001$, Wilcoxon rank sum test, $n=12$ sessions). Bars represent s.e.m.

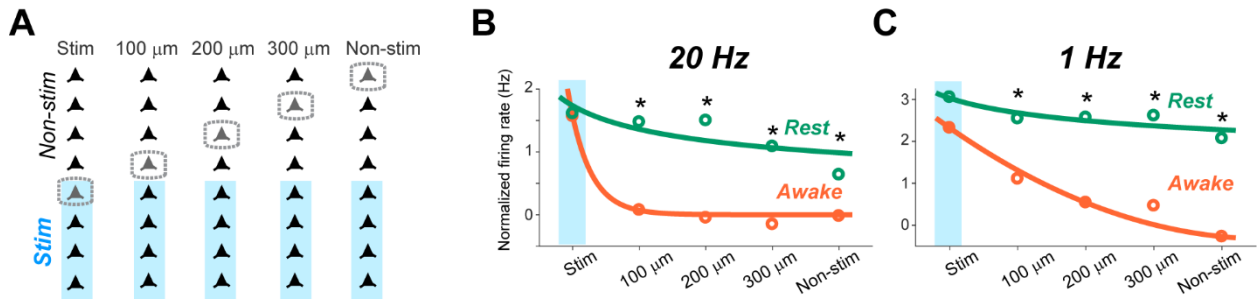


Figure 3.23. Propagation of cortical activity during rest and wakefulness does not depend on laser stimulation frequency. (A) Schematic representation of the subset of units analyzed (gray box) with a sliding window and step size of 1 unit (100 μm) progressively moving away from the stimulated units (blue highlight, 'stim'). (B) Mean firing rates of individual units as a function of distance from the stimulated units in the rest (green) and awake (orange) conditions. Laser stimulation is at 20 Hz (rest vs. awake, $*P < 0.05$, Wilcoxon rank sum test, $n=2$ sessions). Error bars represent s.e.m. (C) Same convention as B but for 1 Hz laser stimulation (rest vs. awake, $*P < 0.05$, Wilcoxon rank sum test, $n=2$ sessions). Error bars represent s.e.m.

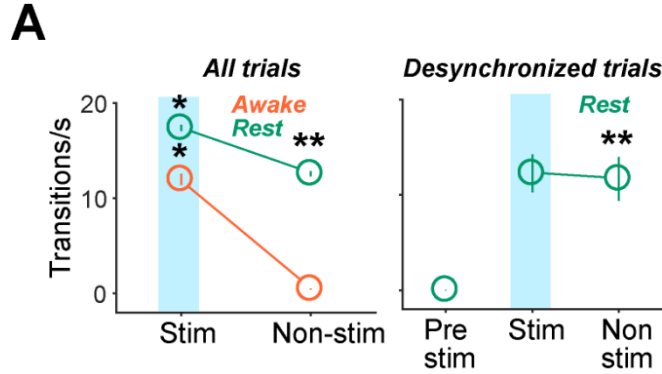


Figure 3.24. (A) Mean transition rate plotted as dots with standard error for stimulated and non-stimulated units (left) during wakefulness and rest (awake vs. rest, $*P < 0.05$, Chi-squared test, $n=12$ sessions). Transition rate in non-stimulated units in rest compared to wakefulness (awake stim vs. awake non-stim, $**P < 0.001$, Chi-squared test, $n=5$ sessions; rest stim vs. rest non-stim, $**P < 0.001$, Chi-squared test, $n=7$ sessions). Mean transition rate plotted as dots with standard error in all units pre-stimulation, in stimulated and non-stimulated units in rest (right; rest pre-stim vs. rest non-stim in synchronized and desynchronized pre-stim conditions, $**P < 0.001$, Chi-squared test, $n=7$ sessions).

Although light-induced synchrony remained mostly local during wakefulness, we found a statistically significant influence of arousal on the extent of signal propagation. That is, we quantified the rate of On-Off state transitions by applying the HMM to subnetworks of fixed size (4 neurons) starting with the stimulated sites and gradually shifting every 100 μm towards the non-stimulated sites (Figure 3.25A). In states of low arousal (small pupil), there was a higher spread of synchrony, i.e., higher rate of transitions between On and Off states, whereas in the high arousal state (large pupil), synchrony was strictly limited to the stimulated sites (Figure 3.25B, Wilcoxon rank sum test, $P < 0.01$). This indicates that, contrary to expectation, alertness limits the extent of signal propagation across laminar cortical populations.

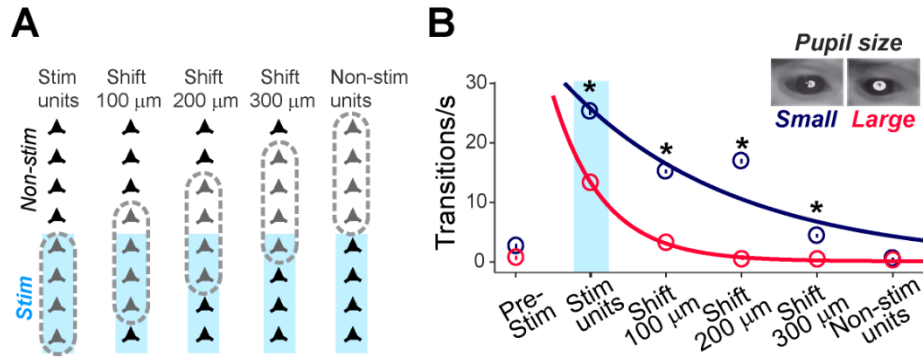


Figure 3.25. (A) Schematic representation of the subset population of units analyzed (gray) with a sliding window of four units with step size of one unit (100 μm) moving away from stimulated units (blue highlight). (B) Mean transition rate plotted as dots with standard error for subset of units analyzed as described in (A). Transition rates plotted for wakefulness trials with larger than average pupil size (red) and smaller than average pupil size (blue) (small pupil vs. large pupil, * $P < 0.01$, Wilcoxon rank sum test, $n=6$ sessions).

Population coupling explains the brain state dependency of signal propagation

What mechanism could underlie the influence of global brain state on the degree of propagation of spiking activity across laminar networks? Since the spread of neural signals was limited during wakefulness but less restricted during rest, we reasoned that the strength of functional connectivity across columnar neurons may exhibit state dependency. We thus computed the strength of coupling between individual neurons and their local population, and hypothesized that coupling would be weak during wakefulness, but strong during rest. Notably, population coupling is a correlate of synaptic connectivity, i.e., the population coupling of a neuron provides an estimate of the number of synapses received by a neuron from its neighbors⁸³. Furthermore, population coupling has been found to be relatively independent of neurons' stimulus preference, such that it reflects a causal relationship that predicts neuronal responses to optogenetically driven increases in local population activity⁸³.

To quantify population coupling, we computed the spike-triggered population rates by correlating the spike train of each neuron with the summed activity of the neural population

(excluding the neuron being examined, Figure 3.26A). Population coupling was remarkably higher in rest compared to wakefulness (Figure 3.26B, left, Wilcoxon rank sum test, $P < 0.01$), and the degree of state modulation was more pronounced during laser stimulation (Figure 3.26B, right, Wilcoxon rank sum test, $P < 0.001$). Thus, increased coupling between individual neurons and their local population may allow a greater spread of synchronous activity during rest, whereas weaker coupling during wakefulness would limit signal propagation (Figure 3.21). This indicates that population coupling changes as a function of brain state, such that the input connection strength dynamically shifts between wakefulness and rest – an underlying mechanism explaining how brain state modulates signal propagation in laminar circuits.

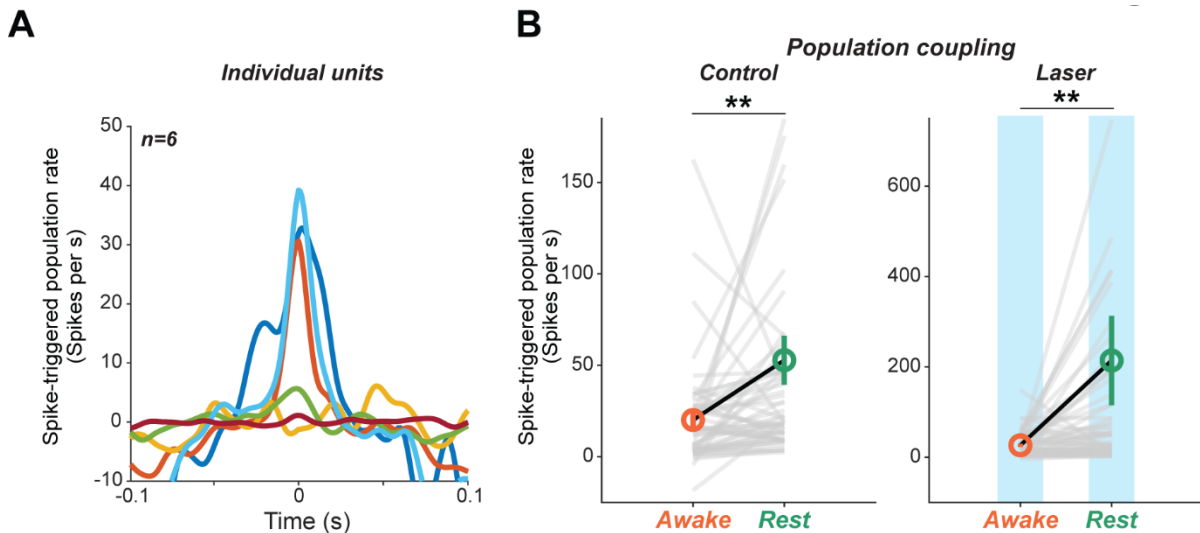


Figure 3.26. State-dependent changes in population coupling. (A) Spike-triggered population rate for six example neurons. (B) Spike-triggered population rate across sessions in wakefulness compared to rest for control and laser conditions; gray lines represent individual units, and circles represent the means. Error bars represent s.e.m. (control awake vs. rest, $**P < 0.001$, laser awake vs. rest, $**P < 0.001$, Wilcoxon rank sum test, $n = 12$ sessions).

3.3 Discussion

The prevailing view of neural dynamics within the cortical microcolumn is that endogenous patterns of spiking activity robustly propagate across layers in a recurrent manner. Using a novel combination of multi-electrode laminar recordings and optogenetics in different brain states, we found that visual cortical layers act as independent functional units during wakefulness. The spiking responses of single neurons are desynchronized within and across layers. In contrast, columnar circuits switch to a synchronized mode during rest. For the first time, we revealed that the propagation of electrical signals is strongly influenced by global brain state. Following optogenetic induction of synchronized activity in a subset of neurons, we found a significantly larger spread of neural signals during rest compared to wakefulness. Furthermore, a global variable controlling the awake state, arousal, was inversely correlated with the spread of neuronal signals. The almost total lack of synchronized fluctuations across layers during wakefulness, when On-Off state transitions were optogenetically induced in one layer, is surprising given the presence of strong inter-layer connections mediating information transfer^{28,60,82}. This suggests a remarkable degree of independence of individual layers, which may act as independent functional units during sensory processing⁹¹.

Mechanistically, our results may be explained by the state-dependent coupling between individual neurons and local population activity. Indeed, we found that neurons are more coupled to their neighbors during rest compared to wakefulness, and that population coupling modulates signal propagation. An additional mechanism could be the state-dependent modulation of the balance between local excitation and inhibition^{84,111}. Previous studies have proposed that the excitation-inhibition (E/I) ratio impacts fluctuations in local populations, including low-frequency synchrony and correlations^{91,93,112}. Furthermore, experiments in

rodents have revealed that sleep regulates cortical E/I balance, with inhibitory interneurons responding only weakly during slow-wave sleep and maximally during REM sleep and wakefulness^{104,113,114}. Indeed, we confirmed in our data set that the E/I ratio (based on functionally defined cell types) is significantly higher in rest compared to wakefulness (Figure 3.27). This raises the possibility that a decrease in E/I ratio from rest to wakefulness along with a decrease in population coupling contribute to restricting the propagation of cortical population activity^{115–117}.

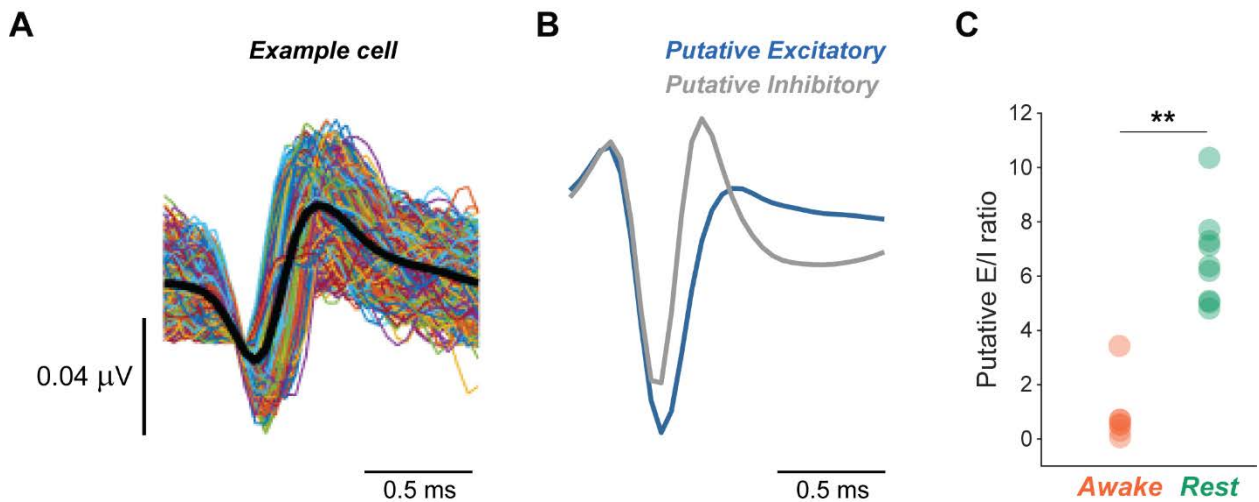


Figure 3.27. Putative excitatory/inhibitory (E/I) ratio is higher in rest. (A) All waveform traces for an example single unit. Black line represents the mean waveform extracted. (B) Mean waveform shape of putative excitatory (blue) and inhibitory (grey) single units across all sessions (177 excitatory cells, 31 inhibitory cells across 13 sessions in wakefulness and 10 sessions in rest). (C) Mean putative E/I ratio per session derived from mean firing rates in excitatory and inhibitory units (rest vs. awake, $**P < 0.001$, Wilcoxon rank sum test, $n=23$ sessions).

What could be the functional significance of the state-dependent propagation of neural signals revealed here? The optimal network state during wakefulness is the desynchronized mode. Indeed, desynchronized cortical activity has been shown to be important for sensory coding and perception^{44,51,91}, i.e., when cells are desynchronized, populations of neurons

encode more information to increase perceptual accuracy. However, the dynamics of neuronal activity across cortical layers and how electrical signals propagate along the cortical column in different brain states has remained unknown. We uncovered a remarkably strong decoupling between layers during wakefulness, which could act as an efficient ‘filtering’ mechanism by only allowing strong stimuli to propagate across cortical layers and influence perception while blocking the propagation of electrical signals elicited by weak stimuli. Indeed, since the generation of action potentials is metabolically expensive, the brain must prevent weak, irrelevant stimuli from eliciting spiking activity in target neurons⁶⁹.

In contrast, rest is associated with significantly stronger coupling of individual neurons to local population activity that contribute to synchronizing laminar networks such as to enhance signal propagation. This is desirable in order to ensure the maintenance of endogenously generated Up and Down states which, although ubiquitously observed during slow-wave sleep, remain poorly understood. Our results reveal a dynamic shift in population coupling from wakefulness to rest, which may be a mechanism by which cortical networks undergo synchronicity, a fundamental phenomenon required for brain’s daily maintenance, e.g., upscaling/downscaling synaptic connections and eliminating metabolic waste¹⁰⁷. Specifically, cells are more coupled during rest (higher population coupling), and hence light-evoked action potentials have a higher probability of being transmitted across layers. In contrast, cells are significantly less coupled during wakefulness, and this reduces the transmission probability of light-evoked action potentials across layers. In addition, we show that this shift occurs across a continuum of brain states – when the animal goes from high arousal to low arousal (drowsiness) to rest.

Our findings provide insight into the brain state-dependent propagation of neural signals across columnar circuits and its functional significance. Revealing the neural network underpinnings of how and why brain switches from asynchronous to synchronous state may pave the way for new approaches on investigating the aberrant synchrony observed in a myriad of neuropsychiatric disorders such as epilepsy, Alzheimer's, schizophrenia, and autism^{118,119}. Given the similarities of columnar microcircuitry associated with different sensory modalities^{25,30,89,120} the brain state control of dynamics and spread of cortical spiking activity revealed here could constitute a general principle of signal propagation across sensory cortical populations.

Chapter 4: Synchrony in NREM sleep desynchronizes cortical circuits and improves behavior

Note: This chapter is based upon: Kharas N, Eagleman S, Chelaru MI, Beaman C, and Dragoi V. Naps improve behavioral performance by desynchronizing cortical circuits. This manuscript is in preparation for submission.

4.0 Abstract

Naps consist of short non-rapid eye movement (NREM) sleep. Although naps have been shown to enhance cognitive performance for over a century, the underlying neural basis for this improvement remains undiscovered. Here, we used non-human primates to record the changes in single neurons, neuronal populations, and local field potentials in V4 that occur before, during, and after NREM sleep. To test the cognitive effects of naps, monkeys performed an orientation discrimination before and after taking a nap. We found that high levels of synchrony during NREM sleep drive the brain to be further asynchronous after sleep compared to before sleep. Thus, synchrony in NREM sleep improved behavior by modulating population level dynamics, which we confirmed by performing local microstimulation to induce synchrony in V4 of awake animals. We uncover the neuronal coding changes in single neurons and in neural ensembles that lead to sleep dependent improvement in cognitive performance. Overall, these findings expand our understanding of the functional significance of synchrony, the neurobiology of sleep, and the neuronal coding driving perception.

4.1 Introduction

Sleep is a universal behavior shared by all animals¹²¹. The depth and complexity of sleep varies across species¹²¹. In humans, sleep is vital for optimal cognitive function. Sleep has been shown to have beneficial effects on cognitive and behavioral performance in a variety of tasks across modalities, including the visual system^{16,122,123}. A century ago, Jenkins and Dallenbach¹²⁴ first showed that sleep improved behavioral performance and yet we still do not fully understand how. The major limitation in our understanding of the function of rest has been the lack of an adequate animal model to study how sleep influences brain networks in real time. Research on the benefits of sleep has been exclusively dominated by invasive neurophysiological investigations in small mammals^{125–127} (e.g., rodents) and non-invasive (fMRI, EEG) investigations in humans^{128,129}. However, the behavioral repertoire of small mammals is relatively limited, and they are primarily nocturnal with polyphasic, fragmented daytime sleep patterns^{121,130}. Additionally, it is currently difficult to perform highly invasive neurophysiological experimentation in humans to understand the mechanistic function of sleep at the single cell or network level. To overcome these limitations, we studied the function of sleep in nonhuman primates, as they offer several key evolutionary advantages, such as a sleep cycle that is very similar to that of humans^{131,132}, and the ability to easily learn complex tasks^{133,134}.

In humans and nonhuman primates, there are four stages of sleep: stage 1, stage 2, stage 3, and REM categorized based on polysomnography (PSG) recordings⁸¹. The early stages 1-3 are grouped as NREM sleep^{71,81}. REM is a late stage of sleep characterized by desynchronized neural activity^{16,66}. Whereas in NREM sleep, neuronal synchrony (robust fluctuations in population firing rates) generates oscillations at frequencies between 0.5 and 4 Hz (delta

waves) recorded in PSG^{135–139}. The amplitude of delta oscillations increases as an animal enters NREM sleep and diminishes as an animal wakes up, suggesting a crucial role for delta in NREM sleep^{140,141}.

There has been a debate on the influence of REM and NREM sleep in memory consolidation and cognitive function. A seminal study in the early 90's by Karni and colleagues¹⁴² showed that REM is required for consolidation, but since then, several other studies have shown that NREM sleep and brief periods of sleep can lead to cognitive improvements^{66,143–147}. Studies in humans have shown that a nap as short as 6 minutes leads to improved cognitive performance¹⁴⁸, and in rodents, short periods of rest alter plasticity in the hippocampus^{71,146,149}. Despite the clear importance of naps, the neural underpinnings of nap-dependent changes in the sensory cortex remain unknown.

Among all sensory cortical areas, the visual cortex is the best understood in terms of receptive field properties and circuitry (sections 1.1. and 1.2)². Thus, visual cortices provide a unique opportunity for investigating the impact of sleep on neural network coding and perceptual performance. Among the visual cortices, the mid-level visual cortex (V4) shows the strongest changes with modulations in brain state such as attention^{14,85,150}. V4 is also hierarchically closer to decision-making areas^{2,5,8}, and lesion studies have suggested that V4 plays a key role in perceptual learning¹⁵¹, making it an ideal brain area to examine how sleep influences perception^{2,4,152}. We hypothesized that perceptual improvement after sleep is associated with specific improvements in the coding of visual information within neuronal circuits in V4.

To test our hypothesis, we examined whether NREM sleep (short 20-min naps) influenced visual perceptual performance and the coding of information across visual cortical

populations. We performed multiple-electrode recordings of single-unit activity and local field potentials (LFPs) in V4 of macaques, while the animals performed a visual discrimination task before and after taking a nap. To record sleep stages, we devised a custom nonhuman primate PSG set-up⁸¹. We examined the mechanistic relationship between sleep and behavior by testing whether or not synchrony during sleep influences synchrony in neuronal populations after sleep. After sleep, we found that neuronal populations were desynchronized to lower levels than before sleep. We postulated that high levels of delta and neuronal synchrony during sleep played a key role in desynchronizing the network after sleep and tested this theory by using electrical microstimulation to induce delta (4 Hz) oscillations in V4 of an awake animal. Local induction of synchrony in V4 replicated the changes in neuronal coding and behavior observed after sleep. Thus, we concluded that synchrony in NREM sleep desynchronizes the brain after sleep, leading to an improvement in cognitive performance.

4.2 Results

We examined the spiking activity of 2080 units using multi-contact laminar arrays and surface arrays in V4 as monkeys performed a visual discrimination task before and after taking a nap (Figures 4.1A and 4.1B; $n = 4$ animals across 47 sessions). Naps were defined using PSG and videography analyses as epochs when monkeys were in sustained non-rapid eye movement (NREM) sleep (Figure 4.2)⁸¹. We used an automated sleep recognition software to define epochs of NREM sleep using all components of PSG including electroencephalography (EEG) to measure electrical activity noninvasively through the scalp, electrooculography (EOG) to measure eye closure, and electromyography (EMG) to measure the slacking of the jaw (Figure 4.4A)⁸¹. Given the novelty of the application of PSG in nonhuman primates, we had expert neurologists verify sleep stages manually (Figure 4.2 and 4.3). We additionally verified sleep

and no sleep sessions by training a deep neural network software⁸⁰ (DeepLabCut) on videos of the faces of monkeys to extract whether a monkey's eyes were open or closed and whether the jaw was slacked (Figure 4.5). We controlled the lights in the room, the monitor darkness, and personnel such that the experimental set-up was identical in the sleep and control (no sleep) conditions.

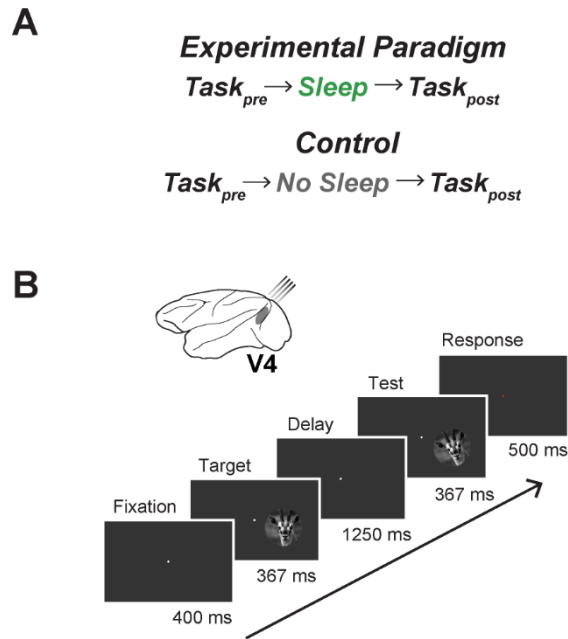


Figure 4.1. (A) Schematic representation of experimental paradigm in sleep and no sleep (control) conditions. (B) Schematic representation of the recording site in V4 and delayed match-to-sample orientation discrimination task. Animals were trained to report whether two briefly flashed successive natural images, target and test, were rotated or no rotated.

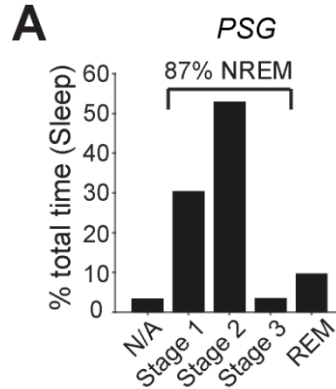


Figure 4.2. (A) Histogram of sleep stages classified into sleep stages based on PSG analysis (n = 47 sessions; see also figures 4.3 and 4.4.). NREM sleep stage breakdown was as follows: stage 1 (61%), stage 2 (35%), and stage 3 (4%).

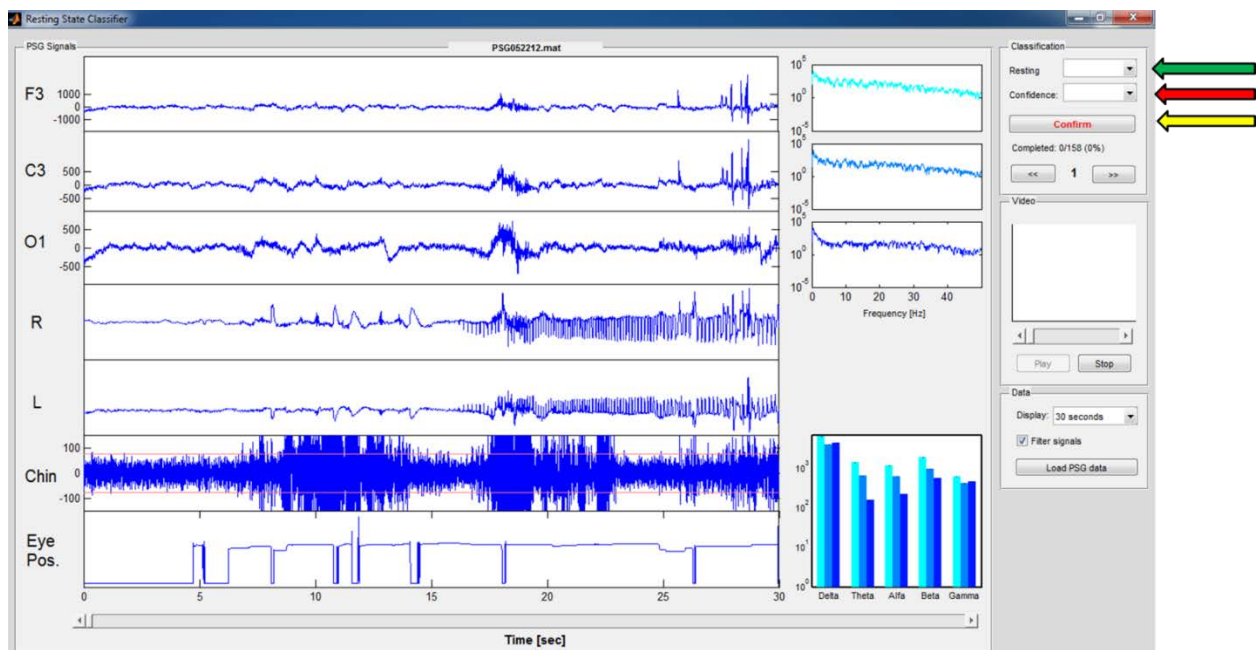


Figure 4.3. PSG software used by expert neurologist technicians to stage sleep. Custom designed graphic user interface (GUI) to load polysomnography data recorded in nonhuman primates. Sleep stage can be selected from dropdown menu as indicated by the green arrow. The confidence level in the sleep stage scored can be selected as indicated by the red arrow (range 0 to 10, no confidence to maximum confidence, respectively). Each scored epoch must be confirmed as indicated by the yellow arrow. The software allows the user to choose the amount of time displayed as indicated by black box.

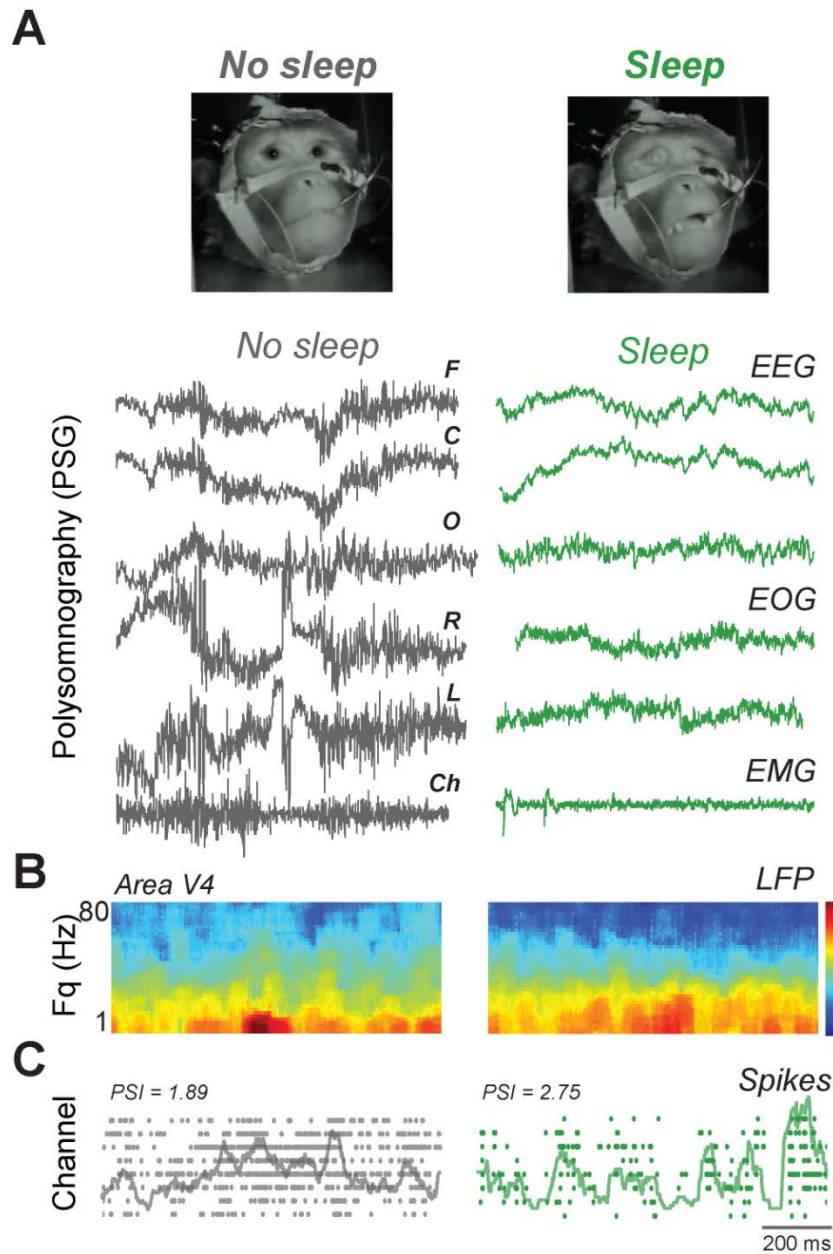


Figure 4.4. Polysomnography (PSG) in nonhuman primates. (A) Example frame from video of monkey in no sleep and sleep sessions (top). Polysomnography consisting of EEG, EOG, and EMG recorded for example time epochs. (B) Time-frequency spectrograms representing changes in local field potential (LFP) power (arbitrary units) in no sleep and sleep example sessions. (C) Raster plots represent single units recorded across channels for example time epochs in no sleep and sleep sessions. Mean population synchrony index (PSI) computed across neuronal population represented as a trace.

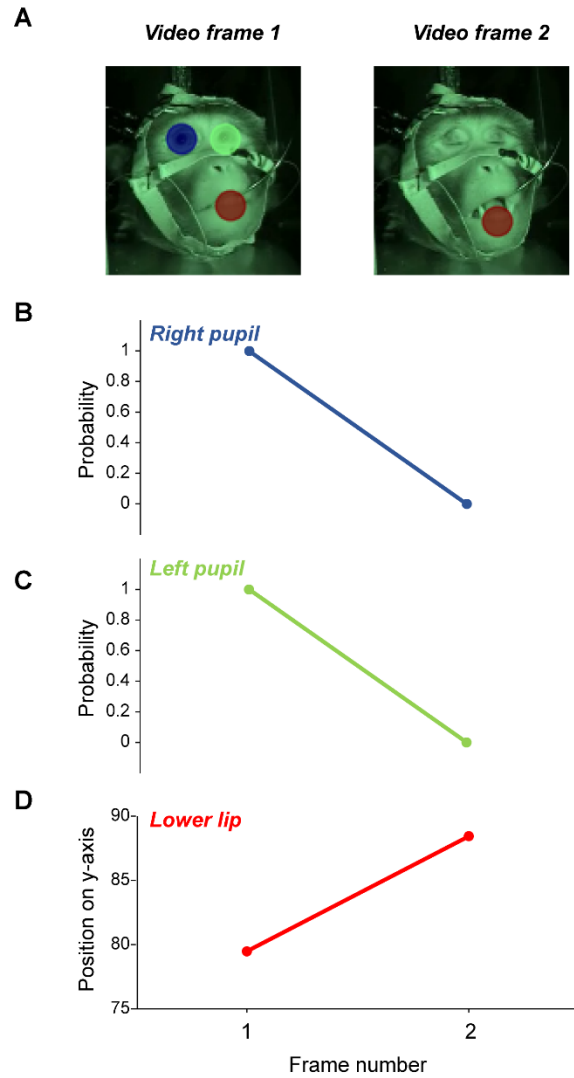


Figure 4.5: Videography analysis using deep neural network-based software (DeepLabCut) identifies eye closure and jaw position. (A) Example video frames where animal is awake (video frame 1) and asleep (video frame 2) labeled with markers for right pupil, left pupil, and lower lip for training the neural network. (B) Likelihood of right pupil being detected in the video frame plotted as dots for video frames 1 and 2. Low probability in frame 2 indicates eye closure. (C) Likelihood of left pupil being detected in the video frame plotted as dots for video frames 1 and 2. Low probability in frame 2 indicates eye closure.

To characterize neuronal and local changes in NREM sleep, we recorded the changes in single neurons, neuronal populations (Figure 4.4C), and local field potentials (Figure 4.4B) before, during, and after naps (Figure 4.1A and 4.4A). Wakefulness was associated with increased power in the high frequency bands (20-80 Hz)⁹² (Figure 4.4B). In contrast, during sleep, LFP analyses revealed increased power in the lower frequency bands (1-20 Hz) and decreased power in higher frequency bands (20-80 Hz)⁹² (Figure 4.4B). As expected^{68,126,140}, among the lower frequencies, delta frequency (0.5-4 Hz) showed the most prominent increase during sleep compared to no sleep (Figure 4.6A, 125.2% increase in delta power in sleep, Chi-squared test, $P < 0.001$). Synchrony, where neural ensembles co-fluctuate in firing, accompanied the increase in delta in NREM sleep (Figure 4.4C). To capture neuronal synchrony, we calculated the population synchrony index (PSI)^{50,51}. As expected^{59,66,67,137}, neuronal populations in sleep were synchronous compared to the no sleep condition (Figure 4.6B, 57.1% increase, Chi-squared test, $P < 0.001$).

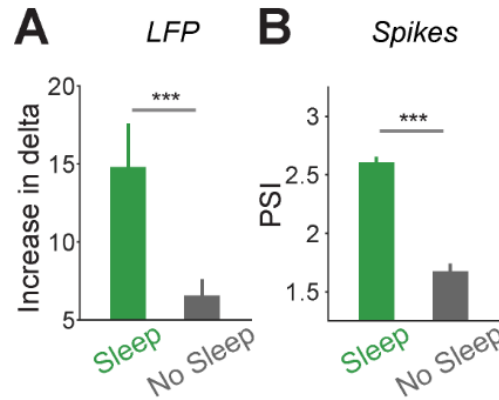


Figure 4.6. (A) Relative increase in delta (0.5-4 Hz) power in sleep vs. no sleep sessions ($P < 0.01$, Chi-squared test, $n = 47$ sessions). Bars represent mean and error bars represent s.e.m. (B) Mean neuronal synchrony (PSI) in sleep vs. no sleep sessions ($P < 0.01$, Chi-squared test, $n = 47$ sessions). Error bars represent s.e.m.

To examine NREM sleep-dependent improvement in behavior, we trained monkeys to report whether two successively flashed natural images were identical (match) or different (non-match) ($n = 47$ sessions, see Methods). In each trial, two identical images flashed for 367 ms, separated by 1250 ms, were either rotated (3° , 5° , 10° , or 20°) or not rotated (0°) (Figure 4.1B). We observed an improvement in behavioral performance in the orientation discrimination task after sleep compared to before sleep (Figure 4.7A and 4.7B; note stable responses throughout a task session). Further, there was significant improvement in discrimination threshold in animals when they napped compared to when they did not nap (no sleep) (Figure 4.7C). NREM sleep improved overall cognitive performance by improving the ability to perceive differences in visual stimuli. Thus, we replicated previous findings by showing sleep dependent improvement in perceptual performance.

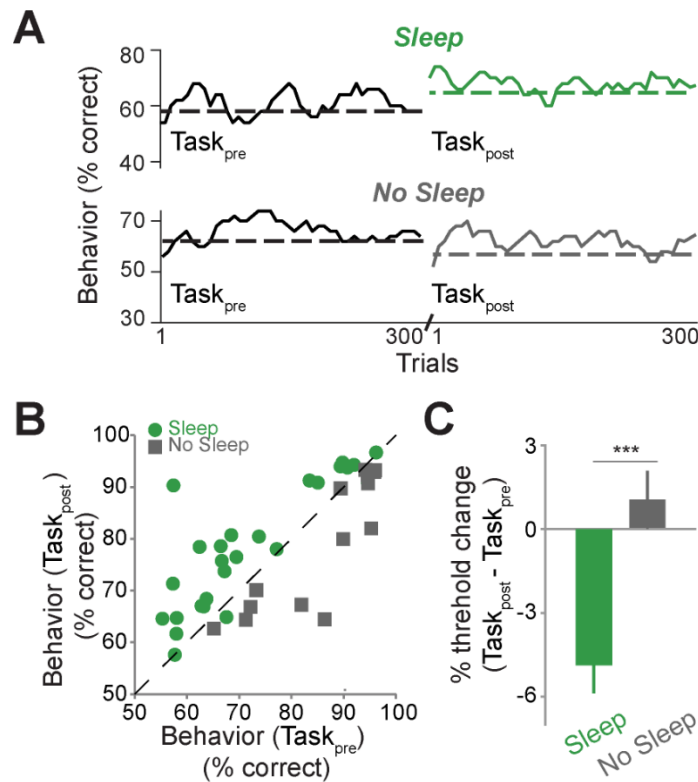


Figure 4.7. Naps (NREM sleep) improve behavioral performance in nonhuman primates. (A) Behavioral performance (% correct responses) per trial in Task_{pre} and Task_{post} periods for example sleep and no sleep sessions. Horizontal dashed line represents the mean behavioral performance across trials for a given task period. (B) Scatter plot of the behavioral performance (% correct responses) in Task_{post} vs. Task_{pre} trials in sleep and no sleep sessions. Each point represents one session (n = 40 sessions: 26 sleep and 14 no sleep). (C) Mean discrimination threshold is significantly lower in sleep sessions compared to no sleep ($P < 0.001$, Chi-squared test, n = 40 sessions: 26 sleep and 14 no sleep). Error bars represent s.e.m.

To investigate the underlying neural basis of the observed sleep dependent improvement in behavioral performance, we analyzed changes in single neurons and neuronal populations before, during, and after NREM sleep. To test sensory information coding in individual neurons, we analyzed firing rates and decoder performance. We examined the changes in firing rates in single and multi-unit activity within the trials only when eye movements were strictly controlled (see methods). We found that after brief naps, firing rates in the task post-sleep were significantly higher compared to before sleep (Figure 4.8A, $P < 0.001$, Wilcoxon rank sum test), whereas there was no difference in firing rates between tasks in the control (no sleep) condition (Figure 4.8B). We used a linear classifier to decode the natural image stimulus identity from single unit activity in tasks before and after sleep. The decoder performance in all task conditions was significantly higher than chance level (25% chance level, $P < 0.001$, Wilcoxon rank sum test). The decoder performance further improved after sleep (Figure 4.9A, $P < 0.001$, Wilcoxon rank sum test). There was no difference in the decoder performance in the control (no sleep) condition (Figure 4.9A, $P > 0.05$, Wilcoxon rank sum test).

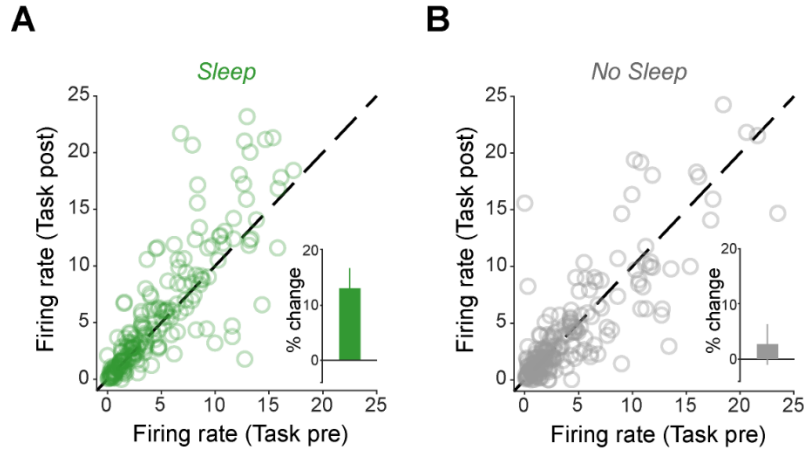


Figure 4.8. NREM sleep dependent changes in individual neurons in V4. (A and B) Scatter plot of neuronal firing rates in Task_{pre} and Task_{post} periods in sleep (A) and no sleep (B) sessions. Each dot represents a single neuron. Inset represents firing rate percent change in Task_{post} vs. Task_{pre} periods across all single units and sessions (n = 197 single units in 26 sleep sessions and n = 201 single units in 14 no sleep sessions; Sleep vs. no sleep, $P < 0.001$, Chi-squared test).

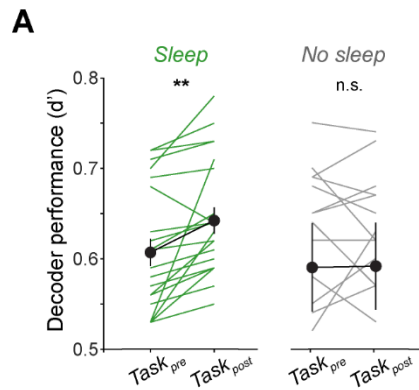


Figure 4.9. (A) Average decoder performance (d') was significantly higher in the Task_{post} period compared to the Task_{pre} period in sleep sessions ($P < 0.01$, Wilcoxon rank sum test, $n = 22$ sessions). Average d' was not significantly different in the task period for the no sleep condition ($P > 0.05$, Wilcoxon rank sum test, $n = 14$ sessions). Average d' was higher than the 25% chance level in all sessions and task periods. Error bars represent s.e.m.

In addition to demonstrating sleep-dependent improvement of sensory information coding in single neurons, we further examined the impact of NREM sleep on population dynamics in neuronal networks by analyzing population synchrony and pairwise correlations between neurons. To capture spontaneous fluctuations in synchrony across the entire neuronal population, we measured the PSI on a trial-by-trial basis in the delay period of the discrimination task (Figure 4.1B; note the lack of visual stimulus in the delay period). PSI levels gauge the readiness of neuronal networks to receive sensory information. We first found that PSI significantly increased during sleep compared to the task period (Figure 4.10A, $P < 0.001$, Wilcoxon rank sum test). Interestingly, we then observed PSI levels in the task after sleep dropped below the PSI levels in the task before sleep (Figure 4.10A). This phenomenon of decreased synchrony after sleep was observed across all sessions (Figure 4.10C, $P < 0.001$, Wilcoxon rank sum test). In the control condition, the synchrony levels were consistent through the tasks and the no sleep period (Figure 4.10B and 4.10C, $P > 0.05$, Wilcoxon rank sum test). Importantly, baseline levels of PSI (task pre) in the sleep and no sleep conditions were not significantly different ($P > 0.05$, Wilcoxon rank sum test, compare task pre in sleep vs no sleep in Figure 4.10C). Lower levels of PSI after sleep indicated that the neural network was optimally ready to receive sensory information after a nap compared to when the monkey did not take a nap. We also tested how robustly the network could encode new sensory information by measuring correlations between pairs of neurons. Studies show that lower levels of correlated variability improve information coding. Indeed, we found lower levels of correlations between neurons after sleep compared to before sleep (Figure 4.11A). Whereas, correlations were unchanged between tasks when the monkey did not sleep (control, Figure 4.11B). When comparing tasks before and after sleep, we found that sleep decreased

correlations across sessions (Figure 4.11C, $P < 0.001$; no change in control/no sleep, $P > 0.05$, Wilcoxon rank sum test). Overall, after naps, we observed a decrease in synchrony and correlations across neuronal populations compared to before naps. As a control, we tested whether changes in underlying brain state could explain the findings after sleep. We found that arousal or attention did not significantly differ in the task periods before and after sleep (Figure 4.12 for arousal and Figure 4.13 for attention). This finding is expected because human and nonhuman primate studies show that large variations in arousal and attention often observed in rodents are rare in large animals.

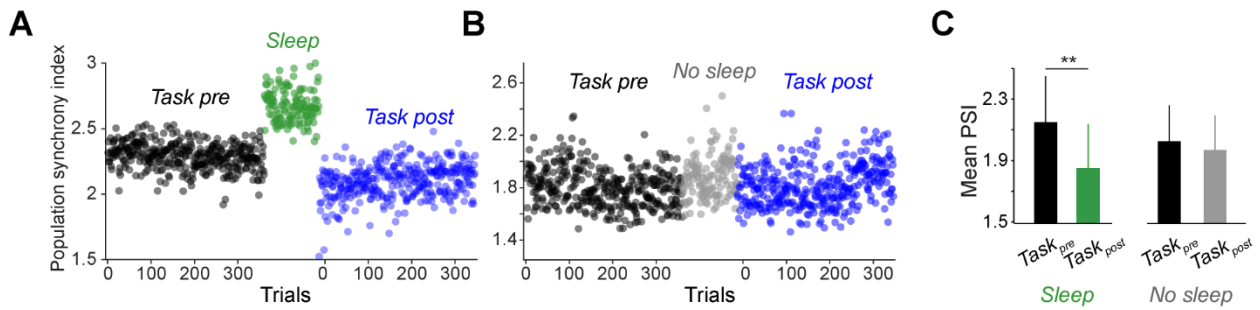


Figure 4.10. (A and B) Population synchrony index (PSI) across neuronal populations represented as dots in task periods in example sleep (A) and no sleep sessions (B). Each dot represents a trial during task periods and each dot represents an epoch of time equivalent to a trial (pseudo-trial) during the sleep or no sleep periods. (C) Mean PSI in Task_{pre} and Task_{post} periods in sleep and no sleep sessions ($P < 0.01$, Wilcoxon rank sum test, $n = 40$ sessions). Error bars represent s.e.m.

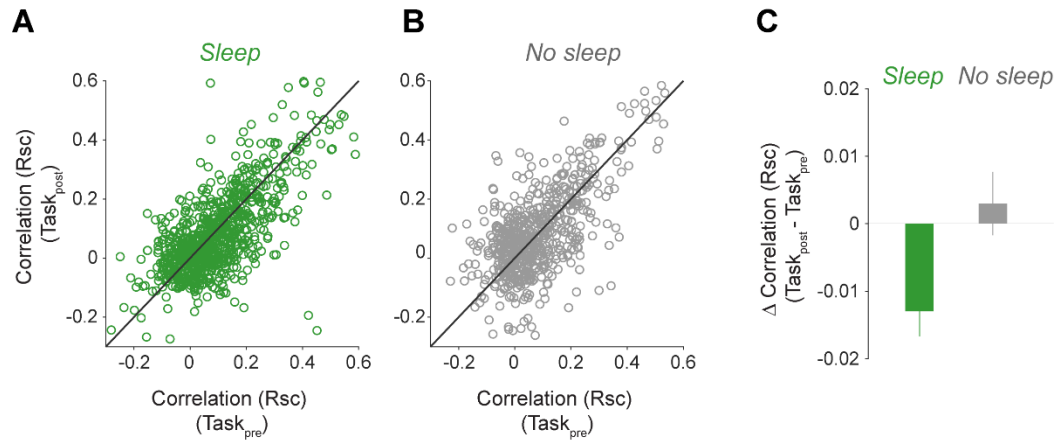


Figure 4.11. (A and B) Scatter plots of the evoked correlation coefficients (Rsc) per trial in Task_{pre} and Task_{post} periods for sleep (A) and no sleep (B) sessions. Each dot represents Rsc for a pair of neurons ($n = 870$ pairs in sleep and $n = 619$ pairs in no sleep sessions). (C) Average change in correlation (Rsc) between pairs of neurons in Task_{post} vs. Task_{pre} periods in sleep and no sleep sessions plotted in panels A and B ($P < 0.01$, Chi-squared test, $n = 1489$ neuron pairs across 40 sessions).

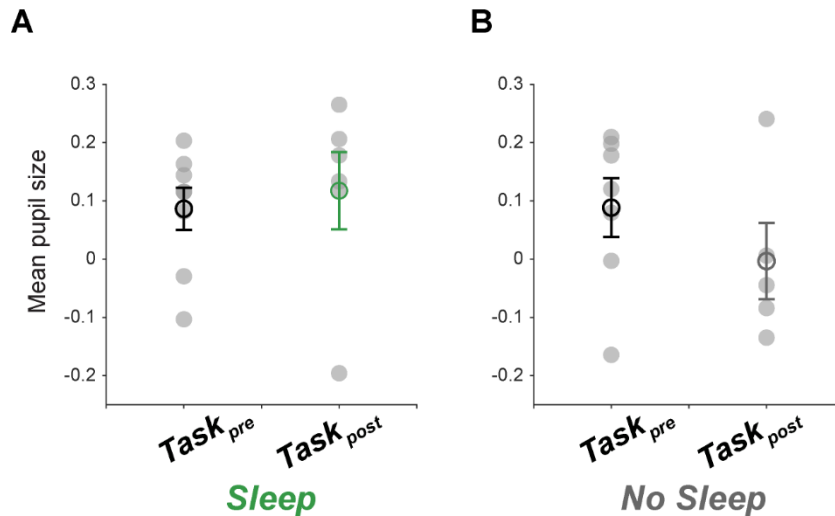


Figure 4.12. Arousal does not significantly differ in sleep and no sleep (control) sessions. Mean pupil size (z-scored) is plotted as dots for Task_{post} and Task_{pre} periods in sleep and no sleep sessions. Each gray dot represents a task period. Black dots represent the mean across sessions and bars represent s.e.m. ($P > 0.05$, Wilcoxon rank sum test, $n = 40$ sessions in 2 monkeys).

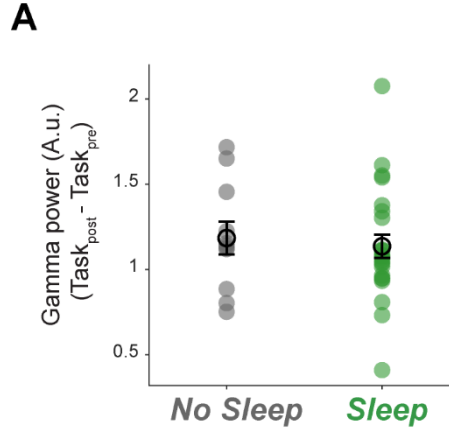


Figure 4.13. Attention does not significantly differ between sleep and no sleep (control) sessions. (A) Mean bandpower in gamma band (30-80 Hz) plotted as dots. Each dot represents a session. Black dots represent the mean across sessions and bars represent s.e.m. ($P > 0.05$, Wilcoxon rank sum test, $n = 40$ sessions in 2 monkeys).

During sleep, we observed that increases in neuronal synchrony positively correlated with the increases in delta power (Figure 4.14A). We further found that the higher the PSI in sleep (between tasks), the lower the PSI dropped after sleep (Figure 4.14B). We were surprised by the paradox that robust synchrony in sleep was followed by lower levels of synchrony after sleep compared to before sleep. Thus, we hypothesized that prominent delta oscillations (Figure 4.6A) and increased neuronal synchrony during naps (Figure 4.6B) robustly decreased synchrony after naps below baseline levels and improved cognitive performance (Figure 4.15A). To test our hypothesis, we repeated the experimental paradigm where the monkey performed the visual discrimination task but instead of the monkey taking a nap between tasks, we electrically stimulated^{153–155} V4 with delta frequency (4 Hz) in an awake animal (Figure 4.15B).

A limitation of performing microstimulation in low frequencies, such as 4 Hz, is that we must use low currents to remain within the safe amount of charge that can be applied to the

brain. Low currents required in low frequency stimulation are not effective in large animals and humans, and thus, most experiments and clinical applications use high frequency stimulation. We overcame this limitation by applying two overlapping high frequency sinusoids (ex. $f_1 = 150$ Hz and $f_2 = 154$ Hz), which allowed us to use high currents. Given the intrinsic low pass filtering of electrical signals by the brain^{1,61}, we theorized that the neurons would perceive the envelope frequency of the two overlapping high frequencies i.e. 4 Hz (Figure 4.15B; $f_2(154 \text{ Hz}) - f_1(150 \text{ Hz}) = 4 \text{ Hz}$, maximum charge of 20 nC/phase). Indeed, there is in-vivo evidence that stimulation with overlapping sinusoids drive neurons at envelope frequencies as efficaciously as direct stimulation with the frequency¹⁵⁶. In this manner, we performed local microstimulation at the 4 Hz delta frequency on 8-contacts of a 96-channel surface array implanted in V4 of an awake animal (Figure 4.15B). We carefully chose contacts to stimulate based on the following criteria: (1) the units shared receptive fields, (2) the units shared stimulus preference, and (3) we could reliably decode visual stimuli from each unit's spiking activity (an indicator that the neuron was involved in visual perception in the behavioral task).

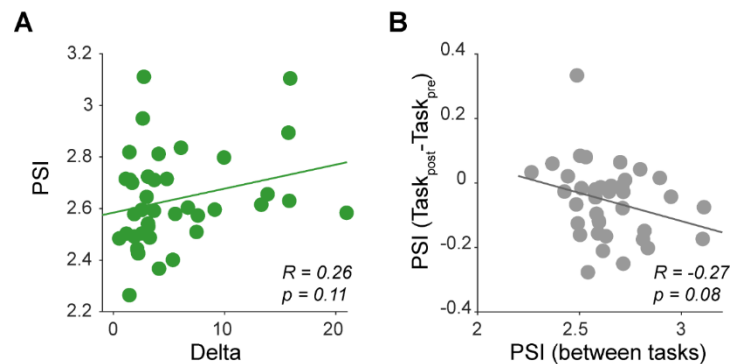


Figure 4.14. Modulations in delta and PSI in tasks and sleep. (A) Scatter plot comparing relative increase in delta power and mean PSI during sleep. (B) Scatter plot comparing relative

changes in mean PSI in task periods compared to mean PSI between task periods. Each dot represents a session (n = 26 sleep sessions and 14 no sleep sessions; Pearson correlation and p values listed on plots).

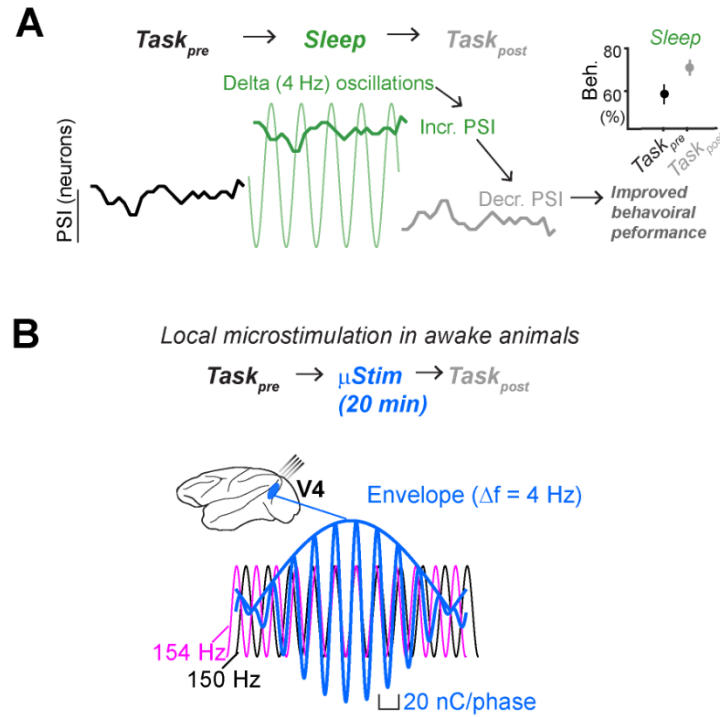


Figure 4.15. Local microstimulation at 4 Hz in V4. (A) Schematic of hypothesis that delta (4 Hz) oscillations during sleep increase neuronal synchrony (PSI), which after sleep leads to a decrease in PSI below baseline levels (PSI in Task_{post} vs. Task_{pre}) and improves behavioral performance. (B) Schematic explaining microstimulation performed in V4 at 4 Hz envelope frequency of superimposed 150 and 154 Hz sinusoids with an amplitude of 0.56 microA current per channel for a maximum charge of 20 nC/phase.

We found that behavioral performance in the visual discrimination task improved after 4 Hz stimulation in V4. We had two control conditions: no stimulation to control for the mere passage of time and one with high frequency (15-40 Hz) stimulation to control for mere sensation and test for selectivity of the stimulation frequency. We verified that the animal was awake using the videography and local field potential analyses described above. In all

conditions and sessions, the experimental room set-up was identical and the conditions were randomly assigned. Behavioral performance improved after the 4 Hz microstimulation but not in the no stimulation or in the high frequency microstimulation conditions (Figure 4.16, $P < 0.001$, Chi-squared test).

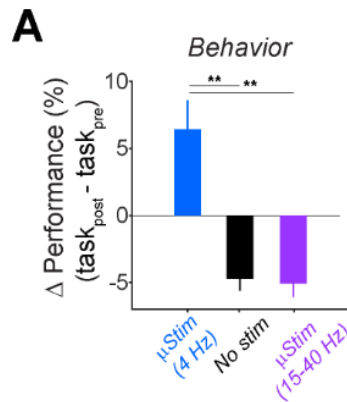


Figure 4.16. (A) Mean change in behavioral performance in 4 Hz microstimulation and control conditions of no stimulation and higher frequency microstimulation. Bars represent s.e.m. ($P < 0.01$, Chi-squared test; $n = 19$ sessions total: 8 microstimulation, 7 high frequency stimulation, and 4 no stimulation sessions).

Local microstimulation with 4 Hz (delta) in V4 also replicated the neuronal coding changes seen after naps – increased firing rate, decreased PSI, and decreased correlations (Figures 4.17B-D). Improvement in behavioral performance accompanied the changes in neuronal coding after naps and delta microstimulation (Figure 4.17A). No significant changes were observed in the control condition (Figures 4.17A-D). The scale of change in neuronal coding and behavior after local delta microstimulation was similar to the nap-driven changes in coding and behavior ($P > 0.05$, Chi-squared test), indicating that the microstimulation successfully mimicked NREM sleep in a local cortical area of an awake animal. The findings that microstimulation in delta (4 Hz) in lieu of a nap decreased synchrony post-stimulation and

improved behavior confirmed our hypothesis that synchrony in NREM sleep drives the brain to be more desynchronized than baseline levels after sleep.

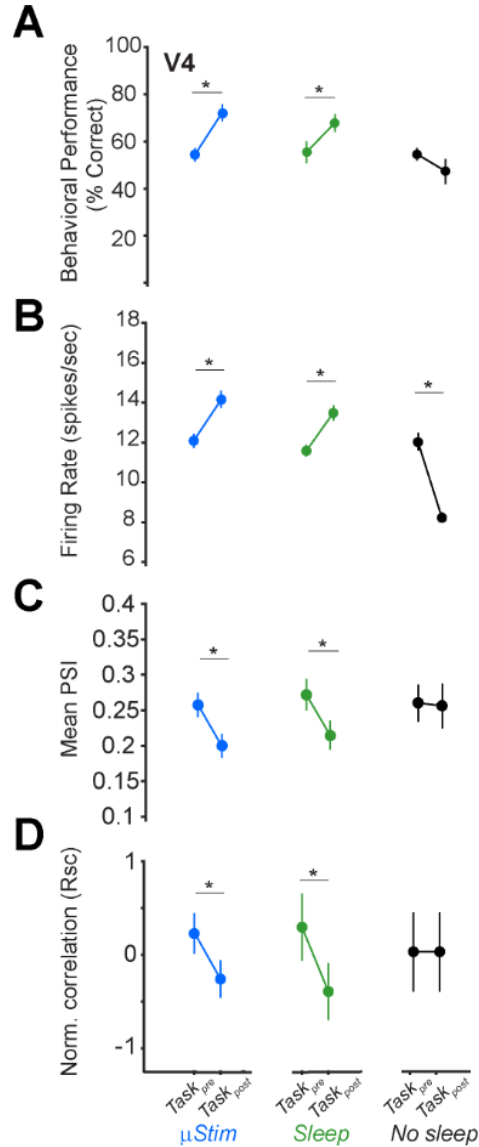


Figure 4.17. Local microstimulation at 4 Hz mimics NREM sleep dependent neuronal and behavioral changes. (A) Mean percent correct responses across sessions plotted as dots with standard error in Task_{post} and Task_{pre} in microstimulation, sleep, and no sleep conditions (* $P < 0.01$, $P > 0.05$ in control, Wilcoxon rank sum test, $n = 18$ sessions total: 8 sessions in microstimulation, 5 sleep and 5 control across 2 animals). (B) Mean firing rate plotted as dots with standard error in Task_{post} and Task_{pre} in microstimulation, sleep, and no sleep conditions (* $P < 0.01$, Wilcoxon rank sum test, $n = 18$ sessions as detailed in legend 4.17A). (C) Mean population synchrony index plotted as dots with standard error in Task_{post} and Task_{pre} in microstimulation, sleep, and no sleep conditions (* $P < 0.01$, $P > 0.05$ in control, Wilcoxon rank sum test, $n = 18$ sessions as detailed in legend 4.17A). (D) Normalized pairwise correlations

between neurons plotted as dots with standard error in Task_{post} and Task_{pre} in microstimulation, sleep, and no sleep conditions (*P < 0.01, P > 0.05 in control, Wilcoxon rank sum test, n = 18 sessions as detailed in legend 4.17A).

4.3 Discussion

How does the increase in population synchrony in sleep desynchronize activity post-sleep? One possible explanation is that the synchronous activity during sleep is likely to cause depression, or downscaling, of local intracortical synapses^{107,157}. However, synaptic depression is an asymmetric process – excitatory synapses are downscaled more than inhibitory ones^{158,159}. Consequently, asymmetric synaptic depression would cause a shift in the balance of local circuits towards inhibition after rest. Because inhibition closely follows excitation to reduce co-fluctuations in cortical responses, and thus reduce correlated variability (even when inhibition increases only modestly), local inhibition has been proposed as a mechanism for decorrelated responses in cortical networks^{91,93,114}. Indeed, our data shows that the increase in synchrony during sleep desynchronized neural activity after sleep, leading to an improvement in behavioral performance.

Our findings complement current theories stating that sleep provides the optimal setting for synaptic downscaling to maintain synaptic homeostasis^{107,160,161} and consolidates information via neuronal re-activation^{71,127,146,149}. These two theories seem contradictory at the synapse level as one states that synapses weaken and the other states that synapses strengthen. Measuring neuronal changes and coupling between neurons at a range of timescales would elucidate how selective synapses can strengthen in an environment of synaptic depression. This sheds light on a potential limitation of our study. We did not measure neuronal coding changes at timescales smaller than 10 milliseconds. A recent study has shown that spike timing between neurons (coordination) in V4 at the 5 ms timescale is crucial for perceptual accuracy⁴⁵. Future

studies could explore the coding changes at the shorter timescales while accounting for neuronal identity^{110,114,162}. Accordingly, future studies might reveal that there is decreased population coupling overall, while increasing spike coordination between neurons selectively engaged in the task. These future experiments and analyses would help reconcile theories of sleep that propose synaptic downscaling and upscaling^{161,163}.

Overall, we tested the interplay of NREM sleep, network coding, and post-sleep perceptual performance. In doing so, we discovered that synchrony in sleep desynchronizes the neural network post-sleep improving neuronal coding and cognitive performance. We also successfully implemented a novel microstimulation paradigm that allows intracranial stimulation at low frequencies, which could serve as a basis for devising neuronal prosthetics in the millions of patients worldwide that suffer from chronic sleep disorders¹⁶⁴. Understanding coding variability revealed here is essential for designing successful neural prosthetics and stimulation paradigms^{165,166}. Thus, our findings lay the groundwork to translate stimulation parameters to treat sleep disruption observed in a variety of neurological disorders, such as Epilepsy and Parkinson's disease, where patients often have implanted electrodes^{118,167–169}. Overall, our findings open novel avenues to treat sleep disruption and expand our basic understanding of the neurobiology of sleep by uncovering the neural underpinnings of sleep dependent improvement in cognitive performance.

Chapter 5: Conclusions and Future Directions

Conclusions

In this dissertation, I examined the prevalence, propagation, and functional significance of synchrony. In chapter 3, I examined whether synchrony propagation in cortical circuits is state-dependent. We used multi-electrode laminar probes to reveal that brain state modulates the propagation of neural activity (synchrony) across the layers of early and mid-level visual cortex (areas V1 and V4). We found high prevalence of neuronal synchrony (vigorous (On) and weak (Off) spiking) in rest but low prevalence of synchrony during wakefulness. We next tested whether propagation of synchrony across cortical circuits is state-dependent. By optogenetically inducing On and Off state transitions within a single cortical layer during wakefulness, we found that synchronized neural activity propagates to other layers only weakly, and the extent of spread is inversely related to arousal level. In contrast, optogenetically-induced population activity robustly propagates throughout the entire cortical column during rest even when neurons are in a desynchronized wake-like state prior to optogenetic stimulation. The influence of global brain state on the propagation of spiking activity across laminar circuits was explained by changes in the coupling between neurons, where neurons were weakly coupled during wakefulness but strongly coupled during rest. The state-dependent propagation of synchronous activity revealed here could constitute a general principle of signal transmission within the sensory cortex.

In addition to understanding how neuronal coupling modulates synchrony propagation in wakefulness and rest, we probed the functional significance of synchrony by studying the influence of NREM sleep (where high levels of synchrony are observed) on coding and behavior. We used non-human primates to record the changes in single neurons, neuronal

populations, and local field potentials in V4 that occur before, during, and after NREM sleep. To test the cognitive effects of naps, monkeys performed an orientation discrimination before and after taking a nap. We found that high levels of synchrony during NREM sleep drive the brain to be further asynchronous after sleep compared to before sleep. Thus, synchrony in NREM sleep improved behavior by modulating population level dynamics, which we tested by performing local microstimulation to induce synchrony in V4 of awake animals. Synchronous local microstimulation replicated the changes in neuronal coding and behavioral performance observed after sleep. We uncovered how synchrony in sleep influences neuronal coding changes in single neurons and in neural ensembles that lead to sleep dependent improvement in cognitive performance. Overall, these findings expand our understanding of the functional significance of synchrony, the neurobiology of sleep, and the neuronal coding driving perception.

Future directions

In chapter 4, we examined how high levels of synchrony in NREM sleep influenced neuronal coding and behavioral performance. To characterize the different stages of sleep accurately, we used a custom-made polysomnography (PSG) setup (Figure 4.4A). And to test the effects of sleep on behavior, we used the visual discrimination task. Both the PSG and the task setup required that our experiments be performed in a head-fixed and restrained body condition (animals comfortably sit in a chair but cannot leave the chair)^{45,52,170}. In this experimental setup, it was easier to train monkeys to nap for short periods of time (20 minutes, NREM sleep) rather than longer periods of sleep (> 45 min, REM sleep). Future studies will use wireless recordings technology implemented in our lab to study sleep in an unrestrained freely moving animal^{50,171}. This is important because several studies show that locomotion

influences neuronal firing by modulating arousal^{75,97}. Perhaps one explanation for why we did not observe the effect of arousal on neuronal coding after sleep is because the animals' movements were restricted in our experiments (Figure 4.12). Studying primates while they freely move and curl up to take a nap as they naturally do would shed light on how other factors, such as attention and arousal, modulate the sleep-dependent effects on neuronal coding and behavioral performance^{99,172–174}. Indeed, we are training freely moving primates to engage in visual discrimination while tracking their eye movements using wireless eye tracking and recording over a hundred neurons to examine network coding^{50,175}. The recent advancements in wireless data transmission and storage make it possible to record from the brain for long periods allowing us to study overnight REM sleep⁵⁰. The combination of recording (1) pupil size as a proxy/indicator for arousal^{173,176}, (2) eye movements and a scene camera to capture natural visual stimuli in the animal's field of view^{23,134}, (3) neuronal activity from multiple brain areas to decode visual stimuli^{55,177}, and (4) videography⁸⁰ to examine behavior in a more natural setting will provide a well-rounded view on the interplay between sleep and perception. Additionally future experiments could use a closed-loop microstimulation paradigm to induce and disrupt synchrony in various sleep stages in a freely moving animal, to examine the components of sleep that influence our daily cognitive performance^{126,178–180}. A colloquial side note: we wirelessly record from the arrays I used for microstimulation in chapter 4 so the proposed future experiments could occur in the not so distant future. The key ingredient is an enthusiastic and motivated graduate student.

In chapter 3, we examined how synchrony spreads in the cortex using optogenetics, and in chapter 4, we examined the functional significance of synchrony by studying sleep-dependent changes in neuronal coding and behavior. While examining how our findings fit

into current theories of synchrony and sleep^{137,149,181}, we postulated that there must be robust changes in synaptic connectivity driving the changes we observed in our data. We examined putative E/I ratios (Figure 3.27) and measured population coupling (Figure 3.26, proxy of synaptic strength) to elucidate the mechanisms underlying our findings^{83,114,117,182}. Since we used electrophysiological techniques, we did not measure molecular changes, an important component that will further our mechanistic understanding of the role of neuronal synchrony.

During wakefulness, several studies have shown that changes in cholinergic drive (arousal) modulates neuronal synchrony^{174,183}. Future studies could use fiber photometry of acetylcholine (ACh) sensors to examine cholinergic changes at the neurochemical level while performing electrophysiological recordings¹⁸⁴. During sleep, waste products are removed from the brain via the recently discovered glymphatic system^{185,186}. Future experiments could utilize microdialysis to capture the local neurochemical changes or utilize cisterna magna taps or a chronic port placed in the 4th ventricle to collect CSF samples and examine them for waste products^{187,188}. This could elucidate the relationship between synchrony and metabolic waste and further our understanding of the role of synchrony as a restorative rhythm.

We used optogenetics in a nonhuman primate model to target excitatory neurons, but, as we know, the repertoire of neuronal subtypes is ever expanding¹⁸⁹. Recording with glassy carbon microelectrodes that report neurotransmitter changes could illuminate how cell-type specific molecular changes during synchrony influence neuronal firing, coding, and behavior^{190,191}. Overall, combining molecular and electrophysiological techniques could provide insights into neuronal dynamics that these techniques alone cannot achieve and move us one step closer to a holistic understanding of how the brain functions.

Bibliography

1. Van Hooser SD, Roy A, Rhodes HJ, Culp JH, Fitzpatrick D. Transformation of receptive field properties from lateral geniculate nucleus to superficial V1 in the tree shrew. *J Neurosci*. 2013;33(28):11494-11505. doi:10.1523/JNEUROSCI.1464-13.2013
2. Nassi JJ, Callaway EM. Parallel processing strategies of the primate visual system. *Nat Rev Neurosci*. 2009;10(5):360-372. doi:10.1038/nrn2619
3. Seidemann E, Geisler WS. Linking V1 activity to behavior. *Annu Rev Vis Sci*. 2018;4:287-310. doi:10.1146/annurev-vision-102016-061324
4. Markov NT, Vezoli J, Chameau P, et al. Anatomy of hierarchy: Feedforward and feedback pathways in macaque visual cortex. *J Comp Neurol*. 2014;522(1):225-259. doi:10.1002/cne.23458
5. Felleman DJ, Van Essen DC. Distributed hierarchical processing in the primate cerebral cortex. *Cereb Cortex*. 1991;1(1):1-47. doi:10.1093/cercor/1.1.1-a
6. Petro LS, Vizioli L, Muckli L. Contributions of cortical feedback to sensory processing in primary visual cortex. *Front Psychol*. 2014;5(OCT). doi:10.3389/fpsyg.2014.01223
7. Budd JML. Extrastriate feedback to primary visual cortex in primates: A quantitative analysis of connectivity. *Proc R Soc B Biol Sci*. 1998;265(1400):1037-1044. doi:10.1098/rspb.1998.0396
8. Ungerleider LG, Galkin TW, Desimone R, Gattass R. Cortical connections of area V4 in the Macaque. *Cereb Cortex*. 2008;18(3):477-499. doi:10.1093/cercor/bhm061
9. Conway BR, Moeller S, Tsao DY. Specialized Color Modules in Macaque Extrastriate Cortex. doi:10.1016/j.neuron.2007.10.008
10. Walsh V, Le Mare C, Blaimire A, Cowey A. Normal discrimination performance

- accompanied by priming deficits in monkeys with V4 or TEO lesions. *Neuroreport*. 2000;11(7):1459-1462.
11. De Weerd P, Peralta MR, Desimone R, Ungerleider LG. Loss of attentional stimulus selection after extrastriate cortical lesions in macaques. *Nat Neurosci*. 1999;2(8):753-758. doi:10.1038/11234
 12. Roland JL, Smyth MD. Recent advances in the neurosurgical treatment of pediatric epilepsy. *J Neurosurg Pediatr*. 2019;23(4):411-421. doi:10.3171/2018.12.PEDS18350
 13. Chawla D, Rees G, Friston KJ. *The Physiological Basis of Attentional Modulation in Extrastriate Visual Areas*; 1999. <http://neurosci.nature.com>. Accessed March 29, 2021.
 14. Fries P, Womelsdorf T, Oostenveld R, Desimone R, Donders FC. The Effects of Visual Stimulation and Selective Visual Attention on Rhythmic Neuronal Synchronization in Macaque Area V4. 2008. doi:10.1523/JNEUROSCI.4499-07.2008
 15. Douglas RJ, Martin KAC. Canonical Cortical Circuits. *Handb Brain Microcircuits*. 2013:15-21. doi:10.1093/med/9780195389883.003.0002
 16. Stickgold R, James L, Hobson JA. Visual discrimination learning requires sleep after training. 2000. https://www.nature.com/articles/nn1200_1237.pdf. Accessed March 27, 2018.
 17. Nigam S, Pojoga S, Dragoi V. A distinct population of heterogeneously color-tuned neurons in macaque visual cortex. *Sci Adv*. 2021;7(8). doi:10.1126/sciadv.abc5837
 18. Conway BR, Tsao DY. Color Architecture in Alert Macaque Cortex Revealed by fMRI. doi:10.1093/cercor/bhj099
 19. Carlson ET, Rasquinha RJ, Zhang K, Connor CE. A sparse object coding scheme in area V4. *Curr Biol*. 2011;21(4):288-293. doi:10.1016/j.cub.2011.01.013

20. Kobatake E, Tanaka K. *Neuronal Selectivities to Complex Object Features in the Ventral Visual Pathway of the Macaque Cerebral Cortex*. Vol 7.; 1994.
21. Hegdé J, Van Essen DC. Stimulus Dependence of Disparity Coding in Primate Visual Area V4. *J Neurophysiol*. 2005;93:620-626. doi:10.1152/jn.00039.2004
22. Hinkle DA, Connor CE. Three-dimensional orientation tuning in macaque area V4. 2002. doi:10.1038/nm875
23. Pasupathy A, Connor CE, Krieger Z, Institute B. *Responses to Contour Features in Macaque Area V4*.; 1999.
24. Roelfsema PR, Singer W. Detecting connectedness. *Cereb Cortex*. 1998;8(5):385-396. doi:10.1093/cercor/8.5.385
25. Hubel DH, Wiesel TN. Uniformity of monkey striate cortex: A parallel relationship between field size, scatter, and magnification factor. *J Comp Neurol*. 1974;158(3):295-305. doi:10.1002/cne.901580305
26. Hubel DH, Wiesel TN. Receptive fields and functional architecture of monkey striate cortex. *J Physiol*. 1968;195:215-243. <https://physoc.onlinelibrary.wiley.com/doi/pdf/10.1113/jphysiol.1968.sp008455>. Accessed July 3, 2019.
27. Hubel DH, Wiesel TN. *SHAPE AND ARRANGEMENT OF COLUMNS IN CAT'S STRIATE CORTEX*. Vol 165.; 1963.
28. Gilbert CD, Wiesel TN. Clustered intrinsic connections in cat visual cortex. *J Neurosci*. 1983;3(5):1116-1133.
29. Hubel DH, Wiesel TN. Receptive fields and functional architecture of monkey striate cortex. *J Physiol*. 1968;195(1):215-243. doi:10.1113/jphysiol.1968.sp008455

30. Mountcastle VB. The columnar organization of the neocortex. 1997;120:701-722.
31. Bastos AM, Usrey WM, Adams RA, Mangun GR, Fries P, Friston KJ. Canonical microcircuits for predictive coding. *Neuron*. 2012;76(4):695-711. doi:10.1016/j.neuron.2012.10.038.Canonical
32. Kohn A, Coen-cagli R, Kanitscheider I, Pouget A. Correlations and Neuronal Population Information. *Annu Rev Neurosci*. 2016;39(April). doi:10.1146/annurev-neuro-070815-013851
33. Abbott LF, Dayan P. The effect of correlated variability on the accuracy of a population code. *Neural Comput*. 1999;11(1):91-101. doi:10.1162/089976699300016827
34. Gur M, Snodderly DM. High response reliability of neurons in primary visual cortex (V1) of alert, trained monkeys. *Cereb Cortex*. 2006;16(6):888-895. doi:10.1093/cercor/bhj032
35. Schölvinck ML, Saleem AB, Benucci A, Harris KD, Carandini M. Cortical state determines global variability and correlations in visual cortex. *J Neurosci*. 2015;35(1):170-178. doi:10.1523/JNEUROSCI.4994-13.2015
36. Gutnisky DA, Beaman CB, Lew SE, Dragoi V. Spontaneous Fluctuations in Visual Cortical Responses Influence Population Coding Accuracy. 2016. doi:10.1093/cercor/bhv312
37. Pouget A, Dayan P, Zemel R. Information processing with population codes. *Nat Rev Neurosci*. 2000;1(2):125-132. doi:10.1038/35039062
38. Cheung KC. Implantable microscale neural interfaces. *Biomed Microdevices*. 2007;9:923-938. doi:10.1007/s10544-006-9045-z
39. GEORGOPOULOS AS. Neuronal Population Coding of Movement Direction .

<http://science.sciencemag.org/>. Accessed March 29, 2021.

40. Montijn JS, Meijer GT, Lansink CS, Pennartz CMA. Population-Level Neural Codes Are Robust to Single-Neuron Variability from a Multidimensional Coding Perspective. *Cell Rep.* 2016;16(9):2486-2498. doi:10.1016/j.celrep.2016.07.065
41. Smith MA, Kohn A. Spatial and temporal scales of neuronal correlation in primary visual cortex. *J Neurosci.* 2008;28(48):12591-12603. doi:10.1523/JNEUROSCI.2929-08.2008
42. Kohn A, Coen-Cagli R, Kanitscheider I, Pouget A. Correlations and Neuronal Population Information. *Annu Rev Neurosci.* 2016;39(1):237-256. doi:10.1146/annurev-neuro-070815-013851
43. Andrei AR, Pojoga S, Janz R, Dragoi V. Integration of cortical population signals for visual perception. *Nat Commun.* 2019;10(1):1-13. doi:10.1038/s41467-019-11736-2
44. Gutnisky DA, Dragoi V. Adaptive coding of visual information in neural populations. *Nature.* 2008;452(7184):220-224. doi:10.1038/nature06563
45. Shahidi N, Andrei AR, Hu M, Dragoi V. High-order coordination of cortical spiking activity modulates perceptual accuracy. *Nat Neurosci.* 2019. doi:10.1038/s41593-019-0406-3
46. Hubel DH, Wiesel TN. *59I RECEPTIVE FIELDS OF SINGLE NEURONES IN THE CAT'S STRIATE CORTEX.* Vol 48.
47. Engel AK, Fries P, Singer W. Dynamic predictions: Oscillations and synchrony in top-down processing. *Nat Rev Neurosci.* 2001;2:704-716.
48. Zagha E, McCormick DA. Neural control of brain state. *Curr Opin Neurobiol.* 2014;29:178-186. doi:10.1016/j.conb.2014.09.010

49. Supè H, Van Der Togt C, Spekrijse H, Lamme VAF. *Internal State of Monkey Primary Visual Cortex (V1) Predicts Figure-Ground Perception.*; 2003.
50. Milton R, Shahidi N, Dragoi V. Dynamic states of population activity in prefrontal cortical networks of freely-moving macaque. *Nat Commun.* 2020;11(1):1-10. doi:10.1038/s41467-020-15803-x
51. Beaman CB, Eagleman SL, Dragoi V. Sensory coding accuracy and perceptual performance are improved during the desynchronized cortical state. *Nat Commun.* 2017;8(1):1308. doi:10.1038/s41467-017-01030-4
52. Nigam S, Pojoga S, Dragoi V. Synergistic Coding of Visual Information in Columnar Networks. *Neuron.* 2019;104(2):402-411.e4. doi:10.1016/j.neuron.2019.07.006
53. Osswald M, Ieng SH, Benosman R, Indiveri G. A spiking neural network model of 3D perception for event-based neuromorphic stereo vision systems. *Sci Rep.* 2017;7(January):1-12. doi:10.1038/srep40703
54. Luczak A, Barthó P, Harris KD. Spontaneous Events Outline the Realm of Possible Sensory Responses in Neocortical Populations. *Neuron.* 2009;62(3):413-425. doi:10.1016/j.neuron.2009.03.014
55. Rubin DB, VanHooser SD, Miller KD. The stabilized supralinear network: A unifying circuit motif underlying multi-input integration in sensory cortex. *Neuron.* 2015;85(2):402-417. doi:10.1016/j.neuron.2014.12.026
56. Pitkow X, Angelaki DE. Inference in the Brain: Statistics Flowing in Redundant Population Codes. *Neuron.* 2017;94(5):943-953. doi:10.1016/j.neuron.2017.05.028
57. Jun JJ, Steinmetz NA, Siegle JH, et al. Fully integrated silicon probes for high-density recording of neural activity. *Nature.* 2017;551(7679):232-236.

doi:10.1038/nature24636

58. Demas J, Manley J, Tejera F, et al. Volumetric Calcium Imaging of 1 Million Neurons Across Cortical Regions at Cellular Resolution using Light Beads Microscopy. *bioRxiv*. 2021. doi:10.1101/2021.02.21.432164
59. Harris KD, Thiele A. Cortical state and attention. *Nat Rev Neurosci*. 2011;12(9):509-523. doi:10.1038/nrn3084
60. Harris KD, Mrsic-flogel TD. Cortical connectivity and sensory coding. *Nature*. 2013;503(7474):51-58. doi:10.1038/nature12654
61. Hutcheon B, Yarom Y. Resonance, oscillation and the intrinsic frequency preferences of neurons. *Trends Neurosci*. 2000;23(5):216-222.
62. Huguenard JR, McCormick DA. Thalamic synchrony and dynamic regulation of global forebrain oscillations. *Trends Neurosci*. 2007;30(7):350-356. doi:10.1016/j.tins.2007.05.007
63. Vyazovskiy V V, Harris KD. Sleep and the single neuron: The role of global slow oscillations in individual cell rest. *Nat Rev Neurosci*. 2013;14(6):443-451. doi:10.1038/nrn3494
64. Sloviter H, Arieli A, Hildesheim R, Grinvald A. Long-Term Voltage-Sensitive Dye Imaging Reveals Cortical Dynamics in Behaving Monkeys. *J Neurophysiol*. 2002;88:3421-3438. doi:10.1152/jn.00194.2002
65. Ohki K, Chung S, Ch YH, Kara P, Clay Reid R. *Functional Imaging with Cellular Resolution Reveals Precise Micro-Architecture in Visual Cortex*; 2005. www.nature.com/nature. Accessed March 29, 2021.
66. Adamantidis AR, Gutierrez Herrera C, Gent TC. Oscillating circuitries in the sleeping

- brain. *Nat Rev Neurosci.* 2019;20(12):746-762. doi:10.1038/s41583-019-0223-4
67. Peter J. Uhlhaas^{1,2}, Gordon Pipa^{1,3}, Bruss Lima¹, Lucia Melloni¹, Sergio Neuenschwander¹, Danko Nikolic^{1,3}, and Wolf Singer^{1,3}. Neural synchrony in cortical networks: history, concept and current status.
 68. Poe GR, Walsh CM, Bjorness TE. *Cognitive Neuroscience of Sleep*. Vol 185. Elsevier B.V.; 2010. doi:10.1016/B978-0-444-53702-7.00001-4
 69. Krueger JM, Huang YH, Rector DM, Buysse DJ. Sleep: A synchrony of cell activity-driven small network states. *Eur J Neurosci.* 2013;38(2):2199-2209. doi:10.1111/ejn.12238
 70. Weber F, Hoang Do JP, Chung S, et al. Regulation of REM and Non-REM Sleep by Periaqueductal GABAergic Neurons. *Nat Commun.* 2018;9(1). doi:10.1038/s41467-017-02765-w
 71. Hobson JA, Pace-Schott EF. The cognitive neuroscience of sleep: Neuronal systems, consciousness and learning. *Nat Rev Neurosci.* 2002;3(9):679-693. doi:10.1038/nrn915
 72. Greenberg DS, Houweling AR, Kerr JND. Population imaging of ongoing neuronal activity in the visual cortex of awake rats. *Nat Neurosci.* 2008;11(7):749-751. doi:10.1038/nn.2140
 73. Poulet JFA, Petersen CCH. Internal brain state regulates membrane potential synchrony in barrel cortex of behaving mice. 2008;454:881-885.
 74. Reimer J, Froudarakis E, Cadwell CR, Yatsenko D, Denfield GH, Tolias AS. Pupil Fluctuations Track Fast Switching of Cortical States during Quiet Wakefulness. *Neuron.* 2015;84(2):355-362. doi:10.1016/j.neuron.2014.09.033.Pupil
 75. Niell CM, Stryker MP. Modulation of visual responses by behavioral state in mouse

- visual cortex. *Neuron*. 2010;65(4):472-479. doi:10.1016/j.neuron.2010.01.033
76. McGinley MJ, Vinck M, Reimer J, et al. Waking State: Rapid Variations Modulate Neural and Behavioral Responses. *Neuron*. 2015;87(6):1143-1161. doi:10.1016/j.neuron.2015.09.012
 77. Ecker AS, Berens P, Cotton RJ, et al. State dependence of noise correlations in macaque primary visual cortex. *Neuron*. 2014;82(1):235-248. doi:10.1016/j.neuron.2014.02.006
 78. Schroeder C. A spatiotemporal profile of visual system activation revealed by current source density analysis in the awake macaque. *Cereb Cortex*. 1998;8(7):575-592. doi:10.1093/cercor/8.7.575
 79. Daley JT, Turner RS, Bs AF, Bliwise DL, Rye DB. Prolonged Assessment of Sleep and Daytime Sleepiness in Unrestrained Macaca Mulatta. *Sleep*. 2017;29(2):221-231.
 80. Mathis A, Mamidanna P, Cury KM, et al. DeepLabCut: markerless pose estimation of user-defined body parts with deep learning. *Nat Neurosci*. 2018;21(9):1281-1289. doi:10.1038/s41593-018-0209-y
 81. Berry R, Brooks R, Gamaldo C, Harding S, Lloyd R. *AASM Manual for the Scoring of Sleep and Associated Events: Rules, Terminology and Technical Specifications*. 2013th ed. Darien, Illinois: American Academy of Sleep Medicine; 2013.
 82. Petreanu L, Mao T, Sternson SM, Svoboda K. The subcellular organization of neocortical excitatory connections. *Nature*. 2009;457:1142-1145. doi:10.1038/nature07709
 83. Okun M, Steinmetz NA, Cossell L, et al. Diverse coupling of neurons to populations in sensory cortex. *Nature*. 2015;521(7553):511-515. doi:10.1038/nature14273
 84. Rudolph M, Pospischil M, Timofeev I, Destexhe A. Inhibition Determines Membrane

- Potential Dynamics and Controls Action Potential Generation in Awake and Sleeping Cat Cortex. *J Neurosci.* 2007;27(20):5280-5290. doi:10.1523/JNEUROSCI.4652-06.2007
85. Mitchell JF, Sundberg KA, Reynolds JH. Differential Attention-Dependent Response Modulation across Cell Classes in Macaque Visual Area V4. *Neuron.* 2007;55(1):131-141. doi:10.1016/j.neuron.2007.06.018
 86. Barthó P, Hirase H, Monconduit L, Zugaro M, Harris KD, Buzsáki G. Characterization of neocortical principal cells and interneurons by network interactions and extracellular features. *J Neurophysiol.* 2004;92(1):600-608. doi:10.1152/jn.01170.2003
 87. Brodmann K. Vergleichende Lokalisationslehre der Grosshirnrinde in ihren Prinzipien dargestellt auf Grund des Zellenbaues. *Barth.* 1909.
 88. Douglas RJ, Martin KAC. Neuronal circuits of the neocortex. *Annu Rev Neurosci.* 2004;27:419-451. doi:10.1146/annurev.neuro.27.070203.144152
 89. Harris KD, Shepherd GMG. The neocortical circuit: Themes and variations. *Nat Neurosci.* 2015;18(2):170-181. doi:10.1038/nn.3917
 90. Hirsch JA, Martinez LM. Laminar processing in the visual cortical column. *Curr Opin Neurobiol.* 2006;16:377-384.
 91. Hansen BJ, Chelaru MI, Dragoi V. Correlated Variability in Laminar Cortical Circuits. *Neuron.* 2012;76(3):590-602. doi:10.1016/j.neuron.2012.08.029
 92. Steriade MM, McCarley R. *Brain Control of Wakefulness and Sleep.* Springer US; 2005.
 93. Renart A, de la Rocha J, Bartho P, et al. Asynchronous state in cortical circuits. *Science* . 2010;328(5974):16–37. doi:10.1126/science.1183640
 94. Cohen MR, Kohn A. Measuring and interpreting neuronal correlations. *Nat Neurosci.*

2011;14(7):811-819. doi:10.1038/nn.2842

95. Anirvan S. Nandy JJN, John H. Reynolds. Laminar Organization of Attentional Modulation in Macaque Visual Area V4. *Neuron*. 2017;93:235–246. [http://www.cell.com/neuron/pdfExtended/S0896-6273\(16\)30867-4](http://www.cell.com/neuron/pdfExtended/S0896-6273(16)30867-4). Accessed March 27, 2018.
96. Smith MA, Jia X, Zandvakili A, Kohn A. Laminar dependence of neuronal correlations in visual cortex. *J Neurophysiol*. 2013;109(4):940-947. doi:10.1152/jn.00846.2012
97. Vinck M, Batista-Brito R, Knoblich U, Cardin JA. Arousal and Locomotion Make Distinct Contributions to Cortical Activity Patterns and Visual Encoding. *Neuron*. 2015;86(3):740-754. doi:10.1016/j.neuron.2015.03.028
98. Gervasoni D, Lin SC, Ribeiro S, Soares ES, Pantoja J, Nicolelis MAL. Global forebrain dynamics predict rat behavioral states and their transitions. *J Neurosci*. 2004;24(49):11137-11147. doi:10.1523/JNEUROSCI.3524-04.2004
99. Li CT, Poo M, Dan Y. Burst Spiking of a Single Cortical Neuron Modifies Global Brain State. *Science* . 2009;324(5927):642-646. <http://science.sciencemag.org/>. Accessed July 3, 2019.
100. Sanchez-Vives M V, McCormick DA. Cellular and network mechanisms of rhythmic recurrent activity in neocortex. *Nat Neurosci*. 2000;3(10):1027-1034.
101. Engel TA, Steinmetz NA, Gieselmann MA, Thiele A, Moore T, Boahen K. Selective modulation of cortical state during spatial attention. *Science* . 2016;354(6316):1140-1144. doi:10.1126/science.aag1420
102. Lakatos P, Chen CM, O’Connell MN, Mills A, Schroeder CE. Neuronal Oscillations and Multisensory Interaction in Primary Auditory Cortex. *Neuron*. 2007;53(2):279-292.

doi:10.1016/j.neuron.2006.12.011

103. Hansen BJ, Dragoi V. Adaptation-induced synchronization in laminar cortical circuits. *Proc Natl Acad Sci U S A*. 2011;108(26):10720-10725. doi:10.1073/pnas.1102017108
104. Tan AYY, Chen Y, Scholl B, Seidemann E, Priebe NJ. Sensory stimulation shifts visual cortex from synchronous to asynchronous states. *Nature*. 2014;509:226-229.
105. Baum L, Petrie T, Soules G, Weiss N. A maximization technique occurring in the statistical analysis of probabilistic functions, of a Markov chains. *Ann Math Stat*. 1970;41(1):164-171.
106. Seidemann E, Meilijson I, Abeles M, Bergman H, Vaadia E. Simultaneously Recorded Single Units in the Frontal Cortex Go through Sequences of Discrete and Stable States in Monkeys Performing a Delayed Localization Task. *J Neurosci*. 1996;76(2):752-768.
107. Tononi G, Cirelli C. Sleep function and synaptic homeostasis. *Sleep Med Rev*. 2006;10:49-62.
108. Ecker AS, Berens P, Keliris GA, Bethge M, Logothetis NK, Tolias AS. Decorrelated Neuronal Firing in Cortical Microcircuits. *Science* . 2010;327(April):584-587.
109. Han X, Qian X, Bernstein JG, et al. Millisecond-timescale optical control of neural dynamics in the nonhuman primate brain. *Neuron*. 2009;62(2):191-198. doi:10.1016/j.neuron.2009.03.011
110. Cardin JA, Carlén M, Meletis K, et al. Driving fast-spiking cells induces gamma rhythm and controls sensory responses. *Nature*. 2009;459(7247):663-667. doi:10.1038/nature08002
111. Dehghani N, Peyrache A, Telenczuk B, et al. Dynamic Balance of Excitation and Inhibition in Human and Monkey Neocortex. *Sci Rep*. 2016;101(3):500-513.

doi:10.1038/srep23176

112. Markram H, Toledo-Rodriguez M, Wang Y, Gupta A, Silberberg G, Wu C. Interneurons of the neocortical inhibitory system. *Nat Rev Neurosci.* 2004;5(10):793-807. doi:10.1038/nrn1519
113. Haider B, Häusser M, Carandini M. Inhibition dominates sensory responses in the awake cortex. *Nature.* 2013;493(7430):97-100. doi:10.1038/nature11665
114. Niethard N, Hasegawa M, Itokazu T, Oyanedel CN, Born J, Sato TR. Sleep-Stage-Specific Regulation of Cortical Excitation and Inhibition. *Curr Biol.* 2016;26(20):2739-2749. doi:10.1016/j.cub.2016.08.035
115. Chagnac-Amitai Y, Connors BW. Horizontal Spread of Synchronized Activity in Neocortex and its Control by GABA-Mediated Inhibition. *J Neurophysiol.* 1989;6(4):747-757.
116. Patel M, Joshi B. Decoding synchronized oscillations within the brain: Phase-delayed inhibition provides a robust mechanism for creating a sharp synchrony filter. *J Theor Biol.* 2013;334:13-25. doi:10.1016/j.jtbi.2013.05.022
117. Xue M, Atallah B V., Scanziani M. Equalizing excitation-inhibition ratios across visual cortical neurons. *Nature.* 2014;511(7511):596-600. doi:10.1038/nature13321
118. Uhlhaas PJ, Singer W. Neural Synchrony in Brain Disorders: Relevance for Cognitive Dysfunctions and Pathophysiology. *Neuron.* 2006;52(1):155-168. doi:10.1016/j.neuron.2006.09.020
119. Uhlhaas PJ, Singer W. Abnormal neural oscillations and synchrony in schizophrenia. *Nat Rev Neurosci.* 2010;11(2):100-113. doi:10.1038/nrn2774
120. Song HF, Kennedy H, Wang X-J. Spatial embedding of structural similarity in the

- cerebral cortex. *Proc Natl Acad Sci U S A*. 2014;111(46):16580-16585.
121. Campbell SS, Tobler I. Animal sleep: A review of sleep duration across phylogeny. *Neurosci Biobehav Rev*. 1984;8(3):269-300. doi:10.1016/0149-7634(84)90054-X
 122. Atienza M, Cantero JL, Stickgold R. Posttraining Sleep Enhances Automaticity in Perceptual Discrimination. *J Cogn Neurosci*. 2004;16(1):53-64. doi:10.1162/089892904322755557
 123. Trettel SG, Trimper JB, Hwaun E, Fiete IR, Colgin LL. Grid cell co-activity patterns during sleep reflect spatial overlap of grid fields during active behaviors. *Nat Neurosci*. 2019;22(4):609-617. doi:10.1038/s41593-019-0359-6
 124. Jenkins J, Dallenbach K. Obliviscence during Sleep and Waking Author (s): John G . Jenkins and Karl M . Dallenbach Source : The American Journal of Psychology , Vol . 35 , No . 4 (Oct . , 1924), pp . 605-612 Published by : University of Illinois Press Stable URL : [http://www.j. Am J Psychol. 1924;35\(4\):605-612. www.jstor.org/stable/1414040](http://www.j. Am J Psychol. 1924;35(4):605-612. www.jstor.org/stable/1414040).
 125. Rosier M, Le Barillier L, Meunier D, El Yacoubi M, Malleret G, Salin PA. Post-learning paradoxical sleep deprivation impairs reorganization of limbic and cortical networks associated with consolidation of remote contextual fear memory in mice. *Sleep*. 2018;41(12):1-18. doi:10.1093/sleep/zsy188
 126. Kim J, Gulati T, Ganguly K. Competing Roles of Slow Oscillations and Delta Waves in Memory Consolidation versus Forgetting Article Competing Roles of Slow Oscillations and Delta Waves in Memory Consolidation versus Forgetting. *Cell*. 2019;179(2):514-526. doi:10.1016/j.cell.2019.08.040
 127. Klinzing JG, Niethard N, Born J. Mechanisms of systems memory consolidation during

- sleep. *Nat Neurosci.* 2019. doi:10.1038/s41593-019-0467-3
128. Yellin D, Berkovich-Ohana A, Malach R. Coupling between pupil fluctuations and resting-state fMRI uncovers a slow build-up of antagonistic responses in the human cortex. *Neuroimage.* 2015;106:414-427. doi:10.1016/j.neuroimage.2014.11.034
 129. Andrillon T, Nir Y, Staba RJ, Ferrarelli F, Cirelli C, Tononi G. Sleep Spindles in Humans : Insights from Intracranial EEG and Unit Recordings. 2011;31(49):17821-17834. doi:10.1523/JNEUROSCI.2604-11.2011
 130. Phillips AJK, Robinson PA, Kedziora DJ, Abeysuriya RG. Mammalian Sleep Dynamics: How Diverse Features Arise from a Common Physiological Framework. *PLoS Comput Biol.* 2010;6(6):1000826. doi:10.1371/journal.pcbi.1000826
 131. Zhdanova I V, Masuda K, Quasarano-Kourkoulis C, Rosene DL, Killiany RJ, Wang S. Aging of Intrinsic Circadian Rhythms and Sleep in a Diurnal Nonhuman Primate, *Macaca mulatta*. *J Biol Rhythms.* 2011;26(2):149-159. doi:10.1177/0748730410395849
 132. Ishikawa A, Sakai K, Maki T, et al. Investigation of sleep-wake rhythm in non-human primates without restraint during data collection. *Exp Anim.* 2016;66(1):51-60. doi:10.1538/EXPANIM.16-0073
 133. Nandy A, Nassi JJ, Reynolds JH. Laminar Organization of Attentional Modulation in Macaque Visual Area V4. *Neuron.* 2017;93(1):235-246. doi:10.1016/j.neuron.2016.11.029
 134. Gutnisky DA, Hansen BJ, Iliescu BF, Dragoi V. Attention Alters Visual Plasticity during Exposure-Based Learning. *Curr Biol.* 2009;19(7):555-560. doi:10.1016/j.cub.2009.01.063
 135. Steriade M, Timofeev I, Grenier F. Natural waking and sleep states: A view from inside

- neocortical neurons. *J Neurophysiol.* 2001;85(5):1969-1985.
doi:10.1152/jn.2001.85.5.1969
136. Buzsáki G, Anastassiou CA, Koch C. The origin of extracellular fields and currents- EEG, ECoG, LFP and spikes. *Nat Rev Neurosci.* 2012;13(6):407-420.
doi:10.1038/nrn3241
 137. Vyazovskiy V V., Olcese U, Lazimy YM, et al. Cortical Firing and Sleep Homeostasis. *Neuron.* 2009;63(6):865-878. doi:10.1016/j.neuron.2009.08.024
 138. Bushey D, Tononi G, Cirelli C. Sleep- and wake-dependent changes in neuronal activity and reactivity demonstrated in fly neurons using in vivo calcium imaging. *Proc Natl Acad Sci U S A.* 2015;112(15):4785-4790. doi:10.1073/pnas.1419603112
 139. Mazzoni A, Whittingstall K, Brunel N, Logothetis NK, Panzeri S. Understanding the relationships between spike rate and delta/gamma frequency bands of LFPs and EEGs using a local cortical network model. *Neuroimage.* 2010.
doi:10.1016/j.neuroimage.2009.12.040
 140. Durkin J, Suresh AK, Colbath J, et al. Cortically coordinated NREM thalamocortical oscillations play an essential, instructive role in visual system plasticity. *Proc Natl Acad Sci U S A.* 2017;114(39):10485-10490. doi:10.1073/pnas.1710613114
 141. Harmony T. The functional significance of delta oscillations in cognitive processing. *Front Integr Neurosci.* 2013;7(DEC):1-10. doi:10.3389/fnint.2013.00083
 142. Karni A, Tanne D, Rubenstein BS, Askenasy JJM, Sagi D. Dependence on REM sleep of overnight improvement of a perceptual skill. *Science* . 1994;265(5172):679-682.
doi:10.1126/science.8036518
 143. Halgren M, Fabó D, Ulbert I, et al. Superficial Slow Rhythms Integrate Cortical

- Processing in Humans. 2018;1-12. doi:10.1038/s41598-018-20662-0
144. Takahashi M. The role of prescribed napping in sleep medicine. *Sleep Med Rev.* 2003;7(3):227-235. doi:10.1053/smr.v.2002.0241
 145. Sallinen M, Härmä M, Åkerstedt T, Rosa R, Lillqvist O. Promoting alertness with a short nap during a night shift. *J Sleep Res.* 1998;7(4):240-247. doi:10.1046/j.1365-2869.1998.00121.x
 146. Marshall L, Helgadóttir H, Mölle M, Born J. Boosting slow oscillations during sleep potentiates memory. *Nature.* 2006;444(7119):610-613. doi:10.1038/nature05278
 147. Fogel SM, Smith CT. Learning-dependent changes in sleep spindles and Stage 2 sleep. *J Sleep Res.* 2006;15(3):250-255. doi:10.1111/j.1365-2869.2006.00522.x
 148. Lahl O, Wispel C, Willigens B, Pietrowsky R. An ultra short episode of sleep is sufficient to promote declarative memory performance. *J Sleep Res.* 2008;17(1):3-10. doi:10.1111/j.1365-2869.2008.00622.x
 149. Diekelmann S, Born J. The memory function of sleep. *Nat Rev Neurosci.* 2010;11(2):114-126. doi:10.1038/nrn2762
 150. Roe AW, Chelazzi L, Connor CE, et al. Toward a Unified Theory of Visual Area V4 HHS Public Access. *Neuron.* 2012;74(1):12-29. doi:10.1016/j.neuron.2012.03.011
 151. Schiller P., Kyoungmin L. *The Role of the Primate Extrastriate Area V4 in Vision.* Vol 251. Springer-Verlag; 1991. <http://science.sciencemag.org/>.
 152. Eagleman SL, Dragoi V. Image sequence reactivation in awake V4 networks. *Proc Natl Acad Sci U S A.* 2012;109(47):19450-19455. doi:10.1073/pnas.1212059109
 153. Fetsch CR, Kiani R, Newsome WT, Shadlen MN. Effects of Cortical Microstimulation on Confidence in a Perceptual Decision. *Neuron.* 2014;83(4):797-804.

doi:10.1016/j.neuron.2014.07.011

154. Salzman CD, Britten KH, Newsome WT. Cortical Microstimulation Influences Perceptual Judgements of Motion Direction. *Nature*. 1990;346(July):174-177. <https://www.nature.com/articles/346174a0.pdf>.
155. Hao Y, Riehle A, Brochier TG. Mapping horizontal spread of activity in monkey motor cortex using single pulse microstimulation. *Front Neural Circuits*. 2016;10(DEC):1-16. doi:10.3389/fncir.2016.00104
156. Grossman N, Bono D, Dedic N, et al. Noninvasive Deep Brain Stimulation via Temporally Interfering Electric Fields. *Cell*. 2017;169(6):1029-1041.e16. doi:10.1016/j.cell.2017.05.024
157. Frank MG. Erasing Synapses in Sleep: Is It Time to Be SHY? *Neural Plast*. 2012;2012. doi:10.1155/2012/264378
158. Chelaru MI, Dragoi V. Efficient coding in heterogeneous neuronal populations. *Proc Natl Acad Sci U S A*. 2008;105(42):16344-16349. doi:10.1073/pnas.0807744105
159. Galarreta M, Hestrin S. Frequency-dependent synaptic depression and the balance of excitation and inhibition in the neocortex. *Nat Neurosci*. 1998;1(7):587-594. doi:10.1038/2822
160. Watson BO, Levenstein D, Greene JP, Gelinas JN, Buzsáki G. Network Homeostasis and State Dynamics of Neocortical Sleep. *Neuron*. 2016. doi:10.1016/j.neuron.2016.03.036
161. Torrado Pacheco A, Bottorff J, Gao Y, Turrigiano GG. Sleep Promotes Downward Firing Rate Homeostasis. *Neuron*. 2021;109(3):530-544.e6. doi:10.1016/j.neuron.2020.11.001

162. Senzai Y, Fernandez-Ruiz A, Buzsaki G. Layer-Specific Physiological Features and Interlaminar Interactions in the Primary Visual Cortex of the Mouse. *Neuron*. 2019;101:500-513. doi:10.1016/j.neuron.2018.12.009
163. Li W, Gan W. Sleep promotes branch-specific formation of dendritic spines after learning. *Science* . 2014;344(6188):1173-1178. doi:10.1126/science.1249098
164. Ting L, Malhotra A. Disorders of sleep: An overview. *Prim Care - Clin Off Pract*. 2005;32(2):305-318. doi:10.1016/j.pop.2005.02.004
165. O'Doherty JE, Lebedev MA, Ifft PJ, et al. Active tactile exploration using a brain-machine-brain interface. *Nature*. 2011;479(7372):228-231. doi:10.1038/nature10489
166. Chen KH, Dammann JF, Boback JL, et al. The effect of chronic intracortical microstimulation on the electrode-tissue interface. *J Neural Eng*. 2014;11(2). doi:10.1088/1741-2560/11/2/026004
167. Britton JW. Electrical stimulation mapping with stereo-EEG electrodes. *J Clin Neurophysiol*. 2018;35(2):110-114. doi:10.1097/WNP.0000000000000443
168. Fridley J, Yoshor D. Brain stimulation for the treatment of epilepsy. *Neurosurg Focus*. 2012;32(March):442-443. doi:10.1017/CBO9781139103992.088
169. Huang J, Zhuo W, Zhang Y, et al. Cognitive function characteristics of Parkinson's disease with sleep disorders. *Parkinsons Dis*. 2017;2017. doi:10.1155/2017/4267353
170. Merritt SL, Schnyders HC, Patel M, Basner RC, O'Neill W. Pupil staging and EEG measurement of sleepiness. *Int J Psychophysiol*. 2004;52(1):97-112. doi:10.1016/j.ijpsycho.2003.12.007
171. Fernandez-Leon JA, Parajuli A, Franklin R, et al. A wireless transmission neural interface system for unconstrained non-human primates. *J Neural Eng*. 2015;12(5).

doi:10.1088/1741-2560/12/5/056005

172. Scammell TE, Arrigoni E, Lipton JO. Neural Circuitry of Wakefulness and Sleep. *Neuron*. 2017;93(4):747-765. doi:10.1016/j.neuron.2017.01.014
173. Reimer J, Froudarakis E, Cadwell CR, Yatsenko D, Denfield GH, Tolias AS. Pupil Fluctuations Track Fast Switching of Cortical States during Quiet Wakefulness - Supplemental. *Neuron*. 2014;84(2):355-362. doi:10.1016/j.neuron.2014.09.033
174. Pinto L, Goard MJ, Estandian D, et al. Fast modulation of visual perception by basal forebrain cholinergic neurons. *Nat Neurosci*. 2013;16(12):1857-1863. doi:10.1038/nn.3552
175. Shahidi N, Schrater P, Wright T, Pitkow X, Dragoi V. Population coding of strategic variables during foraging in freely-moving macaques. *bioRxiv*. 2019. doi:10.1101/811992
176. Suzuki TW, Kunimatsu J, Tanaka M. Correlation between Pupil Size and Subjective Passage of Time in Non-Human Primates. *J Neurosci*. 2016;36(44):11331-11337. doi:10.1523/JNEUROSCI.2533-16.2016
177. Huang C, Ruff DA, Pyle R, Rosenbaum R, Cohen MR, Doiron B. Circuit Models of Low-Dimensional Shared Variability in Cortical Networks. *Neuron*. 2019;101(2). doi:10.1016/j.neuron.2018.11.034
178. Millard DC, Whitmire CJ, Gollnick CA, Rozell CJ, Stanley GB. Electrical and optical activation of mesoscale neural circuits with implications for coding. *J Neurosci*. 2015;35(47):15702-15715. doi:10.1523/JNEUROSCI.5045-14.2015
179. Lafon B, Henin S, Huang Y, et al. Low frequency transcranial electrical stimulation does not entrain sleep rhythms measured by human intracranial recordings. *Nat*

- Commun.* 2017;8(1):1-14. doi:10.1038/s41467-017-01045-x
180. Massimini M, Ferrarelli F, Esser SK, et al. Triggering sleep slow waves by transcranial magnetic stimulation. *Proc Natl Acad Sci U S A.* 2007;104(20):8496-8501. doi:10.1073/pnas.0702495104
 181. Watson BO, Buzsáki G. Sleep , Memory & Brain Rhythms. *AAAS.* 2015:67-82.
 182. Yu X, Li W, Ma Y, et al. GABA and glutamate neurons in the VTA regulate sleep and wakefulness. *Nat Neurosci.* 2019;22(January). doi:10.1038/s41593-018-0288-9
 183. Chen N, Sugihara H, Sur M. An acetylcholine-activated microcircuit drives temporal dynamics of cortical activity. *Nat Neurosci.* 2015;18(6):892-902. doi:10.1038/nn.4002
 184. Patel AA, McAlinden N, Mathieson K, Sakata S. Simultaneous Electrophysiology and Fiber Photometry in Freely Behaving Mice. *Front Neurosci.* 2020;14. doi:10.3389/fnins.2020.00148
 185. Xie L, Kang H, Xu Q, et al. Sleep drives metabolite clearance from the adult brain. *Science .* 2013;342(6156):373-377. doi:10.1126/science.1241224
 186. Ju Y-ES, Ooms SJ, Sutphen C, et al. Slow wave sleep disruption increases cerebrospinal fluid amyloid-b levels Abbreviations: N1/2/3 = non-rapid eye movement sleep stage 1/2/3; SWA = slow wave activity. 2017:2104-2111. doi:10.1093/awx174
 187. Sandberg DI, Kharas N, Yu B, et al. High-dose MTX110 (soluble panobinostat) safely administered into the fourth ventricle in a nonhuman primate model. *J Neurosurg Pediatr.* 2020;26(2):127-135. doi:10.3171/2020.2.PEDS19786
 188. Li X, Han P, Guo Y, Sun H, Xiao Y, Kang YJ. Basic neuroscience An improved technique for cerebrospinal fluid collection of cisterna magna in Rhesus monkeys. *J Neurosci Methods.* 2015;249:59-65. doi:10.1016/j.jneumeth.2015.04.004

189. Choquet D, Sainlos M. Advanced imaging and labelling methods to decipher brain cell organization and function. *Nat Rev Neurosci*. 2021;22:237-255.
190. Vajari DA, Vomero M, Erhardt JB, et al. Integrity assessment of a hybrid DBS probe that enables neurotransmitter detection simultaneously to electrical stimulation and recording. *Micromachines*. 2018;9(10):1-15. doi:10.3390/mi9100510
191. Banerjee S, Mccracken S, Hossain F, Slaughter G. Electrochemical Detection of Neurotransmitters. doi:10.3390/bios10080101

VITA

Natasha Kharas was born in Mumbai, Maharashtra, India, the daughter of Amrit Kaur Kharas and Farokh Rustom Kharas. She graduated with a Bachelor of Science in Neural Science from New York University, with highest honors in May 2011. After graduating, she worked for a start-up company, Cell-centric, for a year and as a research assistant in the Biology Department at Columbia University for a year. In May 2013, she matriculated the MD/PhD program at The University of Texas Health Science Center at Houston McGovern Medical School and MD Anderson Cancer Center.